

DIGITAL ACCESS TO SCHOLARSHIP AT HARVARD
DASH.HARVARD.EDU

HARVARD LIBRARY

Convergent processing of auditory and tactile vibration in the inferior colliculus

Citation

Huey, Erica Lynne. 2025. Convergent processing of auditory and tactile vibration in the inferior colliculus. Doctoral Dissertation, Harvard University Graduate School of Arts and Sciences.

Link

https://dash.harvard.edu/handle/1/42719690

Terms of use

This article was downloaded from Harvard University's DASH repository, and is made available under the terms and conditions applicable to Other Posted Material (LAA), as set forth at

https://harvardwiki.atlassian.net/wiki/external/NGY5NDE4ZjgzNTc5NDQzMGIzZWZhMGFlOWI2M2EwYTg

Accessibility

https://accessibility.huit.harvard.edu/digital-accessibility-policy

Share Your Story

The Harvard community has made this article openly available.
Please share how this access benefits you. Submit a story

HARVARD
Kenneth C. Griffin

GRADUATE SCHOOL
OF ARTS AND SCIENCES

DISSERTATION ACCEPTANCE CERTIFICATE

The undersigned, appointed by the

Division of Medical Sciences

Program in Neuroscience

have examined a dissertation entitled

Convergent processing of auditory and tactile vibration in the inferior colliculus

presented by Erica Huey

candidate for the degree of Doctor of Philosophy and hereby certify that it is worthy of acceptance.

Signature: Chinfei Chen
Chinfei Chen (Sep 13, 2024 22:36 EDT)

Typed Name: Dr. Chinfei Chen

Signature: John A. Assad
John A. Assad (Sep 13, 2024 17:00 EDT)

Typed Name: Dr. John Assad

Signature: Chenghua Gu
Chenghua Gu (Sep 13, 2024 16:10 EDT)

Typed Name: Dr. Chenghua Gu

Signature: Fan Wang
Fan Wang (Sep 13, 2024 18:01 EDT)

Typed Name: Dr. Fan Wang

Date: September 13, 2024

Convergent processing of auditory and tactile vibration in the inferior colliculus

A dissertation presented

by

Erica Huey

to

The Division of Medical Sciences

in partial fulfillment of the requirements

for the degree of

Doctor of Philosophy

in the subject of

Neuroscience

Harvard University

Cambridge, Massachusetts

September 2024

© 2024 Erica Huey

All rights reserved.

Dissertation Advisor: David Ginty Erica Huey

Convergent processing of auditory and tactile vibration in the inferior colliculus

Abstract

Vibrations are ubiquitous in nature, shaping behavior across the animal kingdom. For mammals, mechanical vibrations acting on the body are detected by mechanoreceptors of the skin and deep tissue and processed by the somatosensory system, while sound waves traveling through air are captured by the cochlea and encoded in the auditory system. Here, we report that mechanical vibrations detected by the body's Pacinian corpuscle neurons, which are unique in their ability to entrain to high-frequency (40-1000 Hz) environmental vibrations, are prominently encoded by neurons in the lateral cortex of the inferior colliculus (LCIC) of the midbrain. Remarkably, most LCIC neurons receive convergent Pacinian and auditory input and respond more strongly to coincident tactile-auditory stimulation than to either modality alone. Moreover, the LCIC is required for behavioral responses to high frequency mechanical vibrations. Thus, environmental vibrations captured by Pacinian corpuscles of the body are encoded in the auditory midbrain to mediate behavior.

Table of Contents

Title Page i

Copyright ii

Abstract iii

Table of Contents iv

Acknowledgements v

Chapter 1. Introduction 1

Chapter 2. The auditory midbrain mediates tactile vibration sensing 23

Chapter 3. Discussion 86

References 91

Acknowledgments

First and foremost, I would like to express my deepest gratitude to my advisor, David Ginty. Your unwavering positivity and support have been instrumental in helping me become a more confident and capable scientist. Your enthusiasm for science is infectious. Sharing the joy of scientific discovery with you has been a highlight of my graduate studies. You've taught me to approach science with curiosity, rigor, and generosity. Thanks to your mentorship, I leave the lab as both a better scientist, and a better person.

A special thanks to my past mentors, with whom it has been an honor to work and learn. To my undergraduate mentor, Andrei Popescu, thank you for taking a chance on me when I had no research experience and for sparking my interest in neuroscience. To my technician mentors, Chris Zimmerman and Zachary Knight, thank you for providing me with invaluable experience and guidance, and for encouraging me to pursue a career in research.

I thank my dissertation committee- Chinfei Chen, Susan Dymecki, and Chris Harvey, for their wisdom and support, as well as my Defense Exam Committee- Chinfei Chen, John Assad, Gord Fishell, and Fan Wang. Thank you for engaging with my work and for taking the time to share your expertise.

I thank all Ginty lab members past and present. You make the lab a place I look forward to coming to every day. The ability to brainstorm, exchange ideas, and trouble shoot experiments together is what makes the lab such an enriching environment. I have learned so much by observing how all of you tackle scientific questions, and I am privileged to have worked with so many talented people. Thank you to my postdoc mentors, Brendan Lehnert for taking me under your wing when I first joined the lab, and Josef Turecek for your technical and conceptual guidance on my project. A special thanks to my fellow graduate student "littermates," Lijun Qi

and Dawei Zhang, it's been a pleasure moving through graduate school together. Thanks to my bay mate and close friend, Karina Lezgiyeva, for indulging my need to chat and keeping us fed with baked goods.

I thank the Program in Neuroscience and the Neurobiology department for providing such a nurturing scientific and social environment. A special thank you to my PiN cohort for the support and the comradery. A special thanks to my classmates and close friends, Kelsey Clausing, Rachel Essner, Tess Whitwam, Herriet Hsieh, Maya Jay, Lucy Lai, Nghia Nguyen, and Adam Lowet. It's been so much fun to share this journey with all of you.

I am deeply grateful for my wonderful family. To my brother, Thomas, and my parents, Caryn and Wei, thank you for supporting my decision to pursue my studies in Boston, despite the distance from home. Your infinite love and support have taught me the importance of being kind and generous. I thank my amazing in-laws, Irina Gozman and Yevgeny Portman, for welcoming me into your family. Thank you to my grandparents, aunts, uncles and cousins. I am so fortunate to have grown up surrounded by so many loving family members.

Finally, to my husband, Frank Portman, thank you for uprooting your life and moving to Boston with me. Whether it's traveling around the world or hanging out at home, my life is so much brighter with you by my side. To our fluffy girl, Kona, thank you for bringing so much joy to our lives. If it wasn't so ridiculous to dedicate a dissertation to a dog, this one would be for you.

Chapter 1: Introduction

The sense of touch is central to how we interact with the world, indispensable for crucial functions such as object recognition, social interactions, and motor function. Innocuous touch is detected by low-threshold mechanoreceptors (LTMR) that innervate the skin. The ability to perceive and distinguish the multitude of tactile stimuli that animals encounter is enabled by the diversity of LTMR types and their differing activation properties. The central axons of fast conducting, heavily myelinated LTMRs ascend the dorsal column of the spinal cord, synapsing in the dorsal column nuclei (DCN) of the brainstem. The DCN serves as the entry point for innocuous touch information to the brain, receiving tactile information directly from primary sensory neurons, and indirectly from spinal cord projection neurons. Anatomical tracing studies have revealed multiple, non-overlapping downstream targets of the DCN, the most prominent being the thalamus and tectum (superior and inferior colliculus) (Berkley et al., 1980; Berkley et al., 1986; Lesicko et al., 2016). The majority of research into the neurobiological basis of innocuous touch has focused on the ascending pathway from primary sensory neurons to DCN to thalamus to somatosensory cortex (S1), neglecting pathways that target other brain structures. Since S1 is dispensable for at least some behavioral responses to light touch stimuli (Hong et al., 2018), complete appreciation of tactile perception will require investigation into additional ascending pathways, such as the pathway from the DCN to the colliculus of the midbrain. A deeper understanding of early somatosensory processing will lend insight into how to treat clinical cases where somatosensation is altered, such as neuropathic pain after peripheral injury or hypersensitivity to light touch exhibited by many individuals with autism. By comparing the ascending pathways from primary sensory neurons to distinct central brain regions—the

thalamus and the inferior colliculus—this work aims to elucidate how these pathways contribute to different aspects of tactile perception and reactivity.

Anatomy of somatosensory pathways

Innocuous touch is detected by primary sensory neurons called low-threshold mechanoreceptors (LTMRs), whose cell bodies reside in the dorsal root ganglion (DRG) or trigeminal ganglion. On a gross level, skin can be classified into two categories. Hairy skin covers the majority of the body. Non-hairy, or glabrous skin, covers areas that include the palms of the hand and soles of the feet. Both hairy and glabrous skin are innervated by a diverse range of LTMRs that differ in their associations with end organs in the skin, physiologic conduction properties, and genetic identity (**Figure 1.1)**. Furthermore, these LTMRs differ in their responses to static indentation, as well as dynamic stimuli such as vibration. Primary sensory neurons are designated as Aβ, Aδ, or C based on their conduction velocity. Aβ fibers have the fastest conduction velocities and C fibers have the slowest (Handler & Ginty, 2021). In hairy skin of rodents, LTMRs associate with hair follicles. The Aβ RA-LTMR, Aδ-LTMR and C-LTMR form longitudinal lanceolate endings around hair follicles, and respond to hair deflection (Li et al., 2011). The Aβ field-LTMR also surrounds hair follicles, but forms circumferential endings, and is sensitive to stroking of hairy skin (Bai et al., 2015). The Aβ SA1-LTMR associates with Merkel cells in touch domes around guard hair follicles, responding to indentation of the skin. In glabrous skin, physiological equivalents of a subset of hairy LTMRs can be found, however they associate with different terminal structures. The Aβ RA1-LTMR innervates Meissner corpuscles, which are sensitive to movement across the skin. The Aβ RA2-LTMR, tuned to vibration, innervates the Pacinian corpuscle in the deep dermis of large mammals, including humans. Similar to hairy skin, the glabrous Aβ SAI-LTMR also associates with Merkel cells and responds to indentation. In the mouse, genetic access to Aβ RAI-LTMRs,

Aβ SAI-LTMRs, Aδ-LTMRs, and Aβ field-LTMRs has enabled morphological and physiological characterization in both hairy and glabrous skin (Abraira & Ginty, 2013; Bai et al., 2015; Liu et al., 2012; Luo et al., 2009; Neubarth et al., 2020; Qi et al., 2024; Rutlin et al., 2014; Zimmerman et al., 2014).

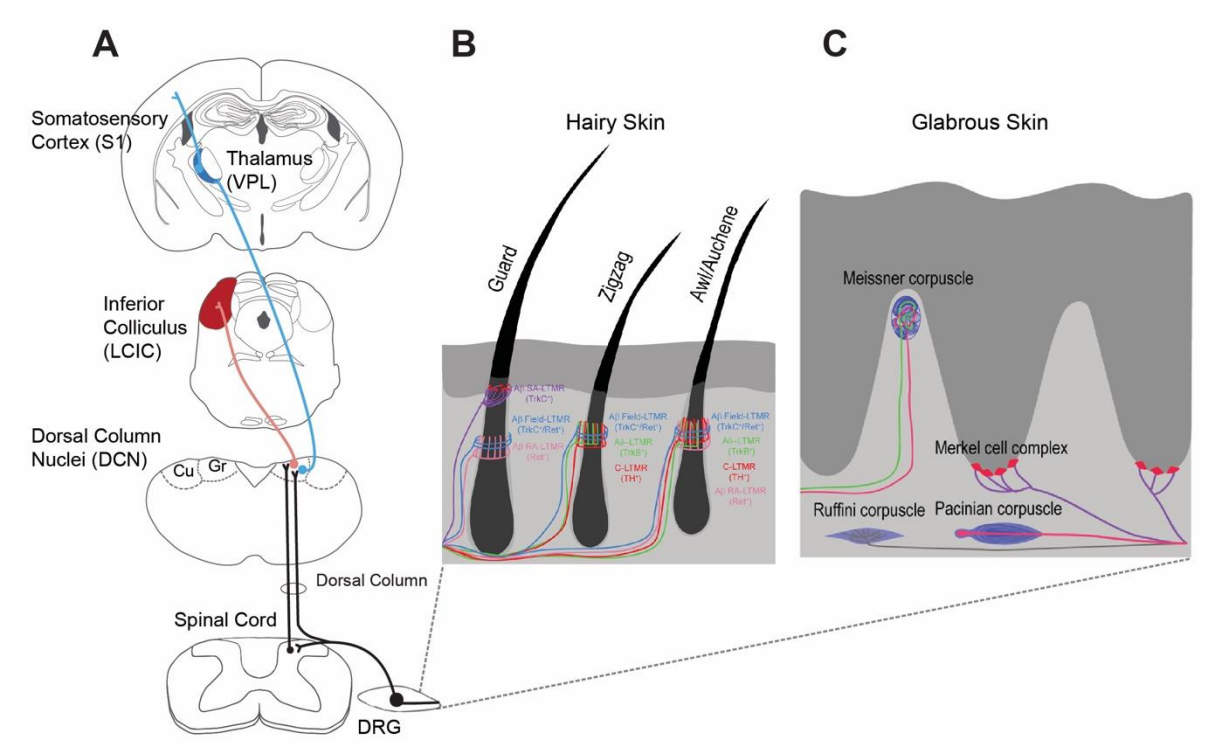


Figure 1.1 Anatomy of ascending light touch pathways

A) The cell bodies of primary sensory neurons that innervate hairy (**B**) and glabrous skin (**C**) reside in the dorsal root ganglion (DRG). The central axons of DRG neurons ascend the dorsal column directly and indirectly through spinal cord projection neurons. The dorsal column terminates in the dorsal column nuclei (DCN), which consists of the gracile nucleus (Gr), receiving inputs from the lower body, and the cuneate nucleus (Cu), receiving inputs from the upper body. The DCN sends non-overlapping projections to the lateral cortex of the inferior colliculus (LCIC) and the ventral posterolateral thalamus (VPL). The VPL then projects to primary somatosensory cortex (S1).

B and C adapted from Handler and Ginty, 2021

While Aβ SA and RA subtypes are named for their rapidly or slowly adapting response properties to static indentation stimuli, these LTMR subtypes also differ in their responses to dynamic stimuli such as vibration. Aβ LTMRs have the ability to entrain, or fire an action potential in response to each cycle of vibration applied to the skin, but differ in the sensitivity and frequencies of vibration that they entrain to. For example, the Aβ RA-LTMR in hairy skin and the Aβ RAI-LTMR that innervates the Meissner corpuscle have U-shaped force frequency tuning curves that are most sensitive at low frequencies (40-150 Hz) (Neubarth et al., 2020; Ribot-Ciscar et al., 1989; Talbot et al., 1968). The SA1-LTMR in hairy and glabrous skin can also entrain to low frequencies of vibration, but has a higher force threshold to entrainment than RA-LTMRs and has a flat rather than U-shaped force frequency tuning curve (Gottschaldt & Vahle-Hinz, 1981; Ribot-Ciscar et al., 1989). Unique amongst the LTMRs in its ability to encode high frequency vibrations is the Aβ RA2-LTMR that innervates the Pacinian corpuscle. The Aβ RA2-LTMR can entrain to stimuli up to 1000 Hz, and is most sensitive at frequencies between 300 and 500 Hz (**Figure 1.2**) (Bell et al., 1994; Salinas et al., 2000; Turecek & Ginty, 2024). The Aβ RAII-LTMR is also unique in its ability to encode environmental vibrations, or vibrations of the substrates that animals interact with (Hulliger et al., 1979; Turecek & Ginty, 2024). Despite progress in defining LTMR subtypes and their responses to ethologically relevant stimuli such as vibration, there is much less known about how the central nervous system organizes information from different modalities to form a cohesive representation of the tactile environment.

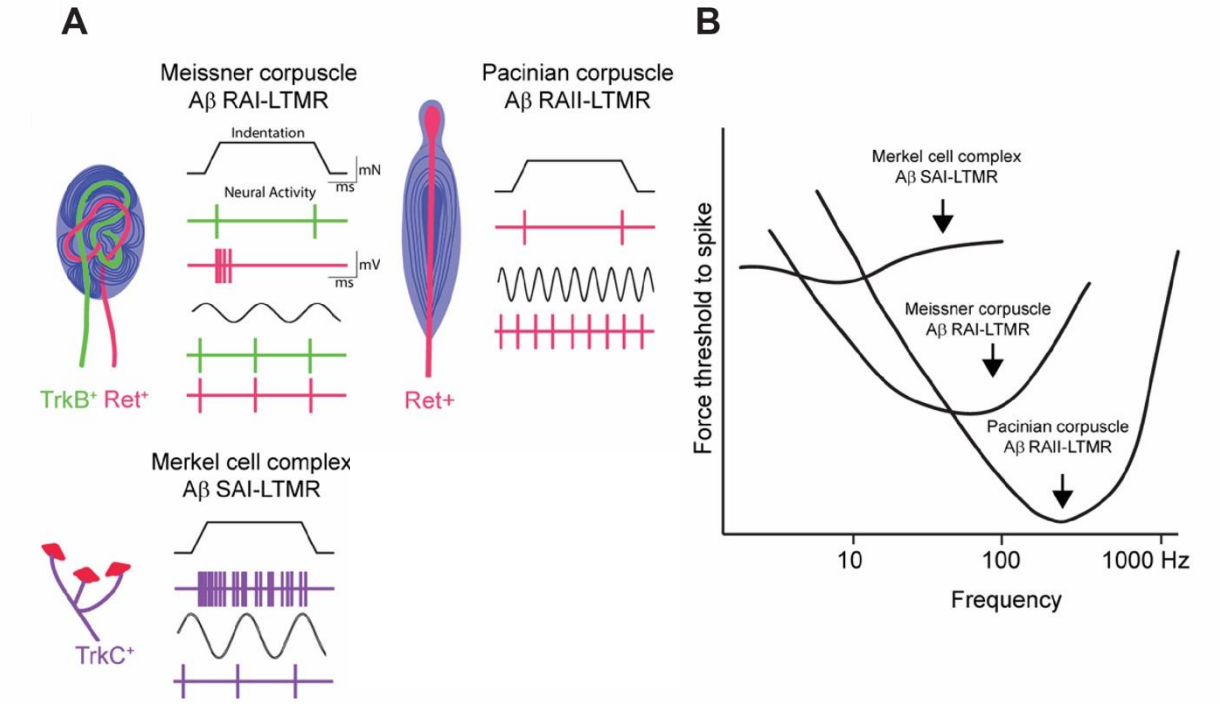


Figure 1.2 LTMR response profiles to static indentation and vibration

A) Each end organ is innervated by distinct LTMR subtypes with unique tuning properties. Two molecularly distinct Aβ LTMR subtypes innervate the Meissner corpuscle located at the apex of dermal papillae. The TrkB+ afferent exhibits the classic Aβ RA1-LTMR response property, with rapidly adapting ON/OFF response to indentation, while the Ret+ afferent is more slowly adapting in its ON response, rarely has an OFF response, and has a higher threshold for activation. Both subtypes are equally sensitive to vibration. In deep dermal tissue, Pacinian corpuscles are innervated by Aβ RA2-LTMRs, which are unique in their capacity to detect high-frequency vibrations. At the rete ridge along the stratum basale are the Aβ SA1-LTMRs that form an intimate, synapse-like association with the mechanically sensitive epidermal Merkel cells (shown in red).

B) Unlike the Aβ SA1-LTMR, the Aβ RA1- and RA2-LTMR sensory afferents associated with the Meissner and Pacinian corpuscle, respectively, have a frequency dependence in their force

Figure 1.2 (Continued)

sensitivity. The Meissner corpuscle is optimally sensitive to light forces in the range of 40–60 Hz. The Pacinian corpuscle is sensitive to force in the range of 100–300 Hz and insensitive to comparable forces delivered at lower frequencies.

Adapted from Handler and Ginty, 2021

The Aβ LTMR subtypes in the skin have two central targets. One branch innervates the deep dorsal horn of the spinal cord, while the other projects directly to the dorsal column nuclei (DCN) of the brainstem. The DCN also receives innocuous touch information from post-synaptic dorsal column (PSDC) neurons, a class of spinal projection neurons that receive and process tactile information from LTMRs. The Aβ-LTMRs project both directly to the DCN and to the spinal cord, while C-LTMRs and Aδ-LTMRs terminate exclusively in the spinal cord (Abraira & Ginty, 2013).

The DCN is comprised of three nuclei: the external cuneate, the cuneate nucleus, and the gracile nucleus. The cuneate nucleus and gracile nucleus process tactile information for the forebody and hindbody, respectively. The trigeminal nucleus plays an analogous role for cutaneous information of the head and face (Abraira & Ginty, 2013). The external cuneate primarily receives proprioceptive information for the upper body, thoracic level 6 and above. In contrast, proprioceptive input from the hindbody projects to Clarke's column of the spinal cord, which is then transmitted from the spinal cord to the brain. While proprioceptors from the hindbody do not synapse in the gracile, there is evidence that proprioceptors from the forebody may project to the cuneate nucleus in addition to the external cuneate (Niu et al., 2013).

Tactile information from the DCN diverges to multiple downstream targets. In the classic dorsal column medial-lemniscal (DCML) pathway that conveys touch information to the cortex, second-order neurons in the DCN send information to the ventral posterolateral nucleus of the thalamus (VPL), where third-order neurons project this information to the primary somatosensory cortex (S1) (**Figure 1.1**). However, anatomical tracing studies conducted in cats, rodents, and primates also describe projections to additional subcortical regions such as the tectum (superior colliculus and inferior colliculus) and cerebellum (Berkley et al., 1980; Berkley et al., 1986; Bjorkeland & Boivie, 1984; Cheek et al., 1975). While the cuneate and gracile nuclei are thought to perform functionally equivalent roles for the hindbody and forebody, they do exhibit some differences in their inputs and outputs. For instance, there is a more substantial cuneate projection to the cerebellum compared to the gracile (Cheek et al., 1975; Quy et al., 2011). This discrepancy could reflect differences in proprioceptive processing between the forebody and hindbody, or a functional specialization of the forepaw. In comparison to the DCML pathway, much less is known about DCN projections to the tectum and cerebellum

While previous anatomical studies indicate a set of DCN projection targets that are conserved between different species, they do not address whether projection neuron populations are non-overlapping or collateralize to target multiple projection targets. To elucidate the anatomy of DCN projections, previous work in the lab utilized viral tracing techniques. To confirm the downstream targets of the DCN in mouse, an AAV encoding synaptophysin-tdTomato was injected into the DCN to label presynaptic terminals of DCN neurons in different target regions of the brain. In line with prior literature, the major targets of the DCN were the VPL, the inferior colliculus, superior

colliculus and cerebellum (Berkley et al., 1980; Berkley et al., 1986; Bjorkeland & Boivie, 1984; Cheek et al., 1975; Niu et al., 2013; Quy et al., 2011). The projection to the VPL was the most robust, while the cerebellar projection was the least prominent. To address the question of overlap between projection neuron populations, distinct fluorophores were injected into the inferior colliculus and the VPL and fluorophore expression was quantified in the DCN. Overlap between projection neurons and inhibitory neuron marker, Gad2, was also assayed by conducing these experiments in *Gad2*$^{2A\text{-}mCherry}$ mice (**Figure 1.3**) (Lehnert et al., 2021). These experiments demonstrate that DCN projection neurons innervating the inferior colliculus and thalamus are likely to be excitatory, and they are largely non-overlapping. These results raise the possibility that diverging tactile processing pathways may have specializations at the level of the DCN PN populations.

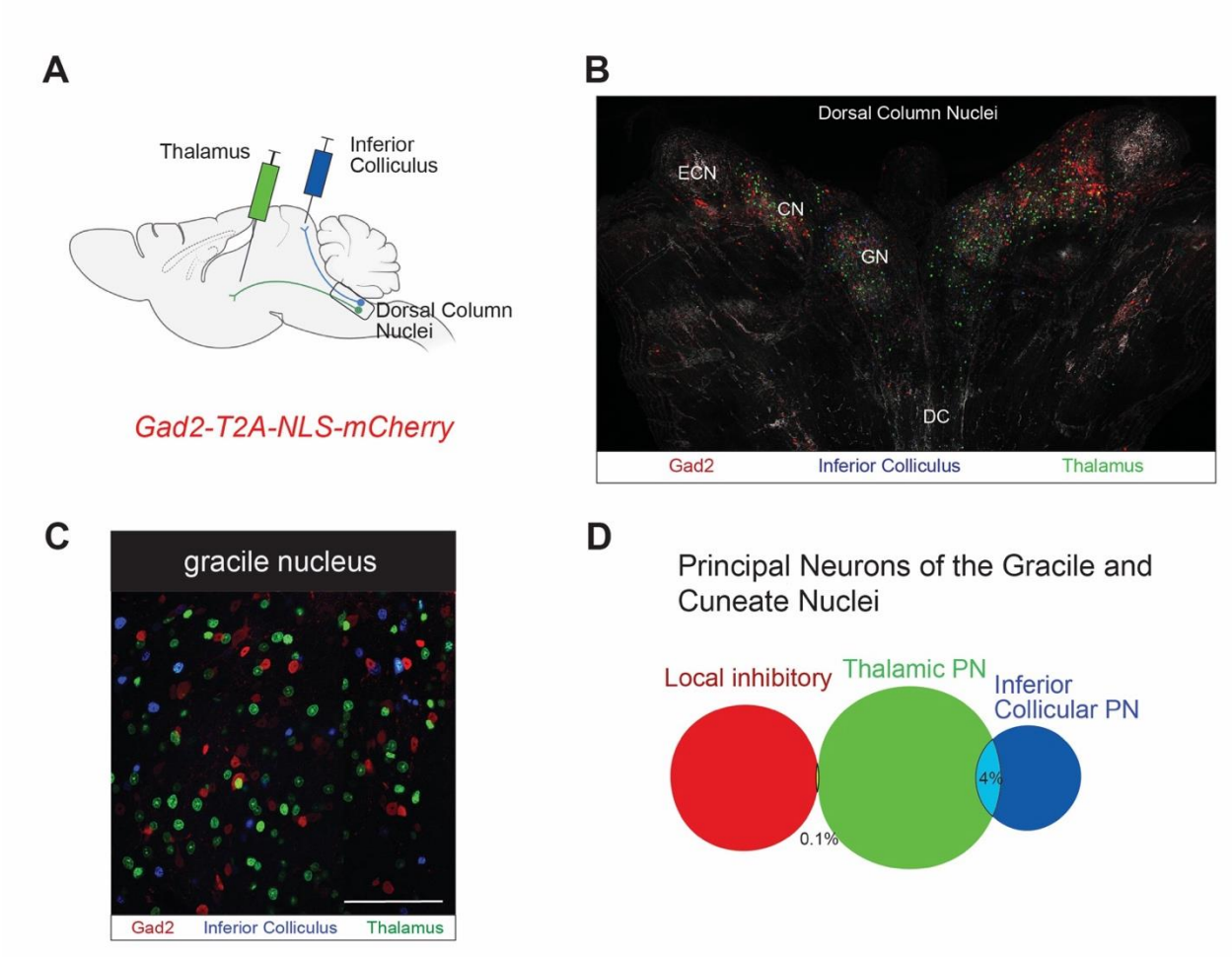


Figure 1.3 Principal neurons of the gracile and cuneate nuclei

A) Strategy for visualizing cell bodies of neurons that project to the ventroposterolateral thalamus and shell of the inferior colliculus. An AAV2-retro-hSyn-H2B-GFP virus was injected into the thalamus and an AAV2-retro-hSyn-H2B-mTagBFP2 virus was injected into the inferior colliculus in Gad2-T2A-nls-mCherry mice.

B) Horizontal section of the brainstem at the level of the dorsal column nuclei, which comprises the external cuneate nucleus (ECN), the cuneate nucleus (CN), and the gracile nucleus (GN). Thalamic projection neuron, inferior collicular projection neuron, and Gad2+ cell bodies are found throughout the CN and GN but excluded from the ECN.

Figure 1.3 (Continued)

C) Higher magnification view of the GN of (B), showing that these three populations of neurons are largely non-overlapping (100 μm scale bar).

D) Quantification of the degree of overlap compiled from two mice.

Adapted from Lehnert et al., 2021

Somatosensory Processing in the DCN

The DCN sits in the medulla of the brainstem and receives tactile information from LTMRs and PSDCs of the spinal cord. Past studies conducting electrophysiological recordings in the DCN have assayed DCN neuron responses to different tactile submodalities, such as hair deflection, pressure, and vibration. Some studies in the cat support a labeled line model of modality transmission where neurons in the DCN represent a single modality, while others report modality integration at the level of the brainstem. Some reports in the cat describe that cutaneous submodalities are restricted to spatially segregated regions in the cuneate and the gracile (Dykes, 1982; Dykes et al., 1982). In contrast, another study in the cat found neurons responsive to multiple tactile modalities. This study reports that while many units recorded from were responsive to a single modality (hair deflection, light pressure, subcutaneous pressure, vibration), a subset of units were responsive to both hair deflection and light pressure (Winter, 1965). These results suggest that the DCN could be a site of early modality integration. However, past studies did not attribute responses properties to identified cell types within the DCN, such as inhibitory neuros or projection neurons.

Recent work has revisited the encoding properties of the DCN in a cell type specific way. The ability to utilize mouse genetic tools to identify inhibitory neurons, and viral or electrophysiologic tools to identify projection neurons has improved our understanding of how the DCN parses tactile information between different ascending pathways, such as the pathways that target the thalamus and inferior colliculus. Our lab has recorded from inhibitory and projection neurons in the DCN using both calcium imaging and electrophysiological techniques (Lehnert et al., 2021; Turecek et al., 2022).

In one such study, we used two-photon calcium imaging neurons in the gracile nucleus to determine whether the somatotopic map in the DCN disproportionately represents glabrous skin compared to hairy skin (Lehnert et al., 2021). We retrogradely labeled DCN projection neurons (PN) by viral injections of an AAV encoding calcium indicator, jGCaMP7s, into the thalamus or the inferior colliculus. We recorded from inhibitory neurons in the gracile by injecting an AAV encoding a cre-dependent GCaMP into the gracile of VGat-Cre animals. By recording from gracile neurons while brushing the animal, we observed thalamic and inferior collicular PNs that respond to brush of the glabrous hindpaw, hairy hindpaw, thigh, or trunk. Both thalamic and inferior collicular PNs exhibited disproportionate representation of glabrous skin, with approximately three times as many inferior collicular and thalamic projection neurons responding to stroke of the glabrous hindpaw compared to the hairy hind paw. In contrast, inhibitory neurons had equal numbers of glabrous and hairy hindpaw responsive neurons, demonstrating no such glabrous emphasis (**Figure 1.4**). These findings reveal that glabrous emphasis emerges at the level of the DCN, highlighting the DCN as a crucial locus for tactile processing.

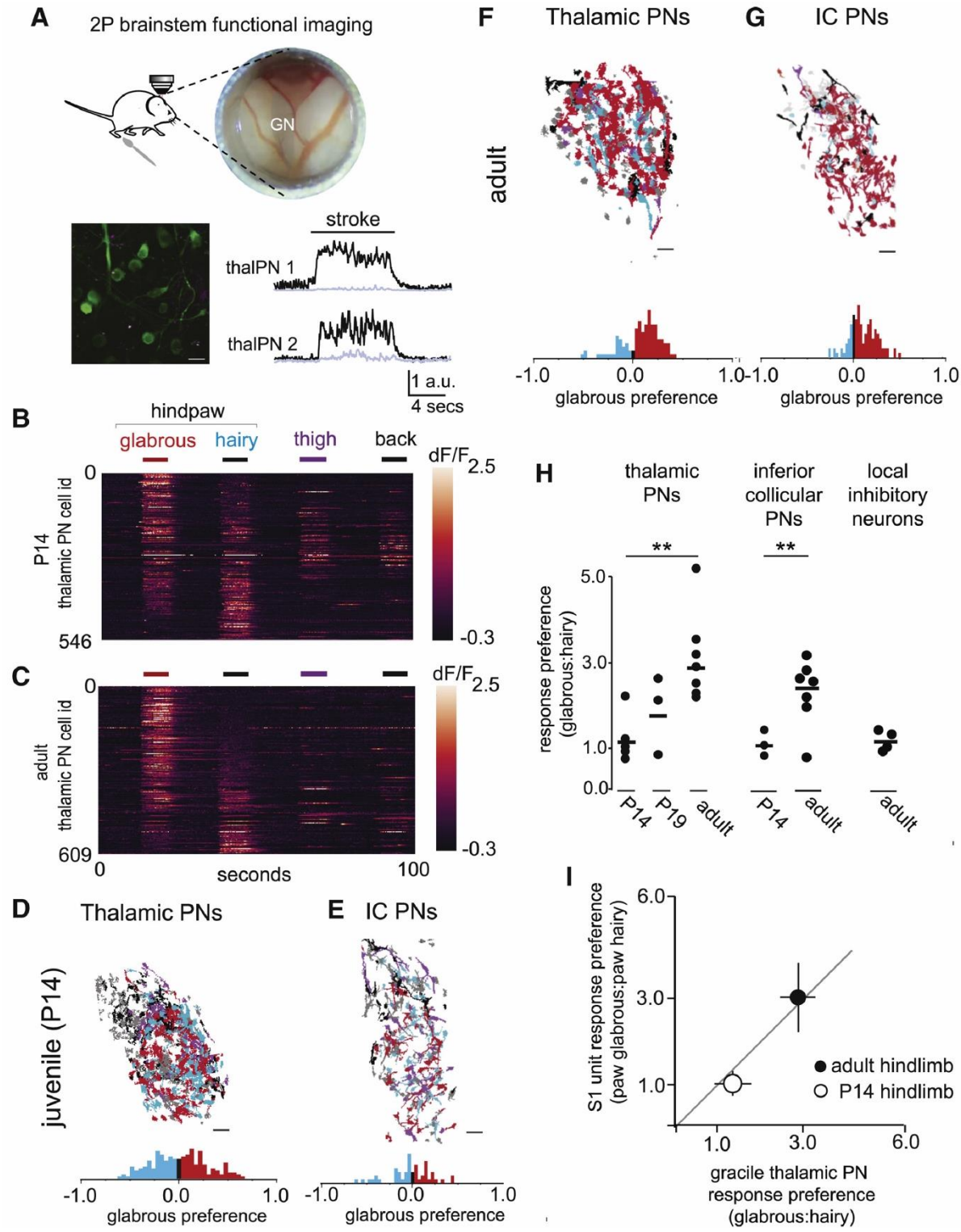

A
2P brainstem functional imaging
GN
stroke
thalPN 1
thalPN 2
1 a.u.
4 secs
B
hindpaw
glabrous
hairy
thigh
back
dF/F
2.5
-0.3
P14 thalamic PN cell id
0
546
C
adult thalamic PN cell id
609
0
seconds
100
D
Thalamic PNs
juvenile (P14)
-1.0
0.0
1.0
glabrous preference
E
IC PNs
F
Thalamic PNs
adult
G
IC PNs
H
thalamic PNs
inferior collicular PNs
local inhibitory neurons
**
response preference (glabrous:hairy)
5.0
3.0
1.0
0.0
P14
P19
adult
I
S1 unit response preference (paw glabrous:paw hairy)
6.0
3.0
1.0
adult hindlimb
P14 hindlimb
gracile thalamic PN response preference (glabrous:hairy)

Figure 1.4 Disproportionate representation of glabrous skin emerges in the brainstem over postnatal development

A) (Top) A preparation allowing in vivo multiphoton imaging of the gracile nucleus (GN) of the brainstem. (bottom) A representative, motion-corrected image of thalamic PNs expressing jGCaMP7, and corresponding raw fluorescence time series extracted from regions of interest (ROIs) centered on two example neurons (black, 100 μm scale bar) and surrounding neuropil fluorescence (gray) during skin stroke.

B) Touch-evoked responses of thalamic projection neurons functionally imaged in the GN. Calcium signals were evoked by stroking equivalent skin areas of the hindpaw glabrous skin (red), hindpaw hairy skin (blue), thigh (purple), and back (black) in P14 mice. Data displayed are pooled across n = 3 mice.

C) Representative response to touch of the body in adult mice, similar to **(B)**.

D) Representative map of the body within thalamic projection neurons of the GN (100 μm scale bar for images shown in D–G). A glabrous skin preference index, (glabrous − hairy)/(glabrous + hairy), was computed for all neurons responding to hindpaw skin stimulation in this and other experiments (bottom). At P14, there are roughly equal proportions of glabrous preferring and hairy preferring cells.

E) Representative map of the body within inferior collicular projection neurons in the GN, similar to **(D).**

F and G) Representative maps of the body in adulthood for thalamic projecting neurons **(F)** and inferior collicular projecting neurons **(G)**.

Figure 1.4 (Continued)

H) The proportion of thalamic or inferior collicular projecting neurons in the GN that preferentially respond to hindpaw glabrous skin touch expands over developmental time ($p < 0.01$, Mann-Whitney U test).

I) The relationship between glabrous preference in the GN of the brainstem and glabrous preference in hindpaw S1 at two developmental time points.

Adapted from Lehnert et al., 2021

Another study conducted in the lab utilized juxtacellular recordings in the DCN to characterize inhibitory interneurons and PNs (Turecek et al., 2022). Thalamic and collicular PNs were identified by electrically stimulating either the thalamus or inferior colliculus while recording juxtacellulary from a cell body in the DCN, thus identifying DCN PNs by antidromic stimulation. Thalamic and collicular PNs differed in their spatial receptive fields and responses to vibratory stimuli. Most thalamic PNs exhibited restrictive receptive fields with inhibitory surrounds, and could entrain well to low frequency vibratory stimuli, but did not respond well to high frequency stimuli. In contrast, many collicular PNs exhibited expansive receptive fields that encompassed the entirety of the hindpaw. Strikingly, most collicular PNs could entrain to vibratory frequencies between 10 and 500 Hz, firing robustly to high frequency stimuli that thalamic PNs did not respond to (**Figure 1.5**). These results identify the DCN as an important node of tactile integration and raise the intriguing possibility that the collicular and thalamic pathways differentially represent vibratory stimuli.

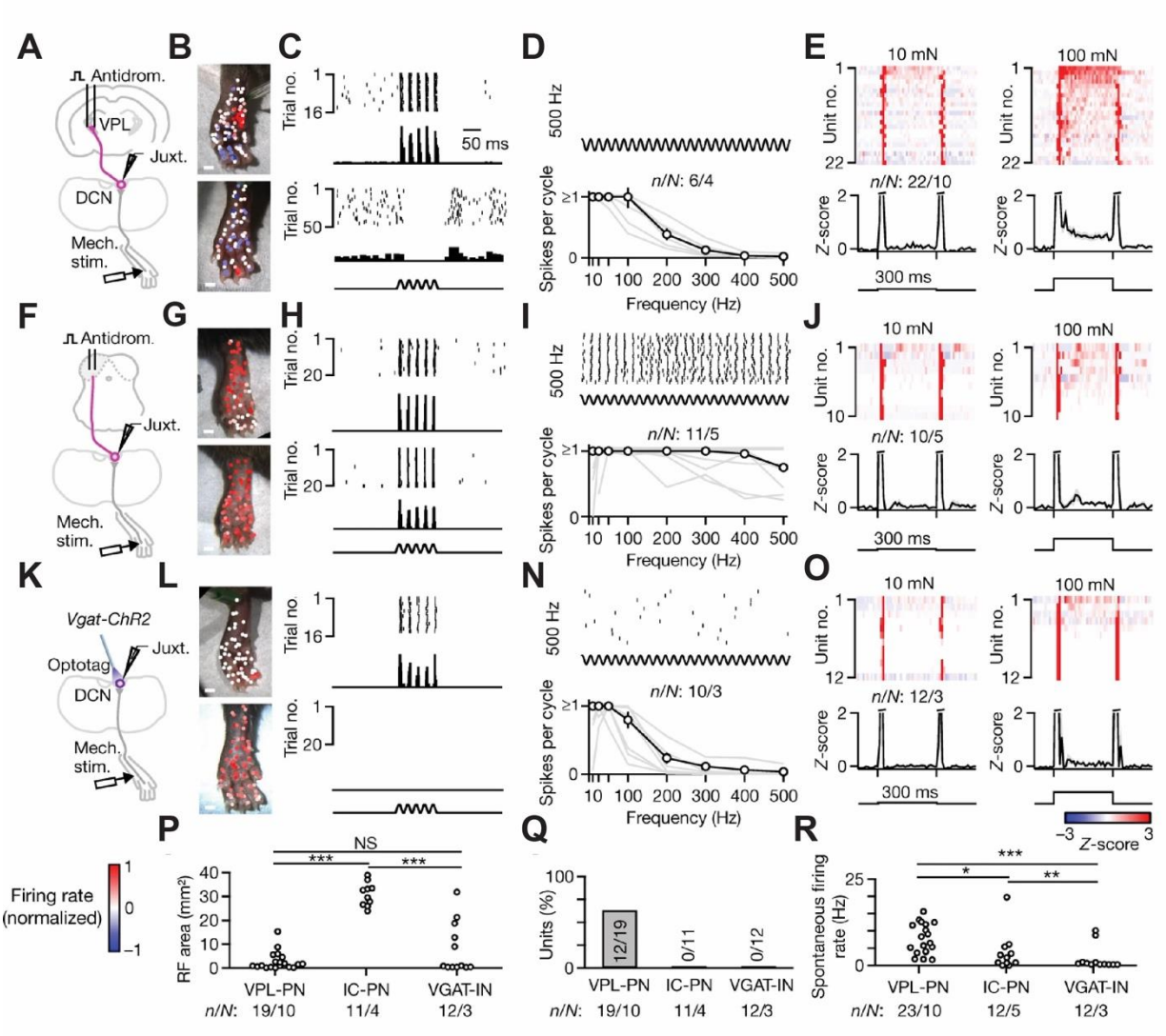


Figure 1.5 Tactile features are directed to distinct targets in the somatosensory hierarchy

A) Schematic of the experiment. Units in the DCN were recorded juxtacellularly (Juxt.) in urethane-anaesthetized mice. Stimulus electrodes were inserted into the VPL, and thalamic PNs (VPL-PNs) were identified through antidromic activation (Antidrom.) and collision testing. Response properties of units were then measured using a mechanical stimulator (Mech. stim.) with a 1 mm probe tip.

B) Receptive fields of two different VPL-PNs. Each point is a single trial colour-coded by the normalized firing rate of the unit in response to 100 ms 50 Hz vibration (10–20 mN).

Figure 1.5 (Continued)

C) Example trials from B with a raster and a histogram for two locations of the receptive field for the same unit: excitatory receptive field (top; 1 ms bins) and inhibitory surround (bottom; 10 ms bins).

D) Top, Example raster of VPL-PN responses to 500 Hz vibration in the excitatory receptive field. Bottom, Vibration tuning of all VPL-PNs with the mean across units ± s.e.m. (black) and individual units (grey).

E) Average responses (Z-scored firing rate) to step indentation in VPL-PN units (top) and mean ± s.e.m. of VPL-PN units (bottom) for 10 mN (left) and 100 mN (right). Mice received 300 ms indentations delivered to the centre of excitatory receptive fields (10 ms bins).

F-J) Same as A-E, but for units identified as projecting to the IC.

K-O) Same as A–E, but for optotagged local inhibitory interneurons (VGAT-INs).

P) Excitatory receptive field (RF) size area for all identified units. Kolmogorov–Smirnov (K-S) test: VPL-PN versus IC-PN, $P < 0.001$; IC-PN versus VGAT-IN, $P < 0.001$; VPL-PN versus VGAT-IN, $P = 0.4$. NS, not significant.

Q) Percentage of DCN cell types with detected inhibitory surrounds.

R) Spontaneous firing rate of all units for each cell type. K–S test: VPL-PN versus IC-PN, $P = 0.012$; IC-PN versus VGAT-IN, $P = 0.008$; VPL-PN versus VGAT-IN, $P < 0.001$. Number of experiments are units/animals (n/N). Scale bars, 1 mm (B,G,L).

Adapted from Turecek et al., 2022

Tactile Processing in DCN Target Regions

Thalamus

The VPL of the thalamus is a primary projection target of the DCN. Tactile information in the VPL is conveyed to S1 of cortex, comprising the canonical dorsal column medial lemniscal pathway. Electrophysiological recordings in the VPL suggest a modularity, with three sub-regions that vary in response characteristics. In the rat, the rostral VPL carries both proprioceptive information, and cutaneous information with large receptive fields. Middle regions of the VPL are reported to have smaller receptive fields, and receive the majority of ascending projections from the DCN (Francis et al., 2008). In both rodents and primates, the forepaw and hindpaw exhibit disproportionately large regions of the nucleus in comparison with their surface area of the body. In addition, neurons representing the paws have smaller receptive fields than other regions of the body (Angel & Clarke, 1975; Emmers, 1965; Francis et al., 2008). Regional heterogeneity observed in the rat appears to be similar to the primate, although subdivisions are less distinct in the rat.

Previous studies in rodents, cats, and primates indicate segregation of submodality representation in the VPL (Francis et al., 2008; Mountcastle & Henneman, 1952). In the primate, neurons responsive to deep pressure are represented in the anterior and posterior ends of the VPL, in anatomically distinct regions from cutaneous representation (Kaas et al., 1984; Loe et al., 1977). Furthermore, response properties to indentation could generally be classified as slowly adapting or rapidly adapting, suggesting a degree of modality segregation in cutaneous inputs within the VPL. In primate VPL, a separate portion of the nucleus contains the majority of Pacinian-like inputs, where VPL neurons were able to entrain to high frequency vibrations (Zhang et al., 2001). Similar to primates, the cat VPL contains neurons with both slowly and rapidly adapting response

profiles. Additionally, some neurons in the cat VPL respond to Pacinian-like inputs, characterized by their ability to entrain to high-frequency vibratory stimuli (Herron and Dykes 1986). Recent work in the rodent suggests that unlike the cat and primate, vibration in the VPL is represented by a rate code rather than by neurons that entrain to vibratory stimuli (Lee et al., 2023; Lee et al., 2024). These results suggest a degree of modality segregation in the VPL, but rely primarily on mechanical or electrical stimuli. Revisiting electrophysiological recordings in the VPL while employing genetic tools that enable activation or loss of function of LTMR subtypes could further our understanding of tactile processing in the VPL.

Inferior Colliculus

The inferior colliculus is primarily an auditory nucleus that processes nearly all ascending and descending auditory information. The inferior colliculus is also thought to play a role in multisensory integration, based on anatomical and physiological studies that have demonstrated the presence of visual and somatosensory representations in the inferior colliculus (Aitkin et al., 1978; Aitkin et al., 1981; Gruters & Groh, 2012; Jain & Shore, 2006; Lesicko et al., 2016; Syka et al., 2000; Tawil et al., 1983). While the role of non-auditory information in the inferior colliculus is poorly understood, there are many ways in which it could be highly adaptive. Multisensory integration could increase the precision of stimulus localization by allowing for the alignment of auditory stimuli with visual or somatosensory cues. Alternatively, somatosensory information could contribute to the cancellation of self-generated sounds to enhance the perception of externally generated sounds (Gruters & Groh, 2012; Wu et al., 2015). Uncovering the role of auditory-somatosensory integration in the inferior colliculus will require an understanding of the source of somatosensory inputs, and the nature of the tactile information they encode.

The inferior colliculus can be divided into multiple subregions including the central nucleus (CNIC) and the lateral cortex of the inferior colliculus (LCIC) (Aitkin et al., 1975; Duque et al., 2012; Lesicko et al., 2016; Pickles, 2015). While the CNIC primarily processes auditory stimuli, the LCIC is a potential region for multisensory processing. Anatomical studies show that the LCIC receives top-down somatosensory input from somatosensory cortex, as well as bottom-up input from the DCN and spinal trigeminal nucleus (Berkley et al., 1980; Berkley et al., 1986; Lesicko et al., 2016). With respect to auditory response properties, the CNIC is tonotopically organized, where neurons that respond to similar sound frequencies are located near one another. Furthermore, CNIC neurons are tuned to narrow ranges of auditory frequency (Duque et al., 2012; Oliver & Morest, 1984). In contrast, the LCIC is not tonotopically organized, and neurons tend to be broadly tuned to a wider range of auditory frequencies (Pickles, 2015). Compared to CNIC neurons, LCIC neurons exhibit stronger stimulus-specific adaptation (SSA), exhibiting a reduction in neural response to repeated sounds (Cohen & Castro-Alamancos, 2007; Malmierca et al., 2009). This property indicates that LCIC neurons are better tuned to new stimuli, suggesting a role for the LCIC in novelty detection. Additionally, one study in the mouse found that the LCIC mediates sound induced escape behavior. Silencing the LCIC impaired an animal's innate flight response to loud, aversive sounds (Xiong et al., 2015). Together, these results suggest that the LCIC may play a role in identifying salient or threatening stimuli in the environment and triggering the appropriate behavioral response.

Compared to auditory coding in the LCIC, there is much less known about somatosensory response properties. The few studies that have addressed somatosensory representation in the inferior

colliculus report that touch responsive neurons represent the contralateral side of the body and have expansive receptive fields (Aitkin et al., 1978; Aitkin et al., 1981). Studies using extracellular recordings in anesthetized cats found representation of the entire body in the LCIC that were mostly low threshold, responding to gentle stimuli such as air-puff or light touch with a feather, while being unresponsive to deep pressure. One study investigated somatosensory and auditory integration in the LCIC through simultaneous application of a tone and electrical stimulations of the dorsal column. Of the units responsive to both auditory and somatosensory input, most were excited by auditory tones and inhibited by dorsal column activation and a smaller proportion were excited by both dorsal column stimulation and auditory stimuli (Aitkin et al., 1978). However, electrical stimulation of the dorsal column is not physiological, and multisensory integration could differ under more natural stimulation paradigms. Previous work in cats has begun to address somatosensory coding in the inferior colliculus, and how tactile and auditory representation may interact (Aitkin et al., 1978; Aitkin et al., 1981; Wu et al., 2015). However, not much is known about the electrophysiologic response properties of LCIC neurons in other model organisms such as the primate and rodent. Furthermore, how the LCIC encodes dynamic somatosensory stimuli such as vibration, remains an open question. Exploring how these somatosensory inputs converge with auditory information will provide further insight into the function of the LCIC.

Parallel tactile processing pathways

The divergence of tactile information between the midbrain and forebrain is reminiscent of parallel processing streams in the visual system. Retinal ganglion cells (RGCs) of the retina transmit visual information to a diverse range of central targets. There are many different types of RGCs. Each type receives distinct combinations of visual input and sends projections to different subsets of

brain regions (Dhande et al., 2015; Martersteck et al., 2017). In particular, RGCs project via anatomically distinct pathways to the superior colliculus and the dorsolateral geniculate nucleus (dLGN) of the thalamus, reminiscent of the collicular and the thalamic divergence observed in the somatosensory system. In mammals, the superior colliculus receives more input from RGCs that can be categorized as feature detectors for motion, contrast, or orientation. In contrast, visual input to the dLGN originates from RGCs with simpler receptive field types, such as center surround. These target nuclei also seem to have distinct roles in visual processing, as lesions in different regions have different effects. In cats, superior colliculus lesions mainly impact orienting, while V1 lesions affect visual processing (Zhaoping, 2016). A recent study conducted in the mouse suggests that visual information from the collicular pathway occupies a dedicated region in the visual cortex. Information from this pathway codes for discriminating moving stimuli better than the LGN to V1 pathway (Beltramo & Scanziani, 2019). These findings indicate that visual streams to the superior colliculus and visual thalamus have different functional roles, and that these functional specializations may be enabled by differential input from dedicated subsets of RGCs. We believe that a similar framework may be involved in the processing of light touch information, where the DCN plays an analogous role to the retina, and feature selection at the level of DCN PNs enables different functional capability between distinct ascending pathways to the somatosensory thalamus and tectum. This hypothesis is supported by our lab's recent work demonstrating that DCN PNs that target the inferior colliculus are better able to encode high frequency vibrations (Turecek et al., 2022) compared to thalamic PNs.

The presence of parallel processing pathways also raises interesting questions regarding how detection and perception of sensory stimuli occurs. Recent work conducted in the barrel cortex of

mice challenges previous notions of the role of primary somatosensory cortex in sensory detection tasks. A study conducted by the Bruno lab discovered that ablation of the barrel region of S1 only transiently prevented animals from performing a whisker detection task (Hong et al., 2018). For these experiments, mice were trained to initiate a trial through a lever press, then report whisker stimulation by licking a spout. Transient optogenetic silencing impaired task performance, but task performance recovered within days of cortical ablation. Surprisingly, cortical ablation also failed to prevent animals from learning the task. These results indicate that somatosensory cortex may not be necessary for active detection or perception of simple tactile stimuli. Similar work conducted in the whisker system of rats demonstrates that animals lacking trigeminal input to either the superior colliculus or to the thalamus are both capable of detection, and only simultaneous loss of both pathways impairs stimulus detection (Cohen & Castro-Alamancos, 2007). While these experiments indicate that either pathway can be used for active detection, further work is necessary to understand the differences in tactile processing between the respective pathways. Collectively, these findings suggest that a fundamental understanding of somatosensory processing will require investigation beyond the dorsal column/medial leminscal projection pathway to the thalamus, and should include collicular pathway. Furthermore, a focus on subcortical regions will be necessary to elucidate the mechanisms underlying sensory detection and perception. In this dissertation, I compare the ascending pathways that target the inferior colliculus and the thalamus, with a focus on vibration tuning. By combining mouse genetic tools to target specific LTMRs and electrophysical recordings, I identify a novel role of the LCIC in detecting and responding to environmental vibrations encoded by Pacinian corpuscles.

Chapter 2. The auditory midbrain mediates tactile vibration sensing

Erica L. Huey, Josef Turecek, Michelle M. Delisle, Ofer Mazor, Gabriel E. Romero, Malvika Dua, Zoe K. Sarafis, Alexis Hobble, Kevin T. Booth, Lisa V. Goodrich, David P. Corey, and David D. Ginty

The original version of this work has been posted on preprint server bioRxiv,

doi: https://doi.org/10.1101/2024.03.08.584077

Vibration sensing is ubiquitous across the animal kingdom, enabling organisms to interpret their dynamic surroundings, communicate, detect predators and prey, and navigate their environment (Cividini et al., 2019; Narins et al., 1992; Nevo et al., 1991; O'Connell-Rodwell, 2007; Virant-Doberlet et al., 2023; Young & Morain, 2002). In mammals, vibrations that propagate through the air in the form of sound waves are transduced into electrical signals in the cochlea and encoded by the auditory system (Pickles, 2015). Analogously, mechanical vibrations acting on the body are detected by fast conducting low-threshold mechanoreceptors (Aβ LTMRs) of the body and encoded by the somatosensory system (Handler & Ginty, 2021; Johnson, 2001). In many animals, including humans, the vibration frequency detection range of the auditory system (20 Hz-20 kHz) partially overlaps with that of the somatosensory system (1-1000 Hz) (Handler & Ginty, 2021; Heffner & Heffner, 2007; Heffner et al., 2001; Yau et al., 2009). In some smaller

mammals, such as mice, the encoding of vibration frequency in the somatosensory system (1-1000 Hz) and auditory system (~1 khz-100 kHz) is largely non-overlapping (Heffner & Heffner, 2007; Heffner et al., 2001; Lee et al., 2023; Neubarth et al., 2020; Prsa et al., 2019; Turecek & Ginty, 2023). The prevailing view is that vibration encoding in the ascending somatosensory and auditory pathways is anatomically and functionally distinct.

Our understanding of LTMRs and their role in detecting mechanical vibrations mainly arises from experiments in which vibratory stimuli are presented directly to the body; however, the somatosensory system can also detect subtle, low amplitude environmental vibrations. In a noteworthy example, elephants can communicate over miles, sensing vocalizations and movements of conspecifics by detecting vibrations of the ground using mechanoreceptors in their feet and trunks (Bouley et al., 2007; O'Connell-Rodwell, 2007). Among the LTMRs, Pacinian corpuscle Aβ rapidly adapting type-2 (RA2)-LTMRs are unique in their capacity to encode high frequency vibrations (Handler & Ginty, 2021). In humans and primates, Pacinians are located in the deep dermis of glabrous skin and also associated with joints and connective tissue (Germann et al., 2021; Kumamoto et al., 1993). In rodents, Pacinians are enriched in the periosteum of wrist and ankle bones, rendering them responsive to vibrations transmitted through the skeleton (Handler & Ginty, 2021; Prsa et al., 2019; Silfvenius, 1970; Turecek & Ginty, 2024; Zelena, 1978). Recordings from Pacinian afferents in awake, behaving mice have recently revealed their exquisite sensitivity to self-movements and substrate vibrations under naturalistic conditions (Turecek & Ginty, 2024). Indeed, Pacinian corpuscle Aβ RA2-LTMRs can fire robustly in response to low-amplitude environmental vibrations, including those initiated by gentle

movements on a surface located meters from where an animal stands (Harvey et al., 2013; Hulliger et al., 1979; Luna et al., 2005; Salinas et al., 2000; Turecek & Ginty, 2024).

The canonical view is that the neural impulses originating in the periphery and encoding mechanical vibrations acting of the body are conveyed via the brainstem dorsal column nuclei (DCN) to the ventroposterolateral thalamus (VPL) *en route* to primary somatosensory cortex (S1) (Abraira & Ginty, 2013; Johnson, 2001). However, our recent work suggests that mechanical vibration sensitive DCN neurons project to the inferior colliculus, a midbrain region involved in auditory information processing (Pickles, 2015; Turecek et al., 2022). The inferior colliculus (IC) is comprised of multiple subregions: the central nucleus of the inferior colliculus (CNIC), which receives auditory input in a tonotopic manner, and the lateral cortex of the inferior colliculus (LCIC), which receives inputs from multiple sensory modalities, including somatosensory inputs from the DCN **(Figure 2.1, Figure 2.2A)** (Aitkin et al., 1978; Aitkin et al., 1981; Aitkin et al., 1975; Berkley et al., 1986; Bjorkeland & Boivie, 1984; Jain & Shore, 2006; Lehnert et al., 2021; Lesicko et al., 2016; Oliver & Morest, 1984; Pickles, 2015; Syka et al., 2000; Turecek et al., 2022; Zhou & Shore, 2006). Here, we use electrophysiological recordings, genetic manipulations, and behavioral analyses to show that most LCIC neurons of the auditory midbrain encode both high frequency mechanical vibrations captured by Pacinian corpuscle LTMRs and auditory vibrations captured by the cochlea to mediate behavioral responses to environmental vibrations.

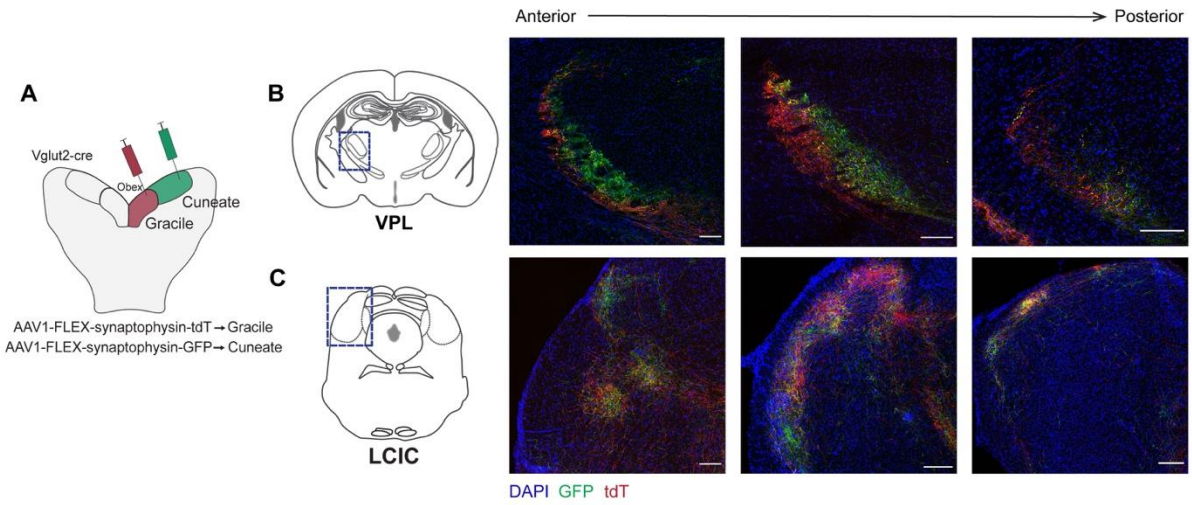


Figure 2.1. Anterograde tracing from the dorsal column nuclei.

A) To identify downstream projections from the dorsal column nuclei (DCN), an AAV encoding Cre-dependent synaptophysin-tdT was injected into the gracile nucleus and an AAV encoding Cre-dependent synaptophysin-GFP was injected into the cuneate nucleus of Vglut2-Cre mice. **B-C)** TdT and GFP positive terminals were observed throughout the ventroposterolateral thalamus (VPL) and lateral cortex of the inferior colliculus (LCIC). Scale bar = 150 μm.

Results

LCIC and VPL neurons are differentially tuned to mechanical vibrations

Distinct populations of DCN neurons send axonal projections to either the VPL of the thalamus or the LCIC of the inferior colliculus (Lehnert et al., 2021). DCN axonal terminals from the gracile nucleus (representing the hindbody) and the cuneate nucleus (representing the forebody) segregate to different regions of the VPL but innervate overlapping regions within the LCIC (**Figure 2.1**). To compare how mechanical vibrations acting on the body are represented in the LCIC and VPL, we performed *in vivo* multi-electrode array (MEA) recordings in these brain regions in urethane anesthetized animals (**Figure 2.3A,E**). We first brushed the animal to identify neurons containing limb receptive fields. Sinusoidal mechanical vibrations of different frequencies and amplitudes were then delivered to the limbs using a mechanical stimulator. While the LCIC and VPL both contain forelimb- and hindlimb-responsive neurons (**Figure 2.2B-C**, **Figure 2.3**), we focused primarily on hindlimb responsive neurons. Vibrations were delivered to the most responsive region, or "hotspot," of a neuron's receptive field. In the VPL, vibratory receptive fields tended to be focal areas such as an individual pad or digit (**Figure 2.2E**). In contrast, receptive fields of LCIC neurons lacked a focal hotspot and were spatially extensive (**Figure 2.2F**). In these cases, the mechanical stimulator was positioned on the heel of the hindlimb. Vibratory stimuli were then delivered at frequencies between 10-900 Hz and forces between 2-50 mN. The majority of VPL neurons responded robustly to low frequency vibrations (<200 Hz), but only transiently to high frequency vibrations (>200 Hz; **Figure 2.2B, Figure 2.3C-D**). While their pre-synaptic DCN inputs are able to entrain (phase-lock firing to each cycle of the stimulus) to vibratory frequencies up to 100 Hz (Turecek et al., 2022), no VPL neurons could entrain to vibratory frequencies up to 100 Hz, although some neurons could entrain up to

50 Hz. Strikingly, LCIC neurons showed an inverse response pattern compared to VPL neurons, with most neurons responding transiently to low frequency vibrations (<200 Hz) but firing robustly to high frequency stimuli (200-900 Hz; **Figure 2.2C, Figure 2.3G-H, Figure 2.8I,M**). While many DCN projection neurons targeting the LCIC entrained to vibratory frequencies from 10-500 Hz (Turecek et al., 2022), LCIC neurons only transiently responded to low frequency stimuli (**Figure 2.2C, Figure 2.3G-H**), suggesting a synaptic filtering mechanism between the DCN and LCIC that preferentially favors high frequency vibratory stimuli. Furthermore, although LCIC neurons responded robustly to high frequency vibrations, they exhibited little or no entrainment **(Figure 2.2C, Figure 2.3G-H)**.

While high frequency vibratory responses were abundant throughout the LCIC, the sparsity of high frequency responses detected in the VPL was surprising and could be attributed to missing a potential "high frequency hotspot" region in the VPL in our recordings. Therefore, considering that the VPL is an elongated structure extending along the anterior-posterior axis of the brain, we next used a four shanked MEA to perform a detailed mapping of somatotopy across the VPL to search for high frequency vibratory responses. We recorded from a minimum of 9 penetrations per animal using the four-shanked probe, enabling sampling across at least 36 regions of the VPL, distributed across the medio-lateral and anterior-posterior axes. The resulting somatotopic map of the VPL aligned well with those previously reported, with receptive fields moving from forelimb to hindlimb to trunk, when moving from medial to lateral within the VPL (**Figure 2.4A, C-D**) (Francis et al., 2008; Horne & Tracey, 1979; Kaas et al., 1984; Mountcastle & Henneman, 1952). A larger proportion of VPL neurons responded to brush of the hindpaw compared to the thigh or the trunk **(Figure 2.4F).** This emphasis on hindpaw representation was less pronounced

in LCIC neurons, which often exhibited expansive receptive fields spanning multiple body regions (**Figure 2.4B, G**). For VPL neurons with brush responses to hindbody regions, high frequency vibration of the hindlimb activated ~9 percent of neurons, and these high frequency responsive neurons were sparsely distributed throughout the VPL, not concentrated in a particular subregion (**Figure 2.2D, Figure 2.4E**). In contrast, >75 percent of brush responsive LCIC neurons responded robustly to high frequency vibrations, indicating that high frequency vibratory information is particularly salient in the LCIC **(Figure 2.2D)**.

To assess the relationship between mechanical force thresholds and vibration frequency in the VPL and LCIC, we next obtained force-frequency tuning curves for vibration sensitive VPL and LCIC neurons by determining force thresholds for individual neurons across a range of vibratory frequencies. The force threshold for a given frequency was defined as the minimum force required to elicit 20 percent of a neuron's maximum firing rate. The tuning curves for VPL and LCIC neurons were approximately U-shaped, although the most sensitive regions of their respective tuning curves were non-overlapping: VPL neurons had the lowest force thresholds to vibrations between 50-200 Hz and LCIC neurons had the lowest force thresholds to vibrations between 300-500 Hz (**Figure 2.5A-E**). Thus, most LCIC neurons are activated by high frequency vibratory stimuli and exhibit expansive receptive fields, while most VPL neurons are preferentially activated by low frequency stimuli in a spatially restricted manner.

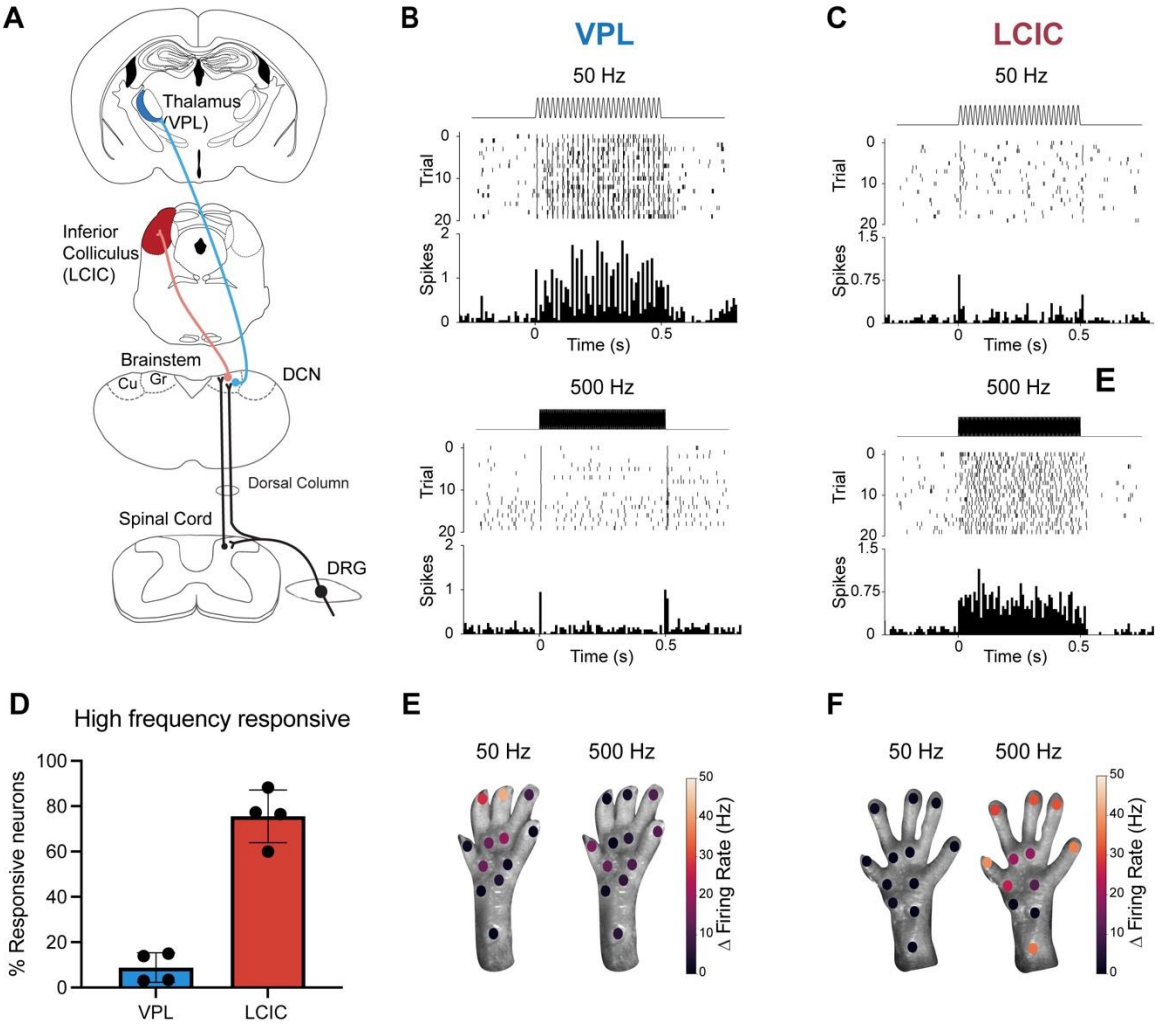


Figure 2.2. LCIC and VPL neurons are differentially tuned to mechanical vibratory stimuli.

A) The brainstem dorsal column nuclei (DCN) receive inputs from dorsal root ganglia (DRG) primary sensory neurons and spinal cord projection neurons. Non-overlapping subsets of DCN projection neurons target the ventroposterolateral thalamus (VPL; blue) and the external nucleus of the inferior colliculus (LCIC; red).

Figure 2.2 (Continued)

B and C) Representative VPL (B) and LCIC (C) neuron spike raster and histogram in response to 50 Hz and 500 Hz vibratory stimuli delivered at a 10 mN force to the hindlimb. Top: spike raster; bottom: average histogram in 10 ms bins.

E) Percentage of neurons (mean ± SD) with hindbody brush receptive fields (tested by brushing the hindpaw, thigh, and trunk) that respond to 500 Hz stimulation of the limb at a 10 mN force in the VPL (n= 182 neurons from 4 animals) and LCIC (n= 76 neurons from 4 animals). Each data point corresponds to measurements in one animal. See also Figure 2.4.

E and F) Example VPL (E) and LCIC (F) neuron receptive field organization for 50 Hz and 500 Hz stimulation to multiple regions across the hindlimb delivered at a 10 mN intensity. Stimulus locations are superimposed on images of the hindpaw.

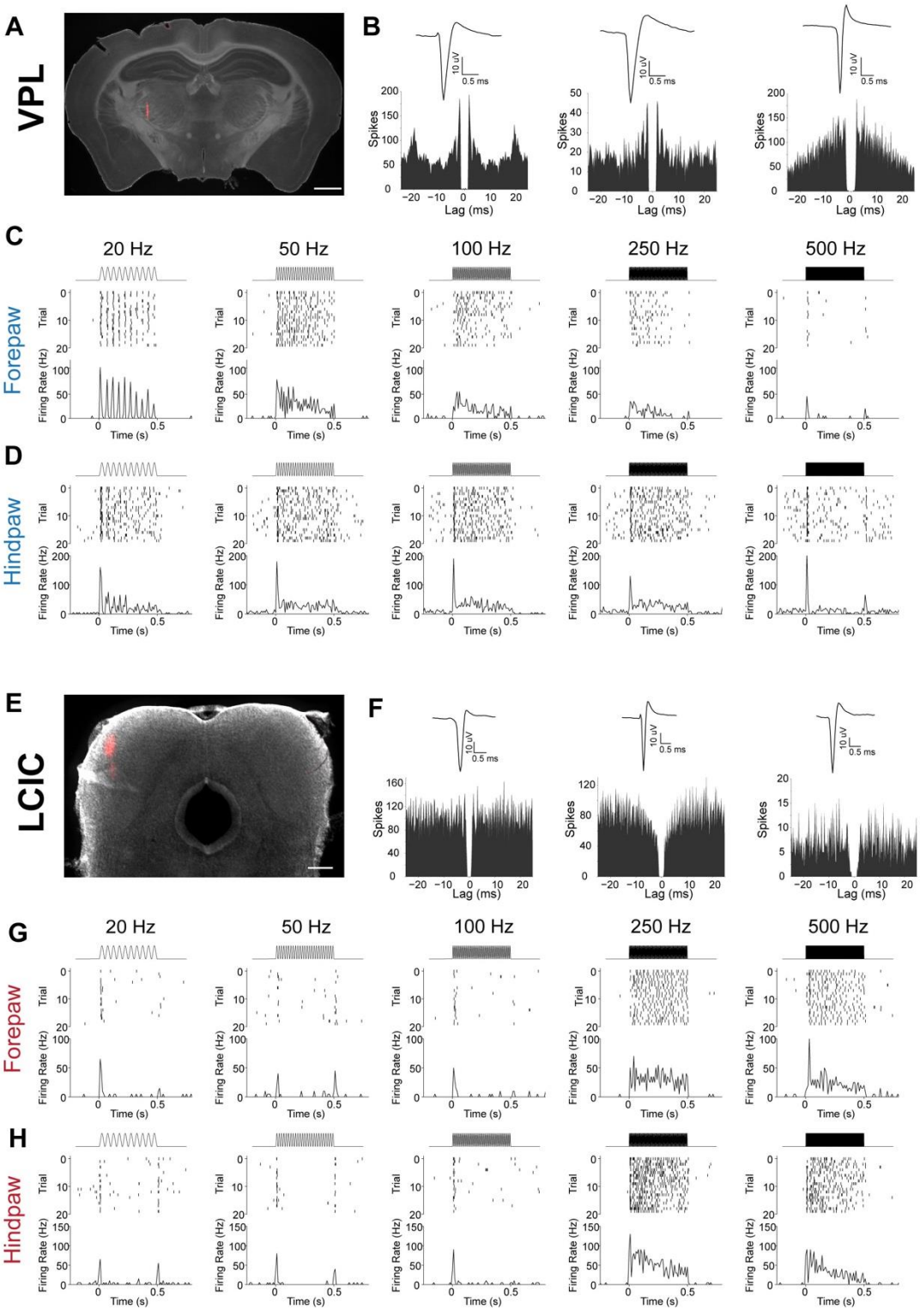

A
VPL
B
10 uV
0.5 ms
Spikes
Lag (ms)
C
20 Hz
50 Hz
100 Hz
250 Hz
500 Hz
Forepaw
Trial
Firing Rate (Hz)
Time (s)
D
Hindpaw
E
LCIC
F
G
Forepaw
H
Hindpaw

Figure 2.3. MEA recordings in the VPL and LCIC to characterize vibratory responses.

A) Representative probe tract from MEA recording in the VPL. Scale bar = 1000 μm.

B) Average waveforms and corresponding autocorrelogram for three example VPL neurons.

C) Example VPL neuron raster and PSTHs in response to vibration of different frequencies delivered at a 10 mN force to the forelimb. Top: spike raster; bottom: PSTHs, which are baseline subtracted and in 10 ms bins.

D) Same as C for a hindlimb responsive neuron.

E) Representative probe tract from MEA recording in the LCIC. Scale bar = 500 μm.

F) Average waveforms and corresponding autocorrelogram for three example LCIC neurons.

G) Same as C for an example LCIC neuron.

H) Same as D for an example LCIC neuron.

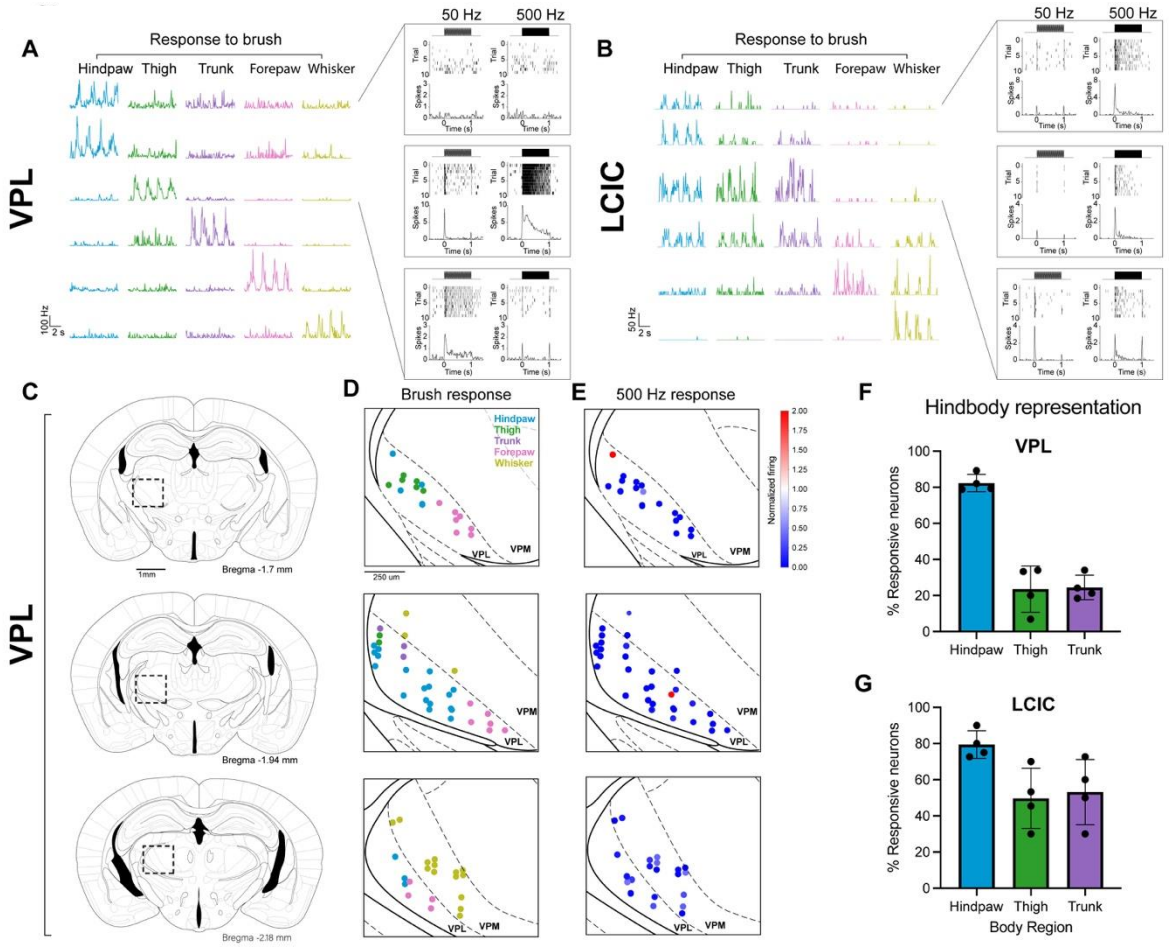


Figure 2.4. Somatotopic and vibratory mapping in the VPL and LCIC.

A) Representative VPL neurons responding to brush of different regions of the body. Each row corresponds to one neuron. Each body region is stroked four times per trial. Right: Example raster plot and PSTHs aligned to hindlimb vibration at 50 Hz and 500 Hz at 10 mN, corresponding to adjacent brush responsive neurons. PSTHs are baseline subtracted and in 10ms bins.

B) As in A, representative LCIC neurons. Note that, unlike VPL neurons, most LCIC neurons respond to brush across multiple body locations.

Figure 2.4 (Continued)

C-E) Example mapping of the VPL in one animal, shown at different coronal planes on the anterior-posterior axis. The approximate atlas location (C) for recorded neurons is shown for the corresponding somatotopic map of the VPL (D), where each neuron is colored for the body region most responsive to brush. The same neurons shown in D are colored by their responsiveness to 500 Hz mechanical vibration, which is normalized to the neuron's response to brush (E). Note that most brush responsive VPL neurons do not respond to the 500 Hz vibration stimulus during the sustained period of the stimulation.

F and G) Percentage of neurons (mean ± SD) with hindbody receptive fields that respond to brush of the hindpaw, thigh, and trunk in the VPL (F) (n= 182 neurons from 4 animals) and LCIC (G) (n= 76 neurons from 4 animals). Each data point corresponds to a single animal.

LCIC vibration responses are mediated by Pacinian corpuscle Aβ RA2-LTMRs

The distinct frequency tuning curves and receptive field properties of VPL and LCIC neurons prompted us to ask whether these brain regions receive inputs from different primary mechanosensory neuron types. Rapidly adapting Aβ LTMRs exhibit distinct force-frequency tuning relationships and receptive fields. Most rapidly adapting LTMRs are optimally sensitive to low frequency vibratory stimuli (40-150 Hz) and exhibit relatively small receptive fields (Handler & Ginty, 2021; Handler et al., 2023; Johnson, 2001; Neubarth et al., 2020; Qi et al., 2024; Saal & Bensmaia, 2014). This includes Meissner corpuscle Aβ RA1-LTMRs, enriched in glabrous skin of pedal pads and digits, hair follicle Aβ RA-LTMRs associated with body hairs, and Krause corpuscle Aβ RA-LTMRs of the genitalia (Handler et al., 2023; Neubarth et al., 2020; Qi et al., 2024; Santiago et al., 2023). In contrast, Pacinian corpuscle Aβ RA2-LTMRs, which in mice are enriched in the periosteum of ankle and wrist bones, are most sensitive to high frequency vibratory stimuli (50-1000 Hz) and have extremely large receptive fields (Alvarez-Buylla & Ramirez de Arellano, 1953; Bell et al., 1994; Bolanowski & Zwislocki, 1984; Hunt & Mc, 1960; Mountcastle et al., 1967; Silfvenius, 1970; Talbot et al., 1968; Turecek & Ginty, 2023). To directly compare the tuning of Meissner corpuscle Aβ RA1-LTMRs and Pacinian corpuscle Aβ RA2-LTMRs to VPL and LCIC neurons, we performed *in vivo* extracellular recordings of DRG neurons and measured force-frequency tuning curves of Meissner and Pacinian afferents **(Figure 2.5F-H)**. As predicted, the force-frequency tuning curves of Pacinian corpuscle Aβ RA2-LTMRs resembled those of LCIC neurons, while the tuning curves of Meissner corpuscle Aβ RA1-LTMRs more closely resembled VPL neurons **(Figure 2.5F-H)**. These findings led us to hypothesize that Pacinian afferents have an outsized role in shaping the

response properties of most LCIC neurons, while Meissner corpuscle afferents and other Aβ RA-LTMRs of the body preferentially contribute to the response properties of most VPL neurons.

To directly test the relationship between primary sensory neuron activity and vibration tuning in the LCIC and VPL, we utilized mouse genetic tools to assess the contributions of Pacinian corpuscles and Meissner corpuscles to LCIC and VPL responses. Ret signaling in somatosensory neurons is necessary for formation of Pacinian corpuscles, and thus $Avil^{Cre}; Ret^{floxGFP/floxGFP}$ (Ret cKO) mice, which lack *Ret* in DRG neurons, lack Pacinian corpuscles (**Figure 2.6B, Figure 2.7F**) (Luo et al., 2009; Luo et al., 2007). Conversely, TrkB signaling is necessary for formation of Meissner corpuscles, and thus $Avil^{Cre}; TrkB^{flox/flox}$ (TrkB cKO) mice lack Meissner corpuscles **(Figure 2.6A)** (Emanuel et al., 2021; Neubarth et al., 2020). Importantly, Ret cKO mice have a normal density of Meissner corpuscles and TrkB cKO mice have a normal density of Pacinian corpuscles **(Figure 2.7)**.

Surprisingly, VPL neurons recorded in TrkB cKO and Ret cKO mice showed no notable shifts in their vibration tuning curves **(Figure 2.6C, F)**. While VPL neurons of TrkB cKO and Ret cKO mice exhibited a decrease in the magnitude of the offset response at certain vibration frequencies, the onset and sustained phases of the response revealed no significant differences **(Figure 2.8A-H)**. Meissner corpuscle and Pacinian corpuscle afferents are not the only primary sensory neurons responsive to vibrations, and indeed Aβ RA-LTMRs associated with hair follicles and other end organs and Aβ SA1-LTMRs found in both hairy and glabrous skin also entrain to vibratory stimuli (Gottschaldt & Vahle-Hinz, 1981; Handler & Ginty, 2021; Ribot-Ciscar et al., 1989; Talbot et al., 1968). Therefore, it is likely that VPL neurons are sensitive to mechanical

vibrations via inputs from both Meissner and Pacinian corpuscle LTMRs or other vibration sensitive LTMRs (Chirila et al., 2022; Emanuel et al., 2021). In stark contrast, vibration responsiveness of LCIC neurons was nearly absent in animals lacking Pacinian corpuscles, although LCIC responses were normal in mice lacking Meissner corpuscles (**Figure 2.6D, E, G, Figure 2.8I-P)**. Taken together, these findings indicate that high frequency mechanical vibrations acting on the body and detected by Pacinian corpuscle Aβ RA2-LTMRs are prominently encoded in the LCIC.

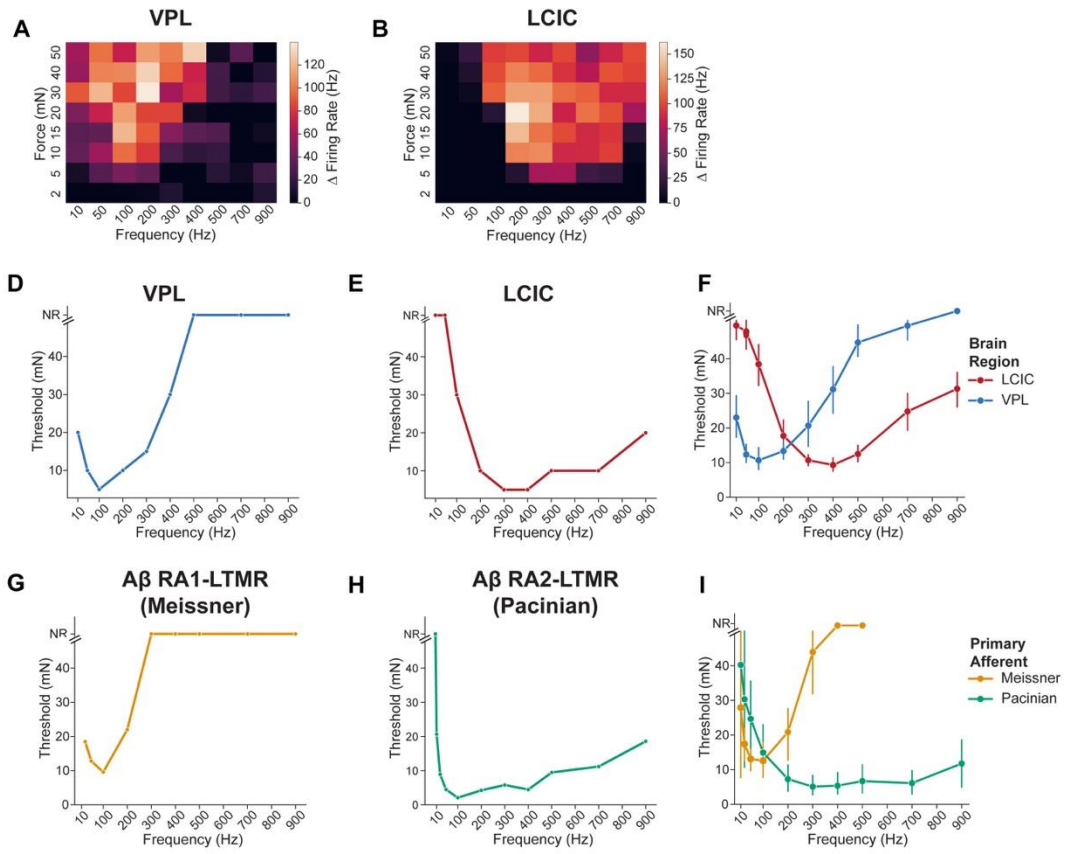


Figure 2.5. LCIC and VPL neurons exhibit distinct force-frequency tuning curves.

A and B) Representative VPL **(A)** and LCIC **(B)** neuron responses to vibrational frequencies delivered at different forces to the hindlimb. Heatmap intensity corresponds to the neuron's average change in firing to the sustained portion of vibratory stimuli (200 ms window beginning 50 ms after stimulus onset).

C and D) Force-frequency threshold curves obtained from heatmaps in A and B, where the force threshold for a vibrational frequency is defined as the minimum force required to elicit 20% of the neuron's maximum firing during the sustained portion of the stimulus. Frequencies in which the highest force tested (50 mN) failed to reach threshold are designated NR (non-responsive).

Figure 2.5 (Continued)

E) Average threshold curves (mean ± 95% confidence interval) for neurons responsive to hindlimb vibration recorded in the VPL (n=15 neurons from 6 animals) and LCIC (n=22 neurons from 6 animals).

F and G) Force-frequency threshold curves for representative Meissner corpuscle innervating Aβ RA1-LTMR afferent (F) and Pacinian corpuscle innervating Aβ RA2-LTMR afferent (G). Threshold is defined as the minimum force necessary for the neuron to reach 50% vibratory entrainment. Frequencies in which the highest force tested (50 mN) failed to reach threshold are designated NR (non-responsive).

H) Average threshold curves (mean ± 95% confidence interval) for hindlimb Meissner A□ RA1-LTMRs (n=4 neurons from 4 animals) and Pacinian A□ RA2-LMTRs (n=6 neurons from 5 animals).

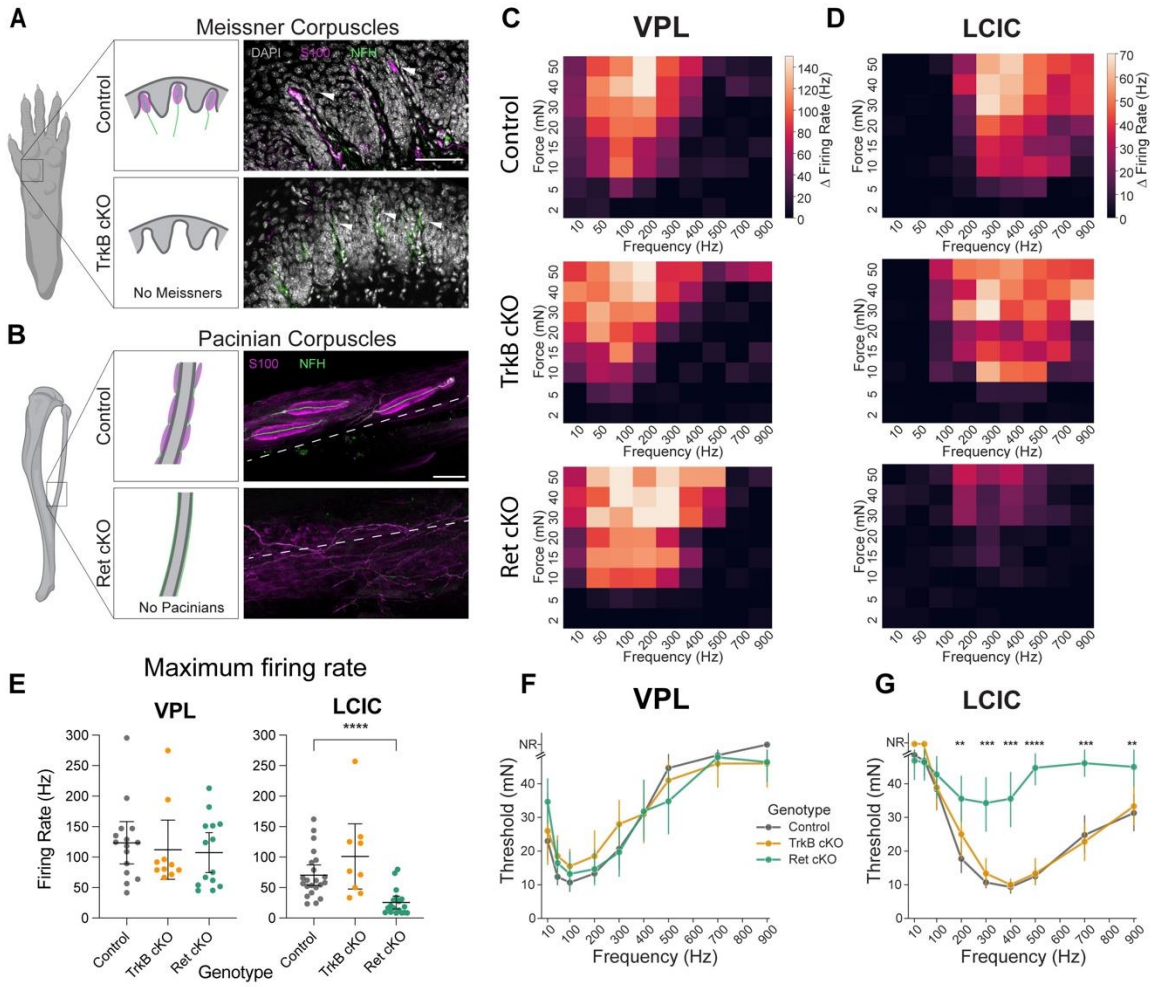


Figure 2.6. LCIC vibration responses are mediated by Pacinian corpuscle Aβ RA2-LTMRs.

A) Meissner corpuscles, located in the plantar pad and digit glabrous skin, are absent in *Avil*^{Cre}*; TrkB*$^{flox/flox}$ (TrkB cKO) mice, which lack TrkB in DRG sensory neurons. Images of skin histology from a TrkB cKO and littermate control, stained for anti-NFH (labels myelinated axons, green) and anti-S100 (labels glial cells, magenta). Scale bar = 50 µm. See also Figure 2.7 for quantification.

B) Pacinian corpuscles, located in the periosteum of the fibula, are absent in *Avil*^{Cre}*; Ret*$^{flox/flox}$ (Ret cKO) mice, which lack Ret in DRG sensory neurons. Images of whole mount histology of

Figure 2.6 (Continued)

the limb of a Ret cKO animal and littermate control, stained for anti-NFH and anti-S100 to visualize Pacinian corpuscles. White dashed line indicates position of the fibula. Scale bar = 100 μm. See also Figure 2.7 for quantification.

C and D) Force-frequency heat maps for representative VPL **(C)** and LCIC **(D)** neurons in control, TrkB cKO and Ret cKO animals. Heatmap intensity corresponds to the neuron's average change in firing to the sustained portion of vibratory stimuli.

E) Maximum firing rate for VPL and LCIC (mean ± 95% confidence interval) neurons to vibratory stimuli in control, TrkB cKO and Ret cKO mice. Firing rates of LCIC neurons in Ret cKO and control mice were significantly different (****$p<0.0001$ Mann-Whitney U test). Firing rates of VPL neurons in TrkB cKO, Ret cKO, and controls were not significantly different. Firing rates of LCIC neurons in TrkB cKO and controls were not significantly different (Mann-Whitney U test).

F) Average threshold curves of VPL neurons (mean ± 95% confidence interval) recorded in control (n=15 neurons from 6 animals), TrkB cKO (n=10 neurons from 3 animals), and Ret cKO (n=14 neurons from 4 animals) mice. Thresholds between Ret cKO, TrkB cKO and controls were not significantly different (Mann-Whitney U Test with Bonferroni correction for multiple comparisons).

G) Average threshold curves of LCIC neurons (mean ± 95% confidence interval) recorded in control (n=22 neurons from 6 animals), TrkB cKO (n=9 neurons from 4 animals), and Ret cKO (n=18 neurons from 4 animals) mice. (*$p<0.05$, **$p<0.01$, ***$p<0.001$, ****$p<0.0001$, Mann-Whitney U test with Bonferroni correction for multiple comparisons). While thresholds between

Figure 2.6 (Continued)

Ret cKO and controls were significantly different, thresholds between TrkB cKO and controls were not (Mann-Whitney U Test with Bonferroni correction for multiple comparisons).

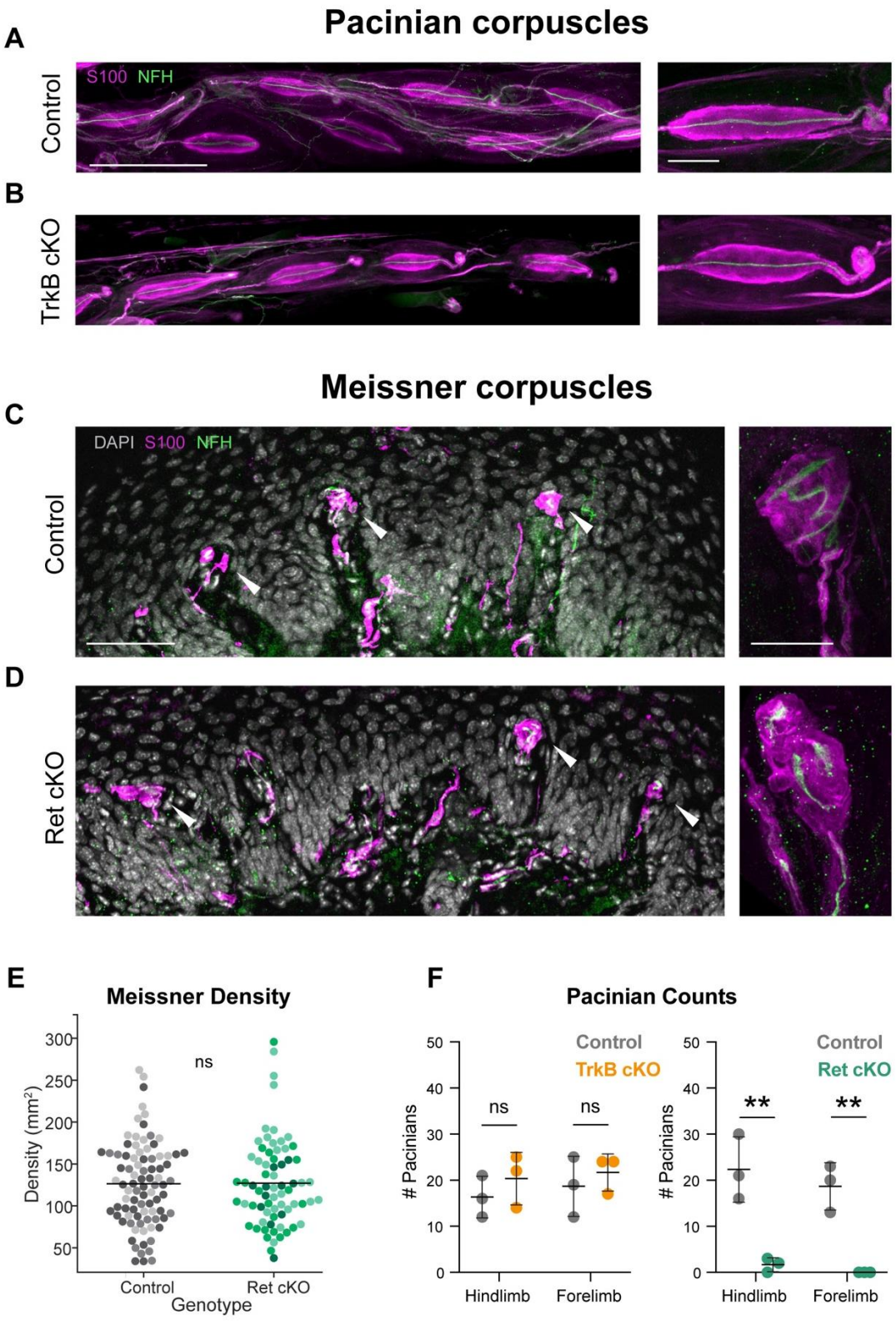

Pacinian corpuscles
A
Control
S100 NFH
B
TrkB cKO
Meissner corpuscles
C
Control
DAPI S100 NFH
D
Ret cKO
E
Meissner Density
Density (mm²)
300
250
200
150
100
50
ns
Control
Ret cKO
Genotype
F
Pacinian Counts
Pacinians
50
40
30
20
10
0
Control
TrkB cKO
ns
ns
Hindlimb
Forelimb
Control
Ret cKO
**
**
Hindlimb
Forelimb

Figure 2.7. Anatomical characterization of LTMR peripheral endings in Ret cKO and TrkB cKO mice.

A-B) Images of Pacinian corpuscles from the limbs of TrkB cKO animals and littermate controls. Limbs were whole-mount stained with antibodies against NFH (green), which labels large caliber axons, and S100 (magenta), which labels lamellar cells of the corpuscle and myelinating Schwann cells. Left scale bar = 250 μm. Right scale bar = 50 μm.

C-D) Images of Meissner corpuscles (indicated by white arrows) from Ret cKO animals and littermate controls. Skin tissue was stained using antibodies against NFH (green) and S100 (magenta). DAPI staining is shown in gray. Left scale bar = 50 μm. Right scale bar =20 μm.

E) Quantification of Meissner density in Ret cKO (n=3 animals) and littermate controls (n=3 animals). Each data point is the Meissner density for a single skin section, and data points of the same color came from the same animal (no significant difference using unpaired t-test).

F) Quantification of Pacinian corpuscles in TrkB cKO (n=3 animals) and littermate controls (n=3 animals), and Ret cKO (n=3 animals) and littermate controls (n=3 animals). The number of Pacinians was counted from wholemount staining of hindlimbs and forelimbs (mean ± SD, **$p<0.001$, unpaired t-test).

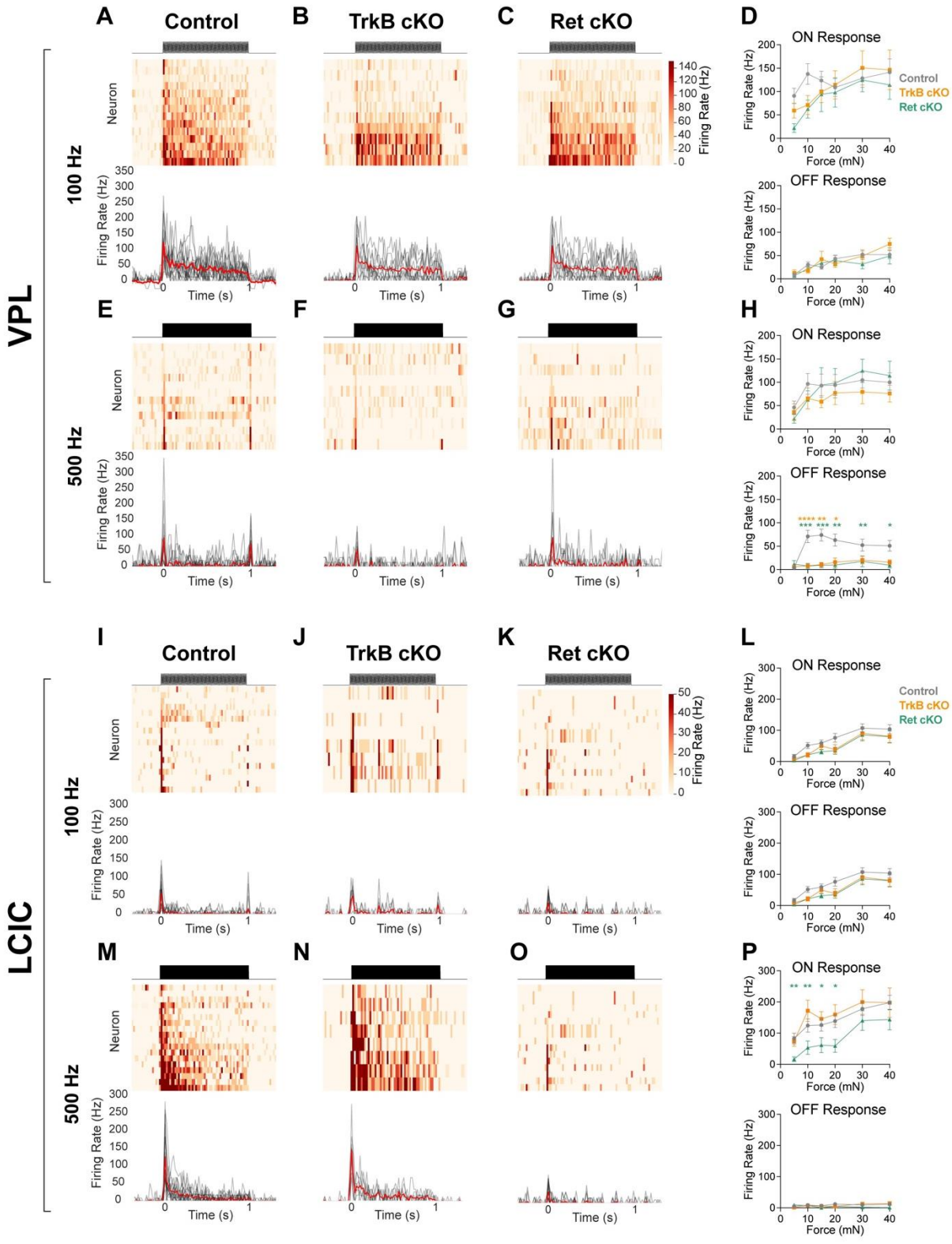

VPL
LCIC
A
Control
B
TrkB cKO
C
Ret cKO
D
ON Response
OFF Response
Control
TrkB cKO
Ret cKO
100 Hz
500 Hz
Neuron
Firing Rate (Hz)
Time (s)
Force (mN)
E
F
G
H
I
J
K
L
M
N
O
P

Figure 2.8. Onset and offset responses to vibratory stimuli in Ret cKO and TrkB cKO mice.

A) Top: Heatmap of neurons in the VPL responding to 100 Hz vibration at a 15 mN force (n=14 neurons from 6 animals). Each row is one neuron. Bottom: PSTHs of each neuron in above heatmap (gray), and population average PSTH (red). PSTHs are in 20ms bins.

B-C) Same as A in TrkB cKO (n=10 neurons from 3 animals) and Ret cKO mice (n=14 neurons from 4 animals).

D) Average firing rate of VPL neurons to the onset (top) and offset (bottom) of the 100 Hz vibration stimulus in control, TrkB cKO, and Ret cKO mice (mean ± SEM, not significantly different, Mann-Whitney U test with Bonferroni correction for multiple comparisons). On period is 20 ms after the stimulus onset, and off period is 20 ms after the end of the stimulus.

E-G) Same as A-C to 500 Hz vibration at 15 mN.

H) Same as D for 500 Hz stimulus (*p<0.05, **p<0.01 , ***p<0.001, ****p<0.0001, Mann-Whitney U test with Bonferroni correction for multiple comparisons).

I-K) Same as A-C for neurons in the LCIC in control (n=18 neurons from 5 animals), TrkB cKO (n=8 neurons from 4 animals), and Ret cKO (n=16 neurons from 5 animals) animals.

L) Average firing rate of LCIC neurons to the onset (top) and offset (bottom) of the 100 Hz vibration stimulus in control, TrkB cKO, and Ret cKO mice (mean ± SEM, not significantly different, Mann-Whitney U test with Bonferroni correction for multiple comparisons).

M-O) Same as I-K to 500 Hz vibration at 15 mN.

P) Same as L for a 500 Hz stimulus (*p<0.05, **p<0.01, Mann-Whitney U test with Bonferroni correction for multiple comparisons).

LCIC neurons integrate multimodal tactile-auditory stimuli in awake mice

Recent recordings from Pacinian afferents under awake conditions revealed that Pacinian Aβ RA2-LTMRs are exquisitely sensitive to environmental vibrations encountered during natural behaviors (Turecek & Ginty, 2024). Because Pacinian corpuscles underlie vibration responses in LCIC neurons **(Figure 2.6D, E, G)** and our recent recordings in awake mice show that they are ultrasensitive to substrate vibrations, we next asked whether LCIC neurons are also sensitive to low amplitude substrate vibrations in awake animals (Turecek & Ginty, 2024). We performed MEA recordings in awake head-fixed mice, but instead of applying vibration directly to the paw, we vibrated the platform the animal stood on **(Figure 2.9A).** Remarkably, in awake mice, 100 percent of LCIC neurons with hindlimb receptive fields responded robustly to 500 Hz stimulation of the surface platform, but few responded to a 50 Hz stimulus, similar to results from direct stimulation of the limb in recordings from anesthetized mice **(Figure 2.9B-C)**. Thus, as with Pacinian corpuscle Aβ RA2-LTMRs, LCIC neurons encode low-amplitude, high frequency environmental vibrations.

The inferior colliculus is primarily an auditory nucleus, and the LCIC receives extensive auditory input from brainstem auditory nuclei (Pickles, 2015), prompting us to ask whether LCIC neurons responsive to high frequency tactile vibrations also respond to sound. Prior findings indicate that many LCIC neurons are broadly tuned to auditory stimuli, and most auditory-sensitive LCIC neurons respond to short pulses of broadband noise (Aitkin et al., 1975; Duque et al., 2012; Perez-Gonzalez et al., 2005; Syka et al., 2000). Therefore, we exposed animals to 100 ms pulses of a broadband white noise stimulus (0-50 kHz) at a 65 dB sound pressure level (SPL) with the goal of activating LCIC neurons that receive auditory inputs. We delivered 500 Hz mechanical

vibrations to the platform surface and white noise pulses in isolation, as well as coincident tactile-auditory stimulation **(Figure 2.9D)** to awake mice while recording in the LCIC. Remarkably, ~75% of LCIC neurons were activated by both high frequency mechanical vibration of the platform and auditory white noise, with a minority of neurons responding to only platform vibration or sound **(Figure 2.9E-H)**. These findings reveal a high degree of convergence of auditory and mechanical vibration signals in the LCIC. Interestingly, of the LCIC neurons that received convergent tactile-auditory input, the majority exhibited a larger response to coincident presentation of mechanical vibration and sound than to either vibration or sound alone **(Figure 2.9I-J)**.

We further assessed the multimodal nature of LCIC responses to environmental vibrations by measuring responses of LCIC neurons in mice lacking either Pacinian corpuscles or cochlear function **(Figure 2.10A-B)**. As predicted from the findings in anesthetized mice **(Figure 2.6D-G)**, LCIC neurons in awake Ret cKO mice, which lack Pacinian corpuscles, were unresponsive to high frequency surface vibrations **(Figure 2.10E, G-H)**. Despite their insensitivity to vibration, LCIC neurons in Ret cKO mice were responsive to brush, suggesting that the LCIC receives inputs from other classes of cutaneous LTMRs. It is noteworthy that the somatosensory neuron deletion of Ret in Ret cKO mice does not impact the auditory system, as the Auditory Brainstem Response (ABR) test in Ret cKO mice indicated similar auditory thresholds to littermate controls **(Figure 2.11A-C)**. Furthermore, LCIC neurons of Ret cKO mice were comparably sensitive to auditory white noise stimuli compared to controls, indicating that developmental loss of Pacinian corpuscles does not alter LCIC sensitivity to broadband auditory stimuli **(Figure 2.10E, G-H)**.

In complementary experiments, we tested whether disrupting auditory system function alters mechanical vibration responsiveness in the LCIC. For this, we utilized *Sox10^{Cre}; GJB2$^{flox/flox}$* mice (GJB2 cKO), which lack connexin 26 expression in epithelial cells of the cochlea (Takada et al., 2014; Yu et al., 2014). GJB2 cKO mice lack cochlear hair cell function but have an intact vestibular system, such that this congenital deafness model exhibits extensive hearing loss but retains normal balance and motor function (Guo et al., 2021; Lalwani, 2002; Lee et al., 2015; Takada et al., 2014; Yu et al., 2014). ABR testing in GJB2 cKO mice confirmed their inability to hear, as none of the GJB2 cKO mice tested had a discernable brainstem response at the highest sound level tested **(Figure 2.11D-F)**. Recordings in anesthetized GJB2 cKO mice revealed that in the absence of normal hearing, LCIC neurons exhibit robust responses to mechanical vibration stimulation of the leg **(Figure 2.11G-J)**. Force-frequency vibration tuning curves in GJB2 cKO showed no difference from controls **(Figure 2.11I-J**). Furthermore, recordings in awake GJB2 cKO mice demonstrated that LCIC neurons responded to substrate vibrations although they showed no responsivity to white noise auditory stimuli **(Figure 2.10F-H)**. Thus, genetically disrupting either somatosensory/Pacinian corpuscle or auditory system function does not grossly alter LCIC neuron responses to the other sensory modality. Together, these findings indicate that most LCIC neurons receive both auditory input emanating from the cochlea and somatosensory input emanating from the body's Pacinian corpuscles. Therefore, the LCIC is a site of auditory-mechanical vibration multisensory integration and enhancement.

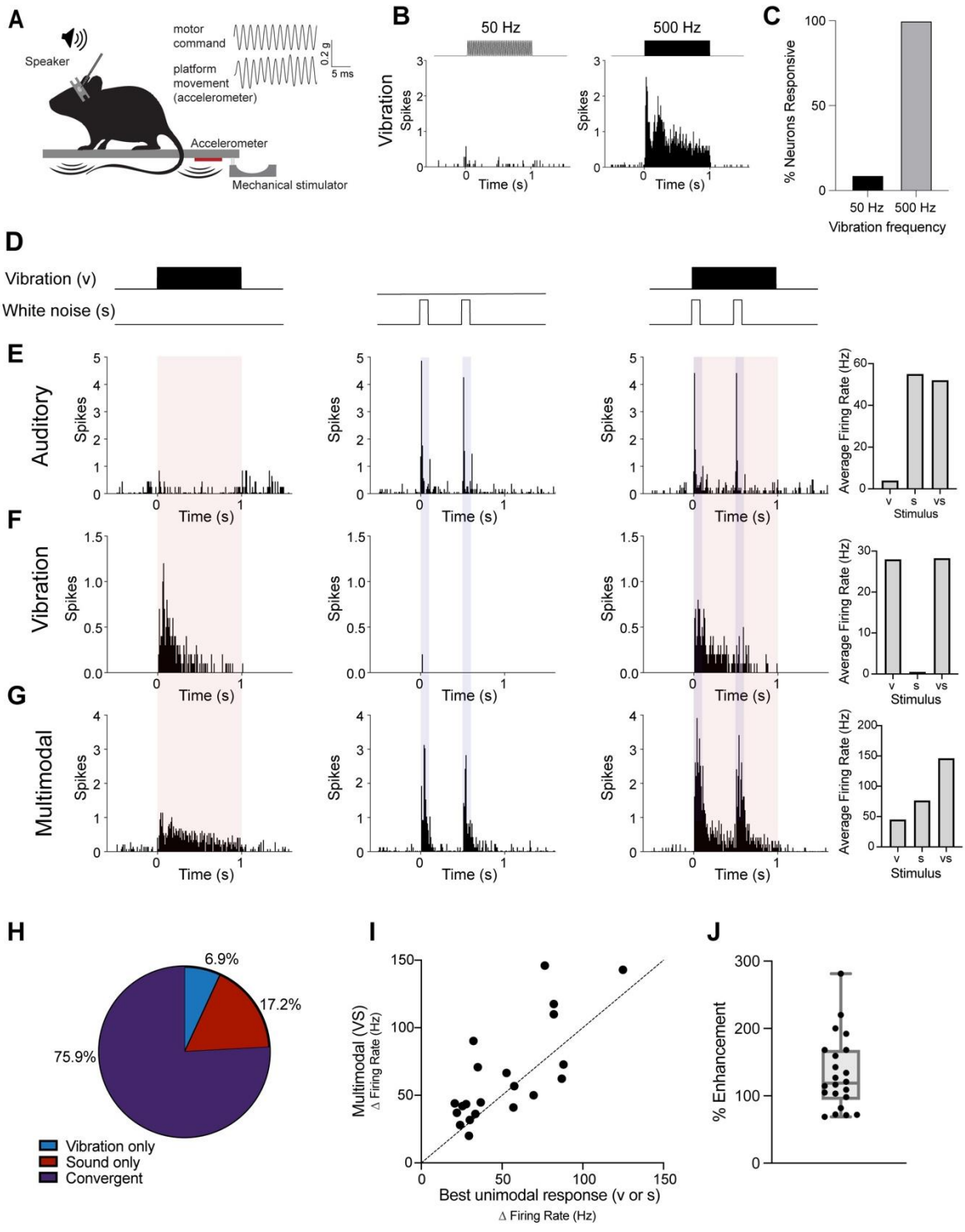

A
Speaker
motor command
platform movement (accelerometer)
0.2 g
5 ms
Accelerometer
Mechanical stimulator
B
50 Hz
500 Hz
Vibration
Spikes
Time (s)
C
% Neurons Responsive
50 Hz
500 Hz
Vibration frequency
D
Vibration (v)
White noise (s)
E
Auditory
F
Vibration
G
Multimodal
Average Firing Rate (Hz)
v
s
vs
Stimulus
H
6.9%
17.2%
75.9%
Vibration only
Sound only
Convergent
I
Multimodal (VS)
Δ Firing Rate (Hz)
Best unimodal response (v or s)
J
% Enhancement

Figure 2.9. Audio-tactile multimodality of LCIC neurons in awake mice.

A) Recordings of LCIC neurons were conducted in awake head-fixed mice as they stood on an acrylic platform, which could be stimulated at different vibratory frequencies. An accelerometer was attached underneath the acrylic platform to measure vibration frequency and amplitude. An example motor command and accelerometer signal are shown for 500 Hz vibration of the platform. A speaker is positioned on the contralateral side of the head from the recording site.

B) Peristimulus time histogram (PSTH) for a representative LCIC neuron, aligned to 50 Hz (left) and 500 Hz (right) vibration stimulation of the acrylic platform at a vibration amplitude of ~0.2 g (gravitational acceleration). PSTHs are baseline subtracted and reported in 10 ms bins.

C) Percentage of hindlimb sensitive LCIC neurons that responded to 50 Hz and 500 Hz vibratory stimuli (n=24 neurons from 5 animals).

D) 500 Hz substrate vibration (amplitude 0.2 g) and auditory white noise (frequency 0-50 kHz, 100 ms pulses, 65 dB SPL) were delivered in isolation and coincidentally to awake head-fixed mice.

E-G) Example PSTHs from LCIC neurons that respond to auditory stimuli (E), vibration (F), or both (G), aligned to vibration (v), sound (s) and convergent (vs) stimuli. PSTHs are baseline subtracted and in 10 ms bins. Right: The example neuron's average firing (during 0-0.1 s and 0.5-0.6 s windows) for each stimulus type.

H) Percentage of neurons in control animals that respond to 500 Hz vibration only, sound only, or convergent stimuli (n=29 neurons from 5 animals).

I) Scatter plot of firing rates in response to combined vibration and sound (vs) plotted against best unimodal response (vibration only or sound only). Unitary line denotes equal firing between best unimodal stimulus and combined stimulus conditions (n=21 neurons from 5 animals).

Figure 2.9 (Continued)

J) Quantification of multisensory enhancement (corresponding to I), calculated using the following equation: $\frac{vs-(Max(v\ or\ s))}{Max(v\ or\ s)}*100$. Neurons above 100% display multisensory enhancement (n=21 neurons from 5 animals)(Holmes & Spence, 2005; Meredith & Stein, 1983).

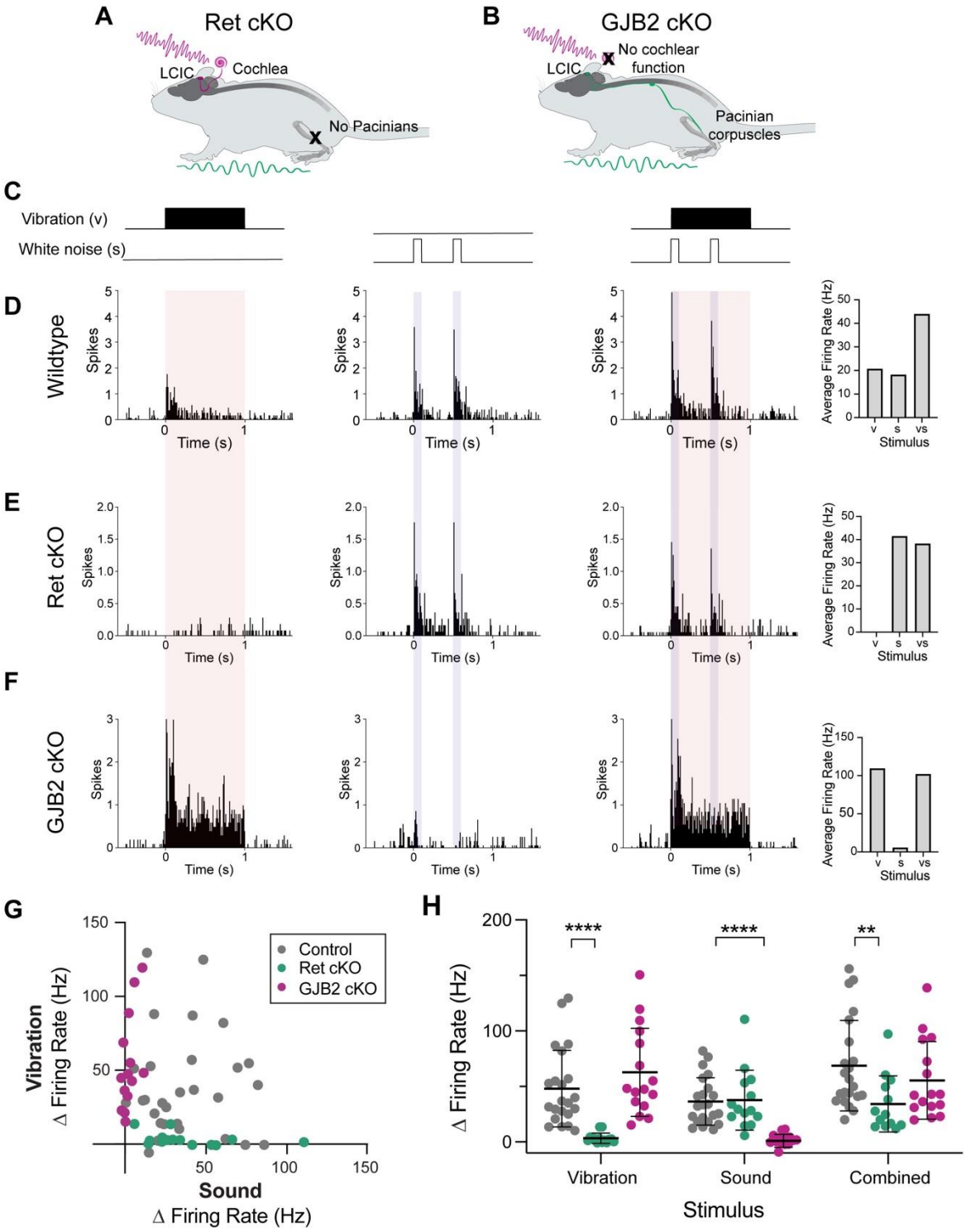

A
Ret cKO
LCIC
Cochlea
No Pacinians
B
GJB2 cKO
LCIC
No cochlear function
Pacinian corpuscles
C
Vibration (v)
White noise (s)
D
Wildtype
E
Ret cKO
F
GJB2 cKO
Spikes
Time (s)
Average Firing Rate (Hz)
v
s
vs
Stimulus
G
Control
Ret cKO
GJB2 cKO
Vibration
Δ Firing Rate (Hz)
Sound
Δ Firing Rate (Hz)
H
Δ Firing Rate (Hz)
****
****
**
Vibration
Sound
Combined
Stimulus

Figure 2.10. LCIC neuron responses in animals that lack Pacinian corpuscles or cochlear function.

A) Schematic of Ret cKO mouse which lacks Pacinian corpuscles, but has intact hearing.

B) Schematic of GJB2 cKO mouse which lacks cochlear function, but has an intact somatosensory system.

C) 500 Hz substrate vibration (amplitude 0.2 g) and auditory white noise (frequency 0-50 kHz, 100 ms pulses, 65 dB SPL) were delivered in isolation and coincidentally to awake head-fixed mice.

D) Example PSTHs from an LCIC neuron of a wildtype mouse aligned to vibration (v), sound (s) and convergent (vs) stimuli. PSTHs are baseline subtracted and in 10 ms bins. Right: The example neuron's average firing (during 0-0.1 s and 0.5-0.6 s windows) for each stimulus type.

E and F) As in (D), example LCIC neurons in a Ret cKO animal, which lacks Pacinian corpuscles **(E)**, and a GJB2 cKO animal, which is unable to hear **(F)**.

G) Scatter plot of each neuron's average change in firing rate to vibration and sound stimuli in control (n=29 neurons from 5 animals), Ret cKO (n=14 neurons from 3 animals) and GJB2 cKO (n=15 neurons from 3 mice) animals.

H) Average change in firing rate to vibration, sound, or combined stimuli (mean ± SD) in control (n=29 neurons from 5 animals), Ret cKO (n=14 neurons from 3 animals) and GJB2 cKO (n=15 neurons from 3 mice) animals (**p<.01, ***p<0.001, ****p<0.0001, Mann-Whitney U test).

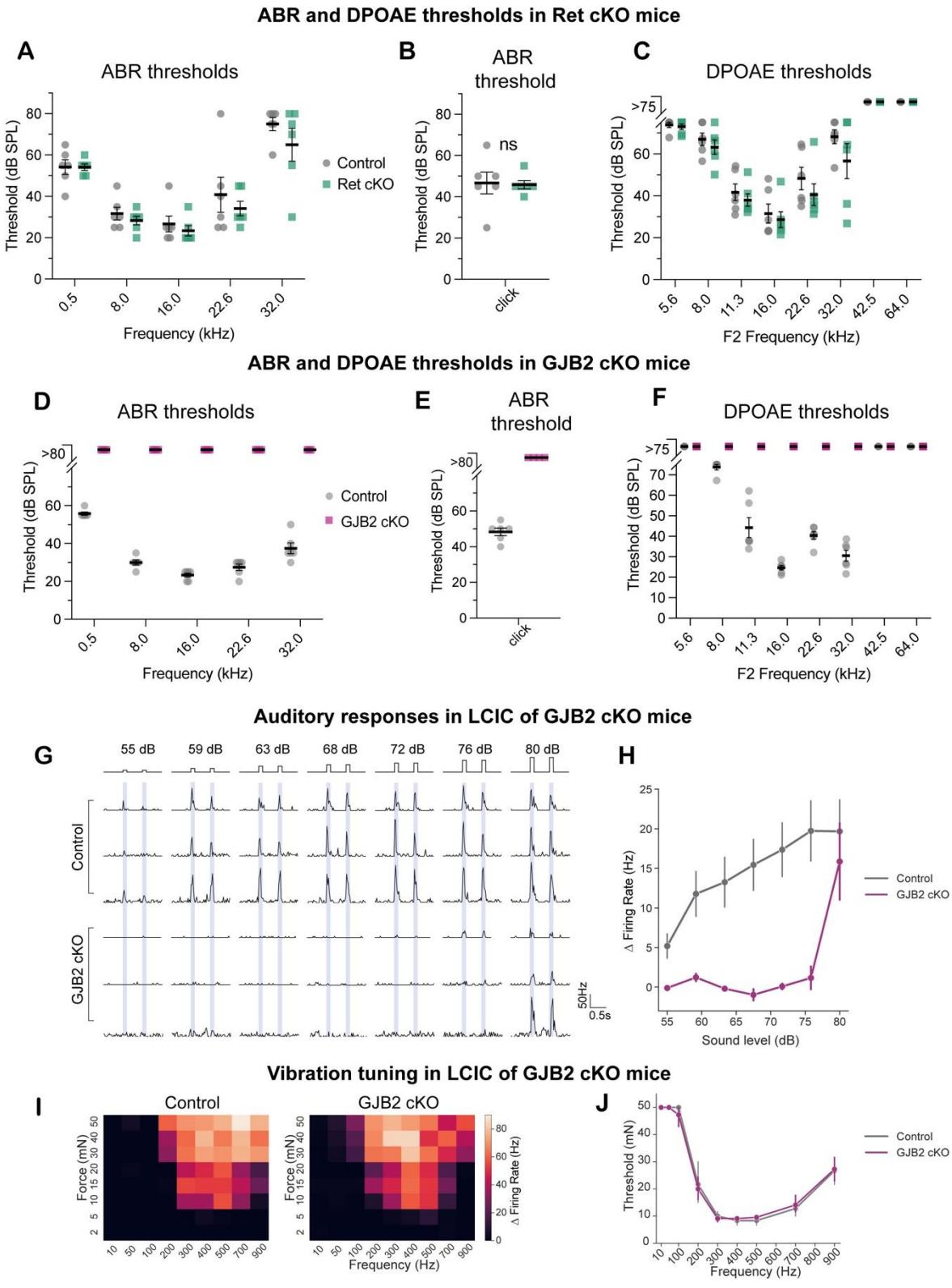

ABR and DPOAE thresholds in Ret cKO mice
A
ABR thresholds
Threshold (dB SPL)
Frequency (kHz)
0.5
8.0
16.0
22.6
32.0
Control
Ret cKO
B
ABR threshold
ns
click
C
DPOAE thresholds
>75
F2 Frequency (kHz)
5.6
11.3
42.5
64.0
ABR and DPOAE thresholds in GJB2 cKO mice
D
ABR thresholds
>80
GJB2 cKO
E
ABR threshold
F
DPOAE thresholds
Auditory responses in LCIC of GJB2 cKO mice
G
55 dB
59 dB
63 dB
68 dB
72 dB
76 dB
80 dB
Control
GJB2 cKO
50Hz
0.5s
H
Δ Firing Rate (Hz)
Sound level (dB)
Vibration tuning in LCIC of GJB2 cKO mice
I
Control
GJB2 cKO
Force (mN)
Frequency (Hz)
Δ Firing Rate (Hz)
J
Threshold (mN)

Figure 2.11 Characterization of auditory and tactile responses in Ret cKO and GJB2 cKO mice.

A) Auditory brainstem response (ABR) thresholds were measured in Ret cKO mice and littermate controls at 5 different auditory frequencies (mean ± SEM). Auditory thresholds between Ret cKO (n=6 animals) and controls (n=6 animals) were not significantly different (Mann-Whitney U Test with Bonferroni correction for multiple comparisons).
B) ABR thresholds to a broadband frequency "click" were measured in Ret cKO mice (n=6 animals) and littermate controls (n=6 animals). Thresholds were not significantly different (Mann-Whitney U Test).
C) Distortion product otoacoustic emissions (DPOAE) thresholds, which are sounds generated by mechanically active cells in the ear in response to sound stimuli, were measured in Ret cKO mice (n=6 animals) and littermate controls (n=6 animals) for 8 different frequency pairs (mean ± SEM). Thresholds were not significantly different (Mann-Whitney U Test with Bonferroni correction for multiple comparisons), suggesting normal function of the sensory cells responsible for fine-tuning cochlear gain.
D) Auditory brainstem response (ABR) thresholds were measured in GJB2 cKO mice (n=4 animals) and littermate controls (n=6 animals) at 5 different auditory frequencies (mean ± SEM). Unlike littermate controls, GJB2 cKO animals had no response at any frequency, even at the highest sound level tested (80 dB).
E) ABR thresholds to a broadband frequency "click" were measured in GJB2 cKO mice (n=4 animals) and littermate controls (n=6 animals). GJB2 cKO animals had no response, even at the highest sound level tested (80 dB).

Figure 2.11 (Continued)

F) Distortion product otoacoustic emissions (DPOAE) thresholds were measured in GJB2 cKO mice (n=4 animals) and littermate controls (n=6 animals) for 8 different frequency pairs (mean ± SEM). GJB2 cKO animals had no DPOAE at any frequency, even at the highest sound level tested (75 dB).

G) Example neurons responding to white noise at varying sound levels (dB) in anesthetized littermate control and GJB2 cKO mice. Each row corresponds to an individual neuron.

H) Average change in firing rate of neurons (mean ± SE) in littermate control (n=13 neurons from 2 mice) and GJB2 cKO mice (n=9 neurons from 2 mice) to white noise at varying sound intensities.

I) Force-frequency heat maps in response to vibration of differing frequencies and intensities in a representative neuron from a littermate control and GJB2 cKO animal.

J) Average force-frequency threshold curves of LCIC neurons (mean ± 95% confidence interval) recorded in control (n=9 neurons from 2 animals), and GJB2 cKO mice (n=11 neurons from 2 animals). Thresholds between GJB2 cKO and controls were not significantly different (Mann-Whitney U Test with Bonferroni correction for multiple comparisons).

The LCIC mediates behavioral avoidance to tactile vibration

The LCIC has been implicated in mediating defensive behaviors in response to auditory cues (Xiong et al., 2015). To begin investigating whether the LCIC can drive behavioral responses to high frequency mechanical vibrations, we developed a behavioral preference assay that relies on an animal's ability to detect and respond to high frequency mechanical vibrations of the environment. Animals were placed in a two-chamber behavioral setup where the floor of one chamber vibrates at 500 Hz, a stimulus that robustly activates Pacinian corpuscle afferents(Turecek & Ginty, 2023, 2024) and most LCIC neurons of awake animals **(Figure 2.9B-C, Figure 2.12A, Figure 2.13)**. Accelerometers were attached to each chamber, confirming the consistency of the stimulus between trials as well as the containment of the vibration to one side of the chamber **(Figure 2.14B-D)**. Wildtype animals had a strong and reliable preference for the non-vibrating chamber, spending ~80% of their time there when the vibration stimulus was on **(Figure 2.12B-D, Figure 2.14E-G)**. This avoidance was present in the two mouse strains tested, C57/Bl6 and CD-1 mice, and persisted in animals that were re-tested one week after the initial behavioral assay **(Figure 2.14E-G)**. Furthermore, whisker trimmed animals showed a preference that was comparable to control animals, indicating that whiskers are not necessary for the behavior **(Figure 2.14E-G)**. Since the production of the 500 Hz vibration generated a low amplitude 500 Hz auditory tone, we also performed a sound-only control. We decoupled the vibration motor from the chamber floor, such that a comparable sound was produced with no surface vibration. In the sound-only paradigm, animals showed no aversion toward the stimulus side of the chamber, demonstrating that sound alone does not drive a preference **(Figure 2.12G-H).** To test whether the high frequency mechanical vibration avoidance behavior is dependent on Pacinian corpuscles, the behavioral preference assay was done using Ret cKO mice, which lack

Pacinian corpuscles. Ret cKO mice did not prefer the non-vibrating side of the chamber over the vibrating side, indicating that avoidance of the 500 Hz vibration stimulus is dependent on Pacinian corpuscles **(Figure 2.12E-F, I-J**).

The Pacinian corpuscle-dependent vibration place preference assay was next used to determine whether the behavioral response to 500 Hz mechanical vibration is dependent on the LCIC. Targeted, bilateral injections of a fluorescently tagged GABA-A receptor agonist, muscimol, were used to silence neural activity in the inferior colliculus (IC; **Figure 2.13A, Figure 2.14H-J**). Post-hoc histology confirmed that muscimol was reliably restricted to the IC and did not extend into neighboring brain regions, including the superior colliculus, periaqueductal gray, or cerebellum **(Figure 2.13A, Figure 2.14H-I)** (Allen et al., 2008; Arikan et al., 2002; Xiong et al., 2015). IC-silenced mice displayed normal locomotor activity, traveling comparable distances during the assay as controls **(Figure 2.13B)**. Strikingly, as with mice lacking Pacinian corpuscles, IC-silenced mice did not exhibit avoidance of the vibratory stimulus compared to saline injected controls, revealing that the IC is required for the behavioral response to high frequency mechanical vibration **(Figure 2.13C-E)**. To determine whether the IC mediates general behavioral avoidance, or whether the effect of IC silencing is specific to vibratory stimuli, we also tested whether IC silencing alters avoidance of other somatosensory stimuli. We first performed a texture preference assay in saline and muscimol treated mice. In a two-chamber setup, one side of the chamber was covered in a smooth construction paper, while the other side was covered with a coarse grit sandpaper, which is aversive **(Figure 2.13F, Figure 2.14K-L)**. Mice injected with either saline or muscimol in the IC showed strong preference for the smooth side of the chamber, revealing that the IC is not necessary for aversive texture avoidance **(Figure**

2.13G). A cold temperature avoidance test was also performed. For this, we used a two-chamber cold avoidance assay in which mice were given a choice between one chamber, which was held at room temperature (30 ºC), and a second chamber, which was held at 18 ºC **(Figure 2.13H, Figure 2.14M)**. Similar to the texture preference assay, both control and IC-silenced animals displayed robust avoidance of the cold chamber **(Figure 2.13I)**. These findings indicate that the IC mediates behavioral response to high frequency mechanical vibrations but is not required for avoidance of an aversive texture or temperature.

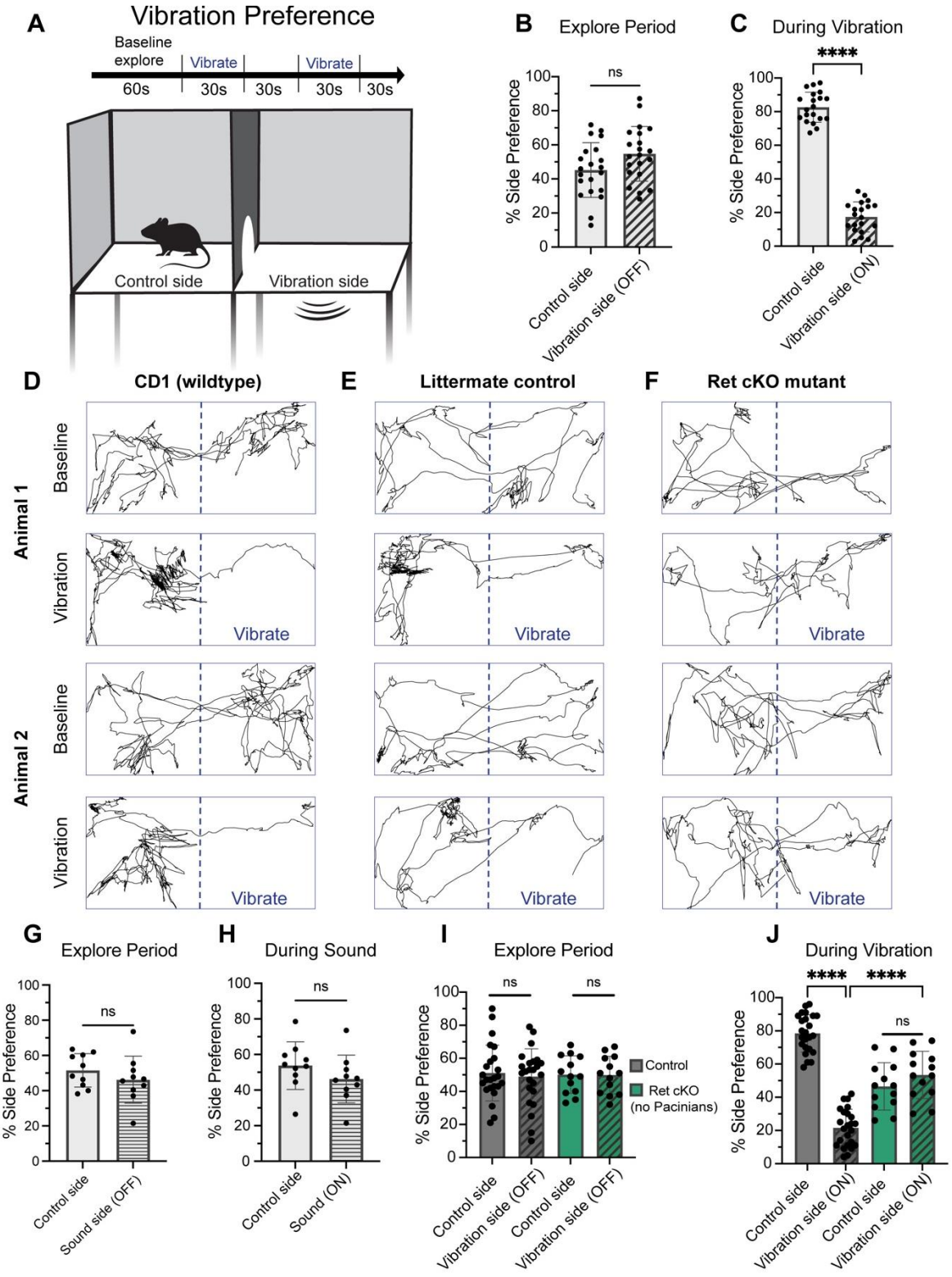

A
Vibration Preference
Baseline explore
Vibrate
Vibrate
60s
30s
30s
30s
30s
Control side
Vibration side
B
Explore Period
ns
% Side Preference
Control side
Vibration side (OFF)
C
During Vibration
****
% Side Preference
Control side
Vibration side (ON)
D
CD1 (wildtype)
E
Littermate control
F
Ret cKO mutant
Animal 1
Animal 2
Baseline
Vibration
Vibrate
G
Explore Period
ns
% Side Preference
Control side
Sound side (OFF)
H
During Sound
ns
% Side Preference
Control side
Sound (ON)
I
Explore Period
ns
ns
% Side Preference
Control
Ret cKO
(no Pacinians)
Control side
Vibration side (OFF)
Control side
Vibration side (OFF)
J
During Vibration
****
****
ns
% Side Preference
Control side
Vibration side (ON)
Control side
Vibration side (ON)

Figure 2.12. A behavioral paradigm to assess behavioral responsiveness to high frequency environmental vibration.

A) Animals were placed in a 2-chamber behavioral setup. The floors of each chamber are disconnected to prevent propagation of vibration between them, and an exciter speaker is attached to the floor of one chamber to generate mechanical vibrations. The chamber walls are partially open to prevent sound resonance from the exciter.

B and C) The percentage of time wildtype CD-1 animals spend on each side of the chamber (mean ± SD) during the 60 s baseline explore period **(B)** and the vibration periods **(C)** of the trial. Each dot represents one animal (n=20 animals, ****p<0.0001 paired t-test).

D-F) Representative activity traces of two example wildtype CD-1 animals **(D)**, littermate control animals **(E)**, and Ret cKO animals **(F)**, tracking movement during the baseline and vibration periods.

G and H) The speaker was detached from the floor of the chamber to test whether the sound of the exciter speaker alone can drive a behavioral preference. Time spent on each side of the chamber during the 60 s baseline explore period **(G)** and the sound on periods **(H)** (not statistically different, n=10 animals, paired t-test).

I and J) The percentage of time Ret cKO mice (n=14 animals) and littermate controls (n=24 animals) spent on each side of the chamber during the 60 s baseline explore period **(I)** and the vibration periods **(J)** of the behavioral trial. (****p<0.0001, paired t-test within group, unpaired t-test between groups).

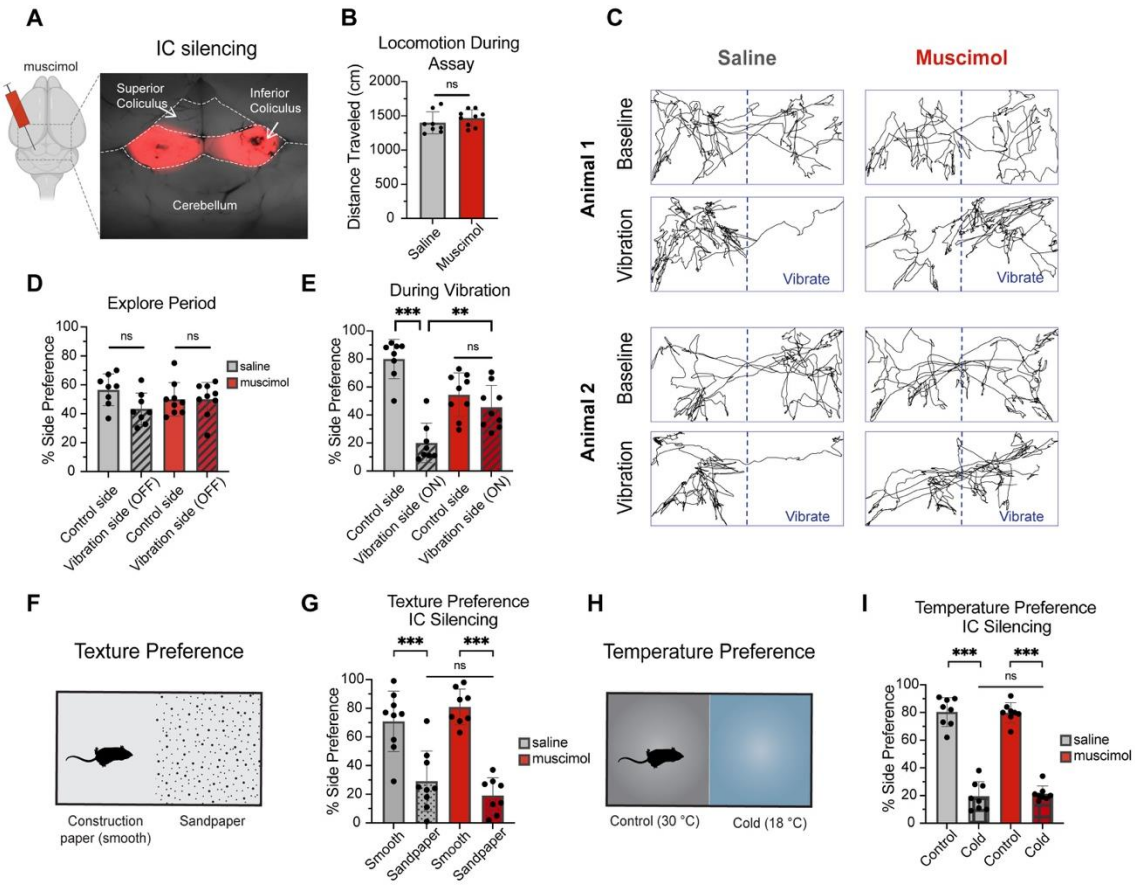


Figure 2.13. The LCIC mediates behavioral avoidance of high frequency mechanical vibration.

A) Targeted injections of TMR-X conjugated to the GABA-A receptor agonist, muscimol, were used to silence neural activity in the inferior colliculus. Top-down view of a schematic (left) and representative muscimol injected brain. Dotted lines depict borders between the inferior colliculus and indicated neighboring brain regions.

B) Total distance traveled during the behavioral assay in saline injected controls (n=8) and muscimol injected animals (n=9 animals, not significant, unpaired t-test).

C) Representative activity traces for 2 saline injected (control) and 2 muscimol injected animals during the baseline and vibration periods of the behavioral trial.

Figure 2.13 (Continued)

D and E) The proportion of time muscimol injected mice (n=9 animals) and saline injected controls (n=8 animals) spent on each side of the chamber during the 60 s baseline explore period (D) and the vibration periods (E) of the trial. (**p<0.01, ***p<0.001, paired t-test within group, unpaired t-test between groups)

F) Schematic of texture preference assay.

G) Percentage of time spent on the smooth and rough sides of the chamber during the 10 min assay for saline controls (n=9 animals) and muscimol silenced animals (n=9 animals, ***p<0.001, paired t-test within group, unpaired t-test between groups).

H) Schematic of temperature preference assay.

I) Percentage of time spent on the control (30 °C) and cold (18°C) sides of the chamber during the 5 min assay for saline controls (n=8) and muscimol silenced animals (n=8, ***p<0.001, paired t-test within group, unpaired t-test between groups).

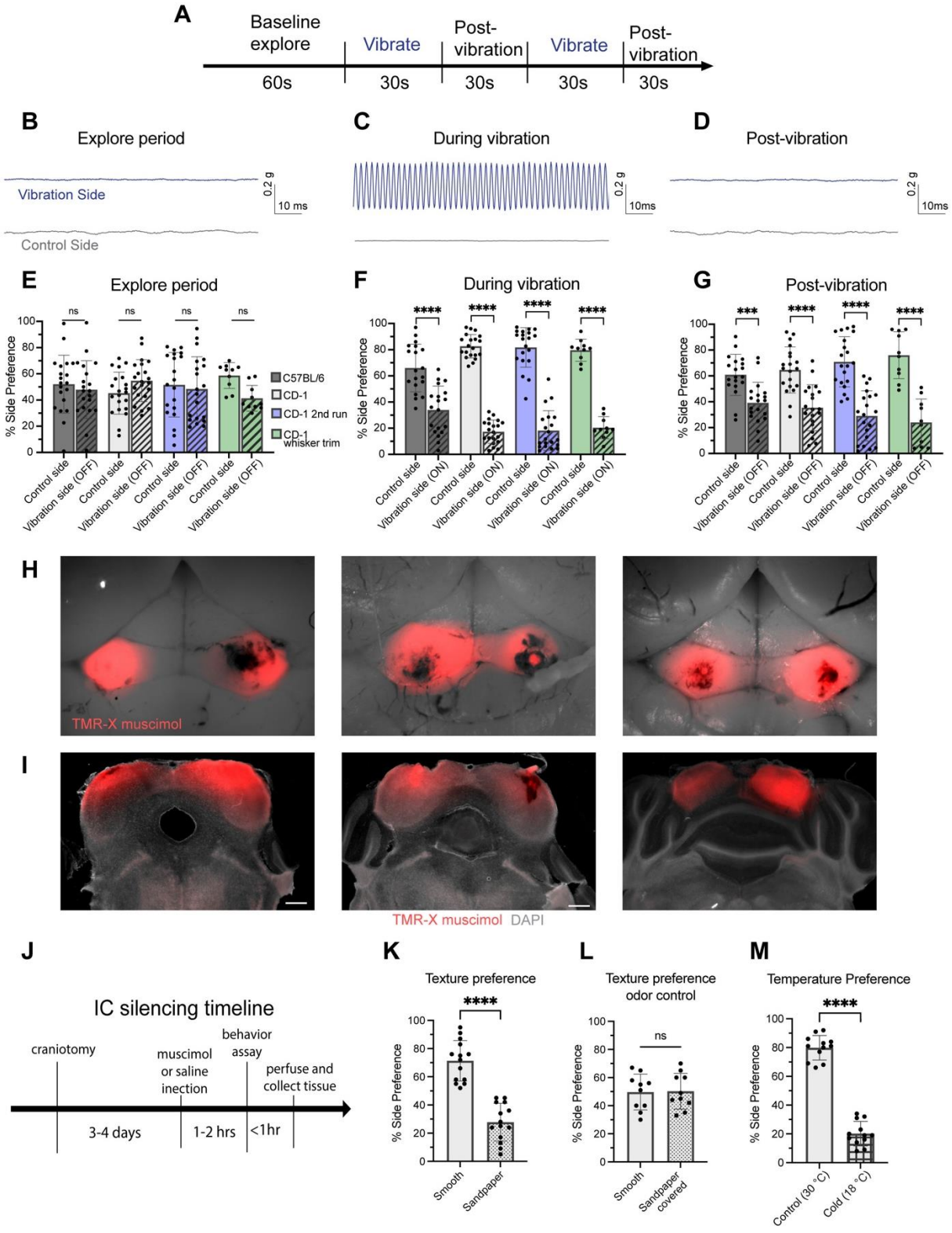

A
Baseline explore
Vibrate
Post-vibration
Vibrate
Post-vibration
60s
30s
30s
30s
30s
B
Explore period
Vibration Side
Control Side
0.2 g
10 ms
C
During vibration
0.2 g
10ms
D
Post-vibration
0.2 g
10ms
E
Explore period
% Side Preference
ns
C57BL/6
CD-1
CD-1 2nd run
CD-1 whisker trim
Control side
Vibration side (OFF)
F
During vibration
****
Control side
Vibration side (ON)
G
Post-vibration
***
****
H
TMR-X muscimol
I
TMR-X muscimol DAPI
J
IC silencing timeline
craniotomy
muscimol or saline inection
behavior assay
perfuse and collect tissue
3-4 days
1-2 hrs
<1hr
K
Texture preference
Smooth
Sandpaper
L
Texture preference odor control
Smooth
Sandpaper covered
M
Temperature Preference
Control (30 °C)
Cold (18 °C)

Figure 2.14. Behavioral analyses in wildtype and LCIC silenced animals.

A) Timeline of behavioral trial.

B-D) Accelerometer traces from vibration side (blue) and control side (gray) of the behavioral chamber during the baseline period **(B)**, vibration period **(C)**, and post-vibration period **(D)** of the behavioral trial. Amplitude of the platform vibration was ~ 0.3 g (gravitational force) when the vibration stimulus was on.

E-G) Percent of time that mice spent on the control and vibration side of the chamber during the explore period **(E)**, vibration period **(F)**, and post-vibration period **(G)** of the behavioral trial for four different conditions: naïve C57BL/6 mice (n=19 animals), naïve CD-1 mice (n=20 animals), CD-1 mice run on the behavior for the second time, one week later (n=20 animals), and naïve CD-1 mice that had been whisker trimmed (n=10 animals; ***$p<0.001$, ****$p<0.0001$, paired t-test).

H) Post-hoc histology of three different TMR-X conjugated muscimol injected animals, showing restriction of the injection to the inferior colliculus.

I) Coronal sections of a representative TMR-X conjugated muscimol injected brain to show ventral spread of the injection. Scale bar = 500 μm.

J) Timeline of IC silencing experiments.

K) Texture preference assay done for naïve CD-1 animals (n=10 animals, ****$p<0.0001$, unpaired t-test). Note, this is a separate cohort from the group used in silencing experiments in Figure 2.13.

L) Some types of sandpaper are aversive to mice due to their odor. To ensure our texture avoidance behavioral measure reflects avoidance of an aversive texture and not odor, the

Figure 2.14 (Continued)

sandpaper was covered by a smooth paper with small holes punched in it, such that the odor of the paper could be sensed, but the texture could not be felt. In this condition, mice (n=10 animals) did not demonstrate an aversion to the sandpaper side. (Not significant, paired t-test.) **M)** Temperature preference assay done for naïve wildtype CD-1 animals (n=10 animals, ****$p<0.0001$, unpaired t-test). Note, this is a separate cohort from the group used in silencing experiments, reported in Figure 2.13.

Methods

Animals

Avil^{Cre}, *TrkB*^{flox}, *Ret*$^{flox(eGFP)}$, and *Vglut2*^{Cre} mouse lines were of mixed background (CD-1 and C57BL/6J). *GJB2*^{flox} and *Sox10*^{Cre} were on a C57BL/6 background. CD-1 animals were imported from Charles River (#022) and C57BL/6 animals were imported from The Jackson Laboratory (#000664). The following mouse lines have been previously described, including: *Sox10*^{Cre} (Ref (Matsuoka et al., 2005), Jax 025807), *Avil*^{Cre}(Ref: (Hasegawa et al., 2007), JAX 032536), *TrkB*^{flox} (Ref:(Liu et al., 2012), *Ret*$^{flox(eGFP)}$ (JAX 029846), and *Vglut2*^{Cre} (JAX 016963). The *GJB2*^{flox} mouse line, in which loxP sites flank the entire coding sequence in exon 2, was generated by KTB in the laboratory of DPC and will be described elsewhere. Mice were handled and housed in standard cages in accordance with Harvard Medical School and IACUC guidelines. Both male and female mice were used in all experiments. Control littermates of *Ret*, *TrkB,* and *GJB2* conditional mutants included Cre-negative animals that were negative, heterozygous, or homozygous for the floxed allele. Our data indicated no difference among controls of different genotypes; therefore, they were combined for statistical analyses and collectively referred to as "controls."

Perfusions

Mice were anesthetized under isoflurane and transcardially perfused with 5-10 mL of PBS, followed by 5-10 mL of 4% paraformaldehyde (PFA) in PBS. After perfusion, the skull was removed and post-fixed in 4% PFA in PBS at 4°C overnight. Skin samples were removed and fixed overnight in Zamboni's fixation buffer with gentle agitation at 4°C. Samples were washed 3x10 min in PBS at room temperature after overnight fixation before fine dissection.

Immunohistochemistry of skin cryosections, brain cryosections and whole-mount tissue

The following dilutions and primary antibodies were used: chicken anti-NFH (Aves # NFH, 1:500), rabbit anti-S100 Beta (VWR/Protein Tech #15146-1-AP, 1:300), rabbit anti-dsRed (Takara #632496. 1:1000), chicken anti-GFP (Abcam #13970, 1:1000), goat anti-GFP (US Biological Life Sciences # G8965-01E, 1:500). The secondary antibodies used were Alexa 488, 546 or 647 conjugated donkey or goat anti-rabbit, chicken, or goat (Life Technologies or Jackson ImmunoResearch) and were prepared at 1:500 or 1:1000 dilutions.

For Meissner corpuscle histology, paws were removed from perfused mice. The pads and fingertips were clipped off of the glabrous skin using small spring scissors and cryoprotected in 30% sucrose in PBS at 4 °C for 1-2 days, embedded in OCT (1437365, Fisher), frozen using dry ice, and stored at −80 °C. The tissues were cryosectioned (25 μm) using a cryostat (Leica) and collected on glass slides (12-550-15, Fisher). Sections were washed 3 times for 5 minutes each with PBS containing 0.1% Triton X-100 (0.1% PBST), incubated with blocking solutions (0.1% PBST containing 5% normal goat serum (S-1000, Vector Labs) or normal donkey serum (005-000-121, Jackson Immuno) for 1 hour at room temperature, incubated with primary antibodies diluted in blocking solutions at 4 °C overnight, washed 3 times for 10 minutes each with 0.1% PBST, incubated with secondary antibodies diluted in blocking solutions at 4 °C overnight, washed again 4 times for 10 minutes each with 0.1% PBST (DAPI solution was included in the second wash at 1:5000 dilution), and mounted in Fluoromount-G mounting medium (Fisher 0100-01).

For whole-mount staining of Pacinian corpuscles, animals were anesthetized under isoflurane and euthanized by cervical dislocation. For Pacinian corpuscle dissections, the tibia and fibula of the ankle, and radius and ulna of the wrists were dissected immediately after euthanasia, keeping muscle and surrounding tissue intact, and fixed overnight in Zamboni's fixative at 4 °C. Limbs were washed 3x10 minutes in PBS and then finely dissected to remove muscle on the bone, while leaving the interosseous membrane of the bone intact. Tissues were then washed every 30 minutes for 5-6 hours with 1% PBST (PBS + triton X-100). Primary antibodies were applied in blocking solution (5% normal goat or donkey serum, 75% PBST, 20% DMSO, 0.01% NaN3) and incubated at room temperature for 3-5 nights with gentle rocking. Tissues were rinsed 3x in PBST, then washed every 30 minutes for 5-6 hours in 1% PBST. Secondary antibodies were applied in blocking solution and incubated at room temperature for 3-5 nights, with gentle rocking. Tissues were rinsed 3x in 1% PBST, washed every 30 minutes for 5-6 hours in 1% PBST, then serially dehydrated (10-15 minutes per wash) in 50%, 75%, and 100% ethanol diluted in distilled water. Tissue was stored at -20 °C in 100% ethanol until clearing and imaging. Tissue was cleared in BABB (1 part benzyl alcohol to 2 parts benzyl benzoate) for 2-12 hours at room temperature and mounted in BABB for imaging. For mounting, chambers were made on slides consisting of a thin layer of vacuum grease to create four walls followed by placement of a coverslip. Tissue was imaged on a Zeiss LSM 900 confocal microscope using the 10x objective.

For brain sections, brains were cryoprotected in 30% sucrose overnight. Tissue was cryosectioned (50 uM sections) and collected in a 12-well plate filled with PBS. Sections were stained free floating using a 12-well plate. Sections were washed 3x5 minutes each with 1x PBS containing 0.1% Triton X-100 (0.1% PBST), incubated with blocking solutions (0.1% PBST

containing 5% normal goat serum (S-1000, Vector Labs) or normal donkey serum (005-000-121, Jackson Immuno) for 1-2 hours at room temperature, incubated with primary antibodies diluted in blocking solutions at 4 °C overnight. Subsequently, sections were washed 3x10 minutes each with 0.1% PBST, incubated with secondary antibodies diluted in blocking solutions at room temperature for 2 hours, and washed again 4x10 minutes each with 0.1% PBST (DAPI solution was included in the second wash at 1:5000 dilution). Sections were mounted onto glass slides and coverslipped in Vectashield (Vector Labs).

Quantification of peripheral anatomy

For quantification of Meissner corpuscles in Ret cKO mice and littermate controls, cryosectioned and stained skin from the pads and fingertips were imaged with a widefield Zeiss LSM 700 microscope. Images of sections were analyzed in the Fiji distribution of Image J (www.fiji.sc). In each section, the number of Meissner corpuscles, visualized by S100 antibody staining, were counted. The length of the surface of the skin was traced and measured in ImageJ, and density was calculated by dividing the number of Meissner corpuscles by the length of the skin surface. Quantification was done blind to genotype.

For quantification of Pacinian corpuscles in Ret cKO mice, TrkB cKO mice, and littermate controls, images of stained and intact limbs were taken using a Zeiss LSM 900 confocal microscope using the 10x objective. The number of Pacinian corpuscles, visualized by S100 antibody staining, were counted. Quantification was done blind to genotype.

DRG recordings

Animals were anesthetized with urethane (1.5 g/kg) or isoflurane (1.5-2%). A skin incision was made over the L3-L5 vertebrae and muscle surrounding the vertebrae was removed. The L3 and L5 vertebrae were fixed in place using custom-built clamps. The L4 DRG was exposed by removing overlaying bone. A borosilicate glass electrode (1 MΩ) was lowered into the DRG using a motorized manipulator (Scientifica) to search for units. Recordings were amplified using a MultiClamp 700B (Molecular Devices) under the 100x AC differential amplification mode with additional 20x gain. Signals were collected with a 0.1 kHz high-pass filter and 3 kHz Bessel filter and acquired using a Digidata 1550B (Molecular Devices) sampled at 20 kHz. For Pacinian corpuscle innervating Aβ-RA2-LTMRs, a search stimulus of 300 Hz vibration (40 mN) was applied to the ankle. Pacinians were identified by their large receptive fields, and their end organ location on the fibula was identified through electrical stimulation following measurements of their vibration tuning. For Meissner corpuscle innervating Aβ-RA1-LTMRs, the hindlimb digits were brushed as the electrode was descended. Aβ-RA1-LTMRs were identified by their small skin receptive fields, adapting responses to indentation, low mechanical thresholds (<10 mN), and cutaneous endings that could be excited by electrical stimulation of the skin. Vibrations (10-900 Hz) of varying intensity (1-50 mN) were delivered to the most sensitive area of the receptive field for each unit, collecting at least 4 trials per force for each frequency.

Craniotomies for MEA recordings

Mice were injected with sustained relesae buprenorphine (0.1 mg/kg), anesthetized with isoflurane, and placed in a small animal stereotaxic frame (David Kopf Instruments). A titanium headplate was cemented to the mouse's skull (C&B Metabond). A craniotomy was made centered over the right inferior colliculus (stereotaxic coordinates: 0.5 mm posterior, 1.8 mm

lateral of lambda), or centered over the right VPL (stereotaxic coordinates: 1.7 mm posterior, 1.9 mm lateral of bregma), keeping the dura intact. Kwik-sil adhesive (World Precision Instruments) was used to cover the craniotomy until the day of recording (within 3 days of the craniotomy).

Multielectrode array (MEA) recordings

For anesthetized recordings, the mouse was injected intraperitoneally with urethane (0.5-1.5 mg/g), placed on a heated platform, and head fixed such that the paws on the side contralateral to the craniotomy were accessible for mechanical stimulation. MEAs were inserted into the LCIC (H6b-32ch or H7b-32ch, Cambridge Neurotech) or VPL (H6b-32ch, H7b-32ch, or E4-64ch, Cambridge Neurotech) with a 3-axes micromanipulator (IVM mini, Scientifica). MEA signals were high-pass filtered at 200 Hz, amplified (RHD2132), and acquired at 20 kHz (RHD2000, Intantech) for offline processing.

For VPL recordings, hindlimb VPL was targeted using coordinates (1.6 mm posterior, 1.9 mm lateral to bregma), and the location was verified by brushing the hindlimb. The LCIC was targeted by positioning the MEA probe posterior to the transverse sinus and ~1.6-1.8 mm lateral, with a 45-degree angle to insert the probe underneath the transverse sinus. In preliminary experiments, probe penetrations that contained only auditory responsive neurons were shown to be in the CNIC, unlike penetrations in the LCIC that contained both mechanical and auditory responses. Therefore, subsequent penetrations that contained only auditory responses were assumed to be in the CNIC and were not included in the analysis. For verification of recording location, after recording was complete, the probe was lifted from the brain, the probe was coated

with DiI (Thermo Fisher) then re-inserted to the same coordinates, and the brain was collected and post-fixed overnight in 4% PFA post-recording. Recordings were performed and analyzed blind to genotype.

Force-frequency tuning experiments (anesthetized): The receptive fields for neurons on the probe were determined by gently brushing the digits or pads using a fine paintbrush. The paw was fixed to the platform with Easy Mold Silicone Putty (Environmental Technologies). The mechanical stimulator (with a blunt 1 mm probe) was then targeted to the receptive fields identified by brush. In the case of LCIC neurons, which had large receptive fields that lacked a hotspot, the probe was targeted to the heel of the hindlimb. As above, for verification of recording location, after recording was complete, the probe was lifted from the brain, the probe was coated with DiI (Thermo Fisher) then re-inserted to the same coordinates, and the brain was collected and post-fixed overnight in 4% PFA post-recording. Thresholds for each vibratory frequency were defined as the force required to elicit 20% of a unit's maximum firing during the sustained portion of the stimulus (200 ms window beginning 50 ms after stimulus onset).

VPL and LCIC mapping experiments (anesthetized): For VPL mapping experiments (Figure 2.4) a 4 shanked probe (E4-64 ch, Cambridge Neurotech) was positioned with the shanks aligned to the antero-posterior axis. Mapping began medially (at ~1.7 mm lateral) and moved 100 μm lateral for each successive penetration. For each probe penetration, the contralateral hindlimb, thigh, trunk, forelimb, and face were stroked with a paintbrush. The hindlimb was fixed to the platform with Easy Mold Silicone Putty and stimulation at 50 Hz and 500 Hz was delivered to the hindpaw with a 10 mN intensity using a mechanical stimulator with a wide blunt tip (3 mm diameter). Complementary LCIC experiments used a single shank probe (H6b or H7b,

Cambridge Neurotech), with probe penetrations also separated by 100 μm intervals. Before each probe penetration the probe was coated with DiI and recording locations were verified post-experiment. Neurons were considered brush responsive to a body region if their change in firing exceeded 10 Hz during the brush period. Similarly, neurons were considered responsive to 500 Hz vibration if their change in firing exceeded 10 Hz during the sustained portion (200 ms period beginning 50 ms after stimulus onset) of the stimulus.

Awake LCIC recordings: For awake LCIC recordings, animals were head-fixed, and the LCIC was targeted as described above. Mechanical stimulation was targeted to the platform the animal stood on rather than the limb. The platform was made of thin (1/8") acrylic. Trials where the animal was moving were excluded.

Mechanical and auditory stimuli

For *in vivo* electrophysiology, vibrations were generated using a DC motor with a blunt 1-mm or 3-mm diameter probe, as previously described(Turecek & Ginty, 2023; Turecek et al., 2022). The motor was driven by a custom-built current supply controlled by Wavesurfer and a multifunction I/O board (USB-6343, National Instruments), and static forces calibrated using a fine scale. For awake recordings, the mechanical stimulator was covered with a sound dampening foam tip, and placed underneath the acrylic platform the animal stands on. The magnitude of vibration was measured using an accelerometer attached to the bottom of the platform and reported in units of gravitational force (g). Brush stimuli were manually delivered with a 4 mm diameter brush at a rate of one stroke per 2 seconds in the rostral to caudal direction.

Auditory stimuli were amplified by an SA1 stereo power amplifier (Tucker-Davis Technologies) and delivered through an MF1 multi-field magnetic speaker (Tucker-Davis Technologies), positioned 14 cm from the ear contralateral to recording site. Auditory stimuli were generated in MATLAB and delivered using WaveSurfer and a multifunction I/O board (USB-6343, National Instruments). Broadband (white) noise (0-50 kHz) was delivered in 100 ms pulses (5 ms rise-fall time) at 65 dB SPL. White noise, vibration, and combined trials were interleaved. For awake recordings, trials where the animal was moving were excluded.

Spike detection and cluster assignment

Data was converted into contiguous binary files (https://github.com/peltonen/kwik-tools) and processed using JRClust (Janelia). Spikes were detected and assigned to clusters corresponding to individual or multiples units with JRClust (https://github.com/JaneliaSciComp/JRCLUST). These initial clusters were manually curated to remove artifacts that did not correspond to spike waveforms, and clusters were examined and split if their PCA decompositions were not monodispersed. This collection of clusters was then examined, and merge operations performed if consideration of the average spike waveform and spiking cross-correlation indicated that two clusters corresponded to the same neuron. Manual curation typically resulted in putative isolated single units with intra-cluster waveform correlations greater than 0.9, inter-cluster waveform correlations less than 0.1, and clusters that did not meet these criteria were not considered in the dataset. Spike event times for each cluster were exported and processed in Python.

Anterograde tracing experiments

For anterograde tracing experiments (Figure 2.1), brainstem DCN neurons of *Slc17a6*^{Cre} (Vglut2) mice were transduced with either an AAV encoding synaptophysin-GFP, AAV1-CAG-FLEX-Synaptophysin-GFP-WPRE (1.088E+14gc/ml), or synaptophysin-tDT, AAV1-CAG-FLEX-Synaptophysin-tdTomato-WPRE (1.1482E+14gc/ml). Viruses were produced and packaged at the Boston Children's Hospital Viral Core Facility. Mice were injected with sustained release buprenorphine (0.1 mg/kg), anesthetized with isoflurane and placed in a small animal stereotaxic frame (David Kopf Instruments) with their neck bent at a 45 degree angle. The dorsal column nuclei were exposed between the base of the skull and C1 through retraction of the paraspinal muscles. A small nick in the overlying dural membrane was made to allow access for the injection pipette. A borosilicate glass pipette was lowered to a depth of 0.5 mm in either the gracile (0.1 mm lateral to obex) or cuneate (0.5mm anterior to obex, 0.1 mm lateral to fourth ventricle) nucleus. 50-100 nL of AAV virus with fast green was injected at a rate of 50 nL min−1 using a Microinject system (World Precision Instruments). Three weeks after injection, mice were perfused, and brain tissue was collected for cryosectioning and immunohistochemistry.

Auditory brainstem responses (ABR) and distortion product otoacoustic emissions (DPOAE)

All measurements and analyses were conducted blind to the animal's experimental condition. For anesthesia, mice were given an IP injection of ketamine (100 mg/kg body weight, BW), xylazine (10 mg/kg BW), and acepromazine (0.3 mg/kg BW) and placed on their side on a 37°C metal heating pad (ATC-2000, World Precision Instruments). Experiments were performed in a sound-attenuating, electrically shielded chamber (IAC Acoustics). After anesthesia induction, eye

lubricant (GenTeal Tears, Alcon) was applied to prevent drying. A ketamine boost (0.3 – 0.5 mg/kg BW) was used to maintain anesthesia at the first sign of movement or elevation in the signal rejection rate (rejection threshold was 15 μV).

An acoustic system consisting of a microphone and dual earphone assembly coupled to a probe tube was used to deliver and measure acoustic stimuli. This custom system was built by the Engineering Core of the Eaton-Peabody Laboratories (EPL) at Massachusetts Eye and Ear (MEE, Boston). The probe end of the acoustic system was placed ~1 mm over the center of the ear canal. Stimuli were digitally generated and then amplified by an SA1 stereo power amp (Tucker Davis Technologies) to drive the acoustic system. The probe tube microphone was amplified by a custom microphone amplifier (EPL at MEE) and sent to a 24-bit I/O board (PXI-4461) installed into a PXI chassis (PXIe-1073, National Instruments).

Bioelectrical signals were recorded using three subdermal electrodes: an active electrode at the vertex, a reference electrode near the pinna, and a ground electrode near the tail. Signals were passed through a custom pre-amplifier (EPL at MEE) before digitization. Acoustic stimuli consisted of clicks and 5 ms tone pips with a repetition rate of 30 s^{-1} and a 0.5 ms rise-fall time at the following frequencies (in kHz): 8, 16, 22.6, and 32. Stimuli were presented in alternating polarity to cancel out the cochlear microphonic potential. Cochlear Function Test Suite (CFTS) software (version 2.37.2; MEE, Boston) amplified (x104), filtered (0.3–3 kHz passband), and averaged 512 responses at each sound pressure level (SPL). ABR thresholds were manually designated blind to genotype using the ABR Peak Analysis Software from the EPL at MEE.

DPOAEs were recorded in response to primary tones f1 and f2 at a frequency ratio of f2/f1 = 1.2, and a SPL level of L1 = L2 + 10 dB. For individual DPOAE trials, f2 consisted of 5.6, 8, 11.3, 16, 22.6, 32, 42.5, or 64 kHz tones that were incremented in 10 dB steps from 10 to 70 dB SPL. The cubic distortion product 2f1-f2 was extracted by Fourier analysis of the ear-canal sound pressure after waveform and spectral averaging. DPOAE threshold was defined as the f1 level required to produce a DPOAE of 5 dB SPL, except at 64 kHz where the threshold was defined as 10 dB SPL due to a higher noise floor.

Muscimol silencing

For muscimol silencing experiments, mice were injected with sustained release buprenorphine (0.1 mg/kg), anesthetized with isoflurane, and placed in a small animal stereotaxic frame (David Kopf Instruments). A small section of skin above the rear of the skull was removed with surgical scissors and the skull was dried. The skin was glued to the skull using Vetbond (3M healthcare), and a small amount of dental cement (C&B Metabond) was used to cover the exposed region of the skull, leaving the area where the craniotomy would be drilled clear. A small craniotomy was drilled approximately 0.5 mm posterior, 1.8 mm lateral to lambda. The craniotomy was covered with Kwik-sil adhesive.

Animals were given 3-4 days to recover. On the day of the behavioral experiment, animals were anesthetized with isoflurane and placed in a small animal stereotaxic frame. A borosilicate glass pipette was used to bilaterally inject into the inferior colliculus (0.5-0.8 mm posterior to lambda, 1.5-1.8 mm lateral, 0.5 mm deep) with TMR-X muscimol dissolved in ACSF (1.5 mM, Invitrogen M23400). 50 nL injections were made in two locations per side (100 nL total per

side). Control mice received the same injection volume of sterile saline. Injections were performed at a rate of 50 nL min−1 using a Microinject system (World Precision Instruments) and the pipette was allowed to sit in the brain for 3 minutes post-injection. Animals were allowed to recover from isoflurane and habituate to the behavior room for ~1 hour, and the behavioral assay (vibration, temperature, or texture) was run within 2 hours. Behavioral assays were run blind to experimental group (saline or muscimol). Post-behavior, animals were perfused. Muscimol spread was confirmed post-hoc following vibratome sectioning the brain and imaging.

Behavior methods for Openfield, Vibration Platform and Temperature Preference assays

To reduce anxiety and improve handling, animals were enriched with Bio-Serv igloos, tunnels, or chew shacks at least one month prior to all behavior testing. One week prior to behavioral testing, animals were moved to the testing room and home cage habituated to the behavior room to acclimate to room lighting (warm white, 2700k), sound (ambient 45-50 dB), odor (cleaned with ECOS unscented dish soap and 70% EtOH), and temperature (73 ºF, 30% humidity). Vibration, temperature, and texture assays were conducted in 3-4 month old CD-1 animals (unless otherwise noted). Vibration assays in Ret cKO and littermate controls were performed at 8 weeks of age and were performed blind to genotype.

Vibration Platform and Sound Only Test: Two days prior to testing, animals were moved to the testing room and habituated to investigator handling. Animals were group habituated to the black matte test chamber (12 in L x 6 in W x 7 in H x 0.25 in), center divided with an arched doorway and allowed to freely explore for 5 minutes. During the three-day room/chamber habituation, animals were also habituated to the vibration motor sound only. The vibration platform was elevated 6 inches above the base. Two flat surface vibration motors, (PUI Audo, ASX08604-

SW-R 4 ohm, BST) were suspended above the base, resting on spring mounted posts, one motor on each side of the chamber to act as the suspension base for the two square white matte acrylic floors, (5.5 in L x 5.5 in W x 0.125 in D) to rest on and provide vibration stimulus to each floor when activated. The acrylic floors were separated by a thin gap and lightly attached to the motor. An accelerometer was attached to each floor to ensure vibration floor displacement was constant for each test animal. The entire floor was covered with a thin stretch white matte cloth napkin (WypAll L30, 05812) to prevent the animals from investigating the gap in the floor and edges of the chamber walls as well as maintain a clean odor free test environment. The black matte acrylic test chamber rested on four pillars (6 inches above the floor) to ensure the chamber walls snugly surrounded the vibration floors without direct contact to prevent the chamber from vibrating when the motor was activated during testing. The room and test platform were lined with odorless 1-inch thick Bonded Logic Natural Fiber Acoustic Sound Absorbing panels (Model #60600-11212).

Vibration Test: The test chamber was modified on test day by removing the front and side wall to create a semi-open and closed end (L-shape) to increase animals' awareness of the floor surface when exploring both sides of the test chamber. The center divider with open doorway was left in place. The semi-closed side of the chamber was the non-stimulus side and the semi-open side was the vibration stimulus side. A custom Bonsai script was used to trigger the vibration motor and camera. The three-minute vibration test sequence was as follows: the animal was placed in the chamber facing the semi-open side which encouraged the animal to walk through the doorway and explore the newly semi-closed side of the chamber.

Stage-1: Start, allow one minute baseline explore of test chamber,

Stage-2: 30 second vibration stimulus on the semi-open side,

Stage-3: 30 second interim period with no stimulus,

Stage-4: 30 second vibration stimulus on the semi-open side,

Stage-5: 30 second final period with no stimulus.

For the sound only test, the motor was disconnected from floor contact and the motor sound only was played for the 30 second stimulus during stage-2 and stage-4. Ambient room and chamber decibel level was 45-50 dB. During sound only and vibration stimulus periods, the background sound in the testing room and chamber was set to 70 dB at 500 Hz. A top video recording device was used to track distance traveled and time exploring the two chambers.

Temperature Preference Test: Two days prior to testing, animals were moved to the testing room and home cage habituated to the behavior. Animals were group habituated for 5 minutes to the black matte test chamber (12 in L x 6 in W x 7 in H x 0.25 in), center divided with an arched doorway, resting on two metal plate floors (5.5 in L x 5.5 in W ea) both set to neutral temperature 30 ºC. On the third day following room habituation, each animal was tested on contrasting temperatures, 30 ºC (warm) vs 18 ºC (cold). Each animal was placed in the test chamber on the warm side facing the doorway to the cold side to encourage the animals to walk through the doorway and freely explore both temperatures for 5 minutes. A top video recording device was used to track distance traveled and time exploring the two chambers.

Texture Preference Assay: Two days prior to testing, animals were moved to the testing room and home cage habituated to the behavior. Animals were group habituated for 10 minutes to the

black matte test chamber (12 in L x 6 in W x 7 in H x 0.25 in) with no divider. On the third day following room habituation, each animal was tested on contrasting floors, construction paper (Tru-Ray Heavyweight, Pacon) vs coarse 60-grit sandpaper (ceramic version, 26060PGP-4, 3M). There was no divider between the smooth and rough textured floors. Each animal was placed in the test chamber on the smooth side and animals were given 10 minutes to freely explore both chambers. A top video recording was used to track distance traveled and time exploring the two chambers.

Quantification and statistical analysis

Statistical tests were conducted in Python 3.7.9 using the SciPy stats module or in GraphPad Prism. Normality of the data was tested using the Shapiro-Wilk test. Comparisons between two independent groups were performed using the unpaired t-test (in the case of two groups distributed normally, with no significant difference between variances), Welch's t-test (in the case of two groups distributed normally, but with unequal variances), or Mann-Whitney test (non-parametric data). When correction for multiple comparisons was necessary, the Bonferroni correction was used. An adjusted p value < 0.05 was considered significant. Additional details on sample sizes and statistical tests for each experiment can be found in figure legends and the main text.

Acknowledgements

We thank A. Handler, H. Kwak, K. Lezgiyeva, R. Martinez-Garcia, J. Peng, K. Ng, A. Emanuel, and A. Shuster for comments on the manuscript. We thank A. Emanuel for code used for the MEA data analysis. This work was supported by a HHMI Hannah Gray fellowship (GER), NEI P30 Core Grant for Vision Research #EY012196 (OM), NIH grants F31 NS097344 (ELH) and R35 5R35NS097344-05 (DDG), the Edward R. and Anne G. Lefler Center for Neurodegenerative Disorders (DDG), and the Hock E. Tan and Lisa Yang Center for Autism Research (DDG). DDG is an investigator of the Howard Hughes Medical Institute. This article is subject to HHMI's Open Access to Publications policy. HHMI lab heads have previously granted a nonexclusive CC BY 4.0 license to the public and a sublicensable license to HHMI in their research articles. Pursuant to those licenses, the author-accepted manuscript of this article can be made freely available under a CC BY 4.0 license immediately upon publication.

Author Contributions

ELH and DDG conceived the study. ELH did the MEA recordings in both anesthetized and awake conditions, with help from JT and MD. JT and ZKS performed primary sensory neuron recordings. ELH, AH, and MD performed anatomy and immunohistochemistry experiments. MMD, OM, and ELH developed the vibration behavioral assay. ELH did the saline and muscimol IC injections, and MMD performed behavioral experiments for vibration, temperature, and texture preference assays, with help from ELH. GER performed auditory brainstem response (ABR) measurements with guidance from LVG. KTB and DPC generated and provided the $GJB2^{flox/flox}$ $Sox10^{Cre}$ mice. ELH and DDG wrote the manuscript with input from all authors.

Chapter 3. Discussion

Organisms across the animal kingdom, including insects, reptiles and mammals, rely on their ability to detect and respond to environmental vibratory cues for their survival. Spider webs are designed to transmit vibrations that spiders utilize to efficiently localize their prey (Virant-Doberlet et al., 2023). Snakes detect the movement of prey by pressing their jaws into the ground to detect subtle substrate vibrations (Young & Morain, 2002). Some subterranean mammals, in the absence of visual cues, rely heavily on vibratory cues for communication, localization of prey, and detection of predators (Cividini et al., 2019; Narins et al., 1992; Nevo et al., 1991). While all mammalian LTMRs are sensitive to mechanical stimuli acting on the body, the Pacinian corpuscle is unique in its exquisite sensitivity to substrate vibrations of the environment and across a broad range of frequencies. Recordings from Pacinian afferents in awake, behaving mice demonstrate their capacity to fire robustly in response to subtle vibrations generated meters away from where an animal stands (Turecek & Ginty, 2024). Here we show that the neural signals encoding mechanical vibrations captured by the body's Pacinian corpuscles converge with the signals encoding auditory vibrations (sound) in the LCIC of the auditory midbrain to create an internal representation of environmental vibration.

Divergent functions of thalamic and collicular pathways

The majority of research into the neurobiological basis of discriminative touch of the body has focused on the ascending pathway through the brainstem to the thalamus (VPL) *en route* to primary somatosensory cortex (S1; **Figure 2.2A**), while somatosensory representations in other brain areas have remained largely unexplored. We found that neurons in the VPL and the LCIC

of the auditory midbrain exhibit highly distinct vibrotactile tuning properties that may underlie unique functions of divergent ascending somatosensory system streams. Most VPL neurons had restrictive receptive fields and were tuned to low frequency vibrations. These properties are well suited for tactile acuity and discrimination—functions hypothesized to be mediated by the VPL to S1 pathway (Kwon et al., 2016; Park et al., 2022; Sathian, 1989; Stuttgen & Schwarz, 2018). Only a small fraction of VPL neurons (~9%) encoded high frequency vibration **(Figure 2.2D)**. In contrast, most LCIC neurons exhibited expansive receptive fields and were tuned to high frequency vibrations (>75%) conveyed by Pacinian corpuscle Aβ RA2-LTMRs **(Figure 2.2D, F)**. These divergent somatosensory streams are reminiscent of the parallel processing streams of the mammalian visual system, where some retinal ganglion cells project to the thalamus (LGN), while others project to the tectum (superior colliculus) or the suprachiasmatic nucleus (SCN) of the hypothalamus (Dhande et al., 2015). Work in the visual system suggests that functional segregation exists between the LGN, collicular, and SCN pathways, whereby the collicular pathway may be optimally tuned for discrimination of moving objects (Beltramo & Scanziani, 2019) and the SCN pathway for circadian entrainment (Dhande et al., 2015). These parallels between visual and somatosensory processing reveal shared organizational principles across sensory systems.

The salience of low amplitude environmental vibrations encoded in the LCIC is highlighted by our finding that IC silencing virtually eliminated animals' avoidance of a 500 Hz vibratory stimulus in a place preference paradigm **(Figure 2.13C-E)**. On the other hand, the IC was not required for avoidance of an aversive texture or temperature, suggesting that the IC does not mediate general avoidance to aversive somatosensory stimuli, rather it plays a more specialized

role in perceiving and reacting to high frequency vibrations **(Figure 2.13G,I)**. It is possible that the divergent ascending streams through the LCIC and VPL underlie distinct responses to high frequency vibrations in different contexts. For example, the sparser representation of high frequency vibration in the VPL to S1 stream may underlie operant tasks that use vibratory cues (Hong et al., 2018; Park et al., 2022; Prsa et al., 2019; Stuttgen & Schwarz, 2018). Future work will discern the relative contributions of distinct ascending streams encoding environmental vibrations in different contexts and downstream targets of the LCIC that underlie environmental vibration sensing.

Tactile-auditory integration in the LCIC

Strikingly, most mechanical vibration sensitive LCIC neurons are also tuned to auditory stimuli. Moreover, the majority of LCIC neurons that received convergent mechanical vibration and auditory inputs exhibited multisensory enhancement, responding more strongly to coincident tactile-auditory stimulation than to either modality alone **(Figure 2.9I-J)**. Furthermore, somatosensory and auditory inputs to the LCIC are independent of one another, as evidenced by the findings that genetically altering the ability to detect either mechanical or auditory inputs did not grossly impact responsivity to the other modality **(Figure 2.10)**. Thus, the LCIC encodes environmental vibrations, whether they are mechanical vibrations propagated through the ground, detected by Pacinian corpuscles, and conveyed via the ascending somatosensory pathway or sound waves traveling through air, captured by the cochlea, and conveyed via the ascending auditory pathway.

We suspect that the LCIC enables enhanced detection or reaction to environmental vibrations through auditory and vibrotactile coincidence detection. A myriad of natural phenomena generates coincident sounds and substrate vibrations, including seismic events or earth movements, objects moving across or falling to the ground, vocalizations of conspecifics, and the motions of prey or predators. Multisensory audio-vibrotactile integration in the LCIC may increase saliency of these ethologically relevant environmental cues and may be particularly relevant under conditions in which cues are weak and difficult to discern. For humans, the connection between vibration and sound is evident when standing in the wind, close to a rushing river or a passing train, in a concert, or playing a musical instrument. We propose that, through their convergent inputs to the LCIC, the somatosensory and auditory systems collaborate to detect, localize, and respond to a wide range of environmental vibrations.

Future Directions

The substantial representation of high frequency tactile vibrations in the LCIC raises interesting questions about how tactile vibrations are encoded in the ascending auditory pathway. Future work will address which brain regions downstream from the LCIC receive tactile information, including candidate regions such as the medial geniculate body (MGB) in the thalamus and primary auditory cortex (A1). Another intriguing area for future investigation is the plasticity in multisensory auditory-somatosensory processing. In humans, there are numerous case studies of musicians with hearing loss who rely on the detection of tactile vibrations to “hear” and produce music (Fulford et al., 2011; Hopkins et al., 2023). Notably, Ludwig Van Beethoven was deaf in the last eight years of his life, and relied on his ability to detect tactile vibrations from musical instruments to compose and play music (Fulford et al., 2011). Thus, exploring how the

representation of tactile vibrations is altered in congenital mouse models of deafness, as well as models of induced hearing loss and in humans, may provide valuable insights into the plasticity observed in humans and aid in the development neural prosthetics.

References

Abraira, V. E., & Ginty, D. D. (2013). The sensory neurons of touch. *Neuron*, *79*(4), 618-639. https://doi.org/10.1016/j.neuron.2013.07.051

Aitkin, L. M., Dickhaus, H., Schult, W., & Zimmermann, M. (1978). External nucleus of inferior colliculus: auditory and spinal somatosensory afferents and their interactions. *J Neurophysiol*, *41*(4), 837-847. https://doi.org/10.1152/jn.1978.41.4.837

Aitkin, L. M., Kenyon, C. E., & Philpott, P. (1981). The representation of the auditory and somatosensory systems in the external nucleus of the cat inferior colliculus. *J Comp Neurol*, *196*(1), 25-40. https://doi.org/10.1002/cne.901960104

Aitkin, L. M., Webster, W. R., Veale, J. L., & Crosby, D. C. (1975). Inferior colliculus. I. Comparison of response properties of neurons in central, pericentral, and external nuclei of adult cat. *J Neurophysiol*, *38*(5), 1196-1207. https://doi.org/10.1152/jn.1975.38.5.1196

Allen, T. A., Narayanan, N. S., Kholodar-Smith, D. B., Zhao, Y., Laubach, M., & Brown, T. H. (2008). Imaging the spread of reversible brain inactivations using fluorescent muscimol. *J Neurosci Methods*, *171*(1), 30-38. https://doi.org/10.1016/j.jneumeth.2008.01.033

Alvarez-Buylla, R., & Ramirez de Arellano, J. (1953). Local responses in Pacinian corpuscles. *Am J Physiol*, *172*(1), 237-244. https://doi.org/10.1152/ajplegacy.1952.172.1.237

Angel, A., & Clarke, K. A. (1975). An analysis of the representation of the forelimb in the ventrobasal thalamic complex of the albino rat. *J Physiol*, *249*(2), 399-423. https://doi.org/10.1113/jphysiol.1975.sp011022

Arikan, R., Blake, N. M., Erinjeri, J. P., Woolsey, T. A., Giraud, L., & Highstein, S. M. (2002). A method to measure the effective spread of focally injected muscimol into the central nervous system with electrophysiology and light microscopy. *J Neurosci Methods*, *118*(1), 51-57. https://doi.org/10.1016/s0165-0270(02)00143-7

Bai, L., Lehnert, B. P., Liu, J., Neubarth, N. L., Dickendesher, T. L., Nwe, P. H., Cassidy, C., Woodbury, C. J., & Ginty, D. D. (2015). Genetic Identification of an Expansive Mechanoreceptor Sensitive to Skin Stroking. *Cell*, *163*(7), 1783-1795. https://doi.org/10.1016/j.cell.2015.11.060

Bell, J., Bolanowski, S., & Holmes, M. H. (1994). The structure and function of Pacinian corpuscles: a review. *Prog Neurobiol*, *42*(1), 79-128. https://doi.org/10.1016/0301-0082(94)90022-1

Beltramo, R., & Scanziani, M. (2019). A collicular visual cortex: Neocortical space for an ancient midbrain visual structure. *Science*, *363*(6422), 64-69. https://doi.org/10.1126/science.aau7052

Berkley, K. J., Blomqvist, A., Pelt, A., & Flink, R. (1980). Differences in the collateralization of neuronal projections from the dorsal column nuclei and lateral cervical nucleus to the thalamus and tectum in the cat: an anatomical study using two different double-labeling techniques. *Brain Res*, *202*(2), 273-290. https://doi.org/10.1016/0006-8993(80)90141-9

Berkley, K. J., Budell, R. J., Blomqvist, A., & Bull, M. (1986). Output systems of the dorsal column nuclei in the cat. *Brain Res*, *396*(3), 199-225. https://doi.org/10.1016/0165-0173(86)90012-3

Bjorkeland, M., & Boivie, J. (1984). An anatomical study of the projections from the dorsal column nuclei to the midbrain in cat. *Anat Embryol (Berl)*, *170*(1), 29-43. https://doi.org/10.1007/BF00319455

Bolanowski, S. J., Jr., & Zwislocki, J. J. (1984). Intensity and frequency characteristics of pacinian corpuscles. II. Receptor potentials. *J Neurophysiol*, *51*(4), 812-830. https://doi.org/10.1152/jn.1984.51.4.812

Bouley, D. M., Alarcon, C. N., Hildebrandt, T., & O'Connell-Rodwell, C. E. (2007). The distribution, density and three-dimensional histomorphology of Pacinian corpuscles in the foot of the Asian elephant (Elephas maximus) and their potential role in seismic communication. *J Anat*, *211*(4), 428-435. https://doi.org/10.1111/j.1469-7580.2007.00792.x

Cheek, M. D., Rustioni, A., & Trevino, D. L. (1975). Dorsal column nuclei projections to the cerebellar cortex in cats as revealed by the use of the retrograde transport of horseradish peroxidase. *J Comp Neurol*, *164*(1), 31-46. https://doi.org/10.1002/cne.901640104

Chirila, A. M., Rankin, G., Tseng, S. Y., Emanuel, A. J., Chavez-Martinez, C. L., Zhang, D., Harvey, C. D., & Ginty, D. D. (2022). Mechanoreceptor signal convergence and transformation in the dorsal horn flexibly shape a diversity of outputs to the brain. *Cell*, *185*(24), 4541-4559 e4523. https://doi.org/10.1016/j.cell.2022.10.012

Cividini, S., Sfenthourakis, S., & Montesanto, G. (2019). Are terrestrial isopods able to use stridulation and vibrational communication as forms of intra and interspecific signaling and defense strategies as insects do? A preliminary study in Armadillo officinalis. *Naturwissenschaften*, *107*(1), 4. https://doi.org/10.1007/s00114-019-1656-3

Cohen, J. D., & Castro-Alamancos, M. A. (2007). Early sensory pathways for detection of fearful conditioned stimuli: tectal and thalamic relays. *J Neurosci*, *27*(29), 7762-7776. https://doi.org/10.1523/JNEUROSCI.1124-07.2007

Dhande, O. S., Stafford, B. K., Lim, J. A., & Huberman, A. D. (2015). Contributions of Retinal Ganglion Cells to Subcortical Visual Processing and Behaviors. *Annu Rev Vis Sci*, *1*, 291-328. https://doi.org/10.1146/annurev-vision-082114-035502

Duque, D., Perez-Gonzalez, D., Ayala, Y. A., Palmer, A. R., & Malmierca, M. S. (2012). Topographic distribution, frequency, and intensity dependence of stimulus-specific adaptation in the inferior colliculus of the rat. *J Neurosci*, *32*(49), 17762-17774. https://doi.org/10.1523/JNEUROSCI.3190-12.2012

Dykes, R. W. (1982). Parallel processing of cutaneous information in the somatosensory system of the cat. *Can J Neurol Sci*, *9*(1), 9-19. https://doi.org/10.1017/s0317167100043560

Dykes, R. W., Rasmusson, D. D., Sretavan, D., & Rehman, N. B. (1982). Submodality segregation and receptive-field sequences in cuneate, gracile, and external cuneate nuclei of the cat. *J Neurophysiol*, *47*(3), 389-416. https://doi.org/10.1152/jn.1982.47.3.389

Emanuel, A. J., Lehnert, B. P., Panzeri, S., Harvey, C. D., & Ginty, D. D. (2021). Cortical responses to touch reflect subcortical integration of LTMR signals. *Nature*, *600*(7890), 680-685. https://doi.org/10.1038/s41586-021-04094-x

Emmers, R. (1965). Organization of the First and the Second Somesthetic Regions (Si and Sii) in the Rat Thalamus. *J Comp Neurol*, *124*, 215-227. https://doi.org/10.1002/cne.901240207

Francis, J. T., Xu, S., & Chapin, J. K. (2008). Proprioceptive and cutaneous representations in the rat ventral posterolateral thalamus. *J Neurophysiol*, *99*(5), 2291-2304. https://doi.org/10.1152/jn.01206.2007

Fulford, R., Ginsborg, J., & Goldbart, J. (2011). Learning not to listen: the experiences of musicians with hearing impairments. *Music Education Research*, *13*(4), 447-464. https://doi.org/10.1080/14613808.2011.632086

Germann, C., Sutter, R., & Nanz, D. (2021). Novel observations of Pacinian corpuscle distribution in the hands and feet based on high-resolution 7-T MRI in healthy volunteers. *Skeletal Radiol*, *50*(6), 1249-1255. https://doi.org/10.1007/s00256-020-03667-7

Gottschaldt, K. M., & Vahle-Hinz, C. (1981). Merkel cell receptors: structure and transducer function. *Science*, *214*(4517), 183-186. https://doi.org/10.1126/science.7280690

Gruters, K. G., & Groh, J. M. (2012). Sounds and beyond: multisensory and other non-auditory signals in the inferior colliculus. *Front Neural Circuits*, *6*, 96. https://doi.org/10.3389/fncir.2012.00096

Guo, J., Ma, X., Skidmore, J. M., Cimerman, J., Prieskorn, D. M., Beyer, L. A., Swiderski, D. L., Dolan, D. F., Martin, D. M., & Raphael, Y. (2021). GJB2 gene therapy and conditional deletion reveal developmental stage-dependent effects on inner ear structure and function. *Mol Ther Methods Clin Dev*, *23*, 319-333. https://doi.org/10.1016/j.omtm.2021.09.009

Handler, A., & Ginty, D. D. (2021). The mechanosensory neurons of touch and their mechanisms of activation. *Nat Rev Neurosci*, *22*(9), 521-537. https://doi.org/10.1038/s41583-021-00489-x

Handler, A., Zhang, Q., Pang, S., Nguyen, T. M., Iskols, M., Nolan-Tamariz, M., Cattel, S., Plumb, R., Sanchez, B., Ashjian, K., Shotland, A., Brown, B., Kabeer, M., Turecek, J., DeLisle, M. M., Rankin, G., Xiang, W., Pavarino, E. C., Africawala, N.,…Ginty, D. D. (2023). Three-dimensional reconstructions of mechanosensory end organs suggest a unifying mechanism underlying dynamic, light touch. *Neuron*, *111*(20), 3211-3229 e3219. https://doi.org/10.1016/j.neuron.2023.08.023

Harvey, M. A., Saal, H. P., Dammann, J. F., 3rd, & Bensmaia, S. J. (2013). Multiplexing stimulus information through rate and temporal codes in primate somatosensory cortex. *PLoS Biol*, *11*(5), e1001558. https://doi.org/10.1371/journal.pbio.1001558

Hasegawa, H., Abbott, S., Han, B. X., Qi, Y., & Wang, F. (2007). Analyzing somatosensory axon projections with the sensory neuron-specific Advillin gene. *J Neurosci*, *27*(52), 14404-14414. https://doi.org/10.1523/JNEUROSCI.4908-07.2007

Heffner, H. E., & Heffner, R. S. (2007). Hearing ranges of laboratory animals. *J Am Assoc Lab Anim Sci*, *46*(1), 20-22. https://www.ncbi.nlm.nih.gov/pubmed/17203911

Heffner, R. S., Koay, G., & Heffner, H. E. (2001). Audiograms of five species of rodents: implications for the evolution of hearing and the perception of pitch. *Hear Res*, *157*(1-2), 138-152. https://doi.org/10.1016/s0378-5955(01)00298-2

Holmes, N. P., & Spence, C. (2005). Multisensory integration: space, time and superadditivity. *Curr Biol*, *15*(18), R762-764. https://doi.org/10.1016/j.cub.2005.08.058

Hong, Y. K., Lacefield, C. O., Rodgers, C. C., & Bruno, R. M. (2018). Sensation, movement and learning in the absence of barrel cortex. *Nature*, *561*(7724), 542-546. https://doi.org/10.1038/s41586-018-0527-y

Hopkins, C., Maté-Cid, S., Fulford, R., Seiffert, G., & Ginsborg, J. (2023). Perception and learning of relative pitch by musicians using the vibrotactile mode. *Musicae Scientiae*, *27*(1), 3-26. https://doi.org/10.1177/10298649211015278

Horne, M. K., & Tracey, D. J. (1979). The afferents and projections of the ventroposterolateral thalamus in the monkey. *Exp Brain Res*, *36*(1), 129-141. https://doi.org/10.1007/BF00238473

Hulliger, M., Nordh, E., Thelin, A. E., & Vallbo, A. B. (1979). The responses of afferent fibres from the glabrous skin of the hand during voluntary finger movements in man. *J Physiol*, *291*, 233-249. https://doi.org/10.1113/jphysiol.1979.sp012809

Hunt, C. C., & Mc, I. A. (1960). Characteristics of responses from receptors from the flexor longus digitorum muscle and the adjoining interosseous region of the cat. *J Physiol*, *153*(1), 74-87. https://doi.org/10.1113/jphysiol.1960.sp006519

Jain, R., & Shore, S. (2006). External inferior colliculus integrates trigeminal and acoustic information: unit responses to trigeminal nucleus and acoustic stimulation in the guinea pig. *Neurosci Lett*, *395*(1), 71-75. https://doi.org/10.1016/j.neulet.2005.10.077

Johnson, K. O. (2001). The roles and functions of cutaneous mechanoreceptors. *Curr Opin Neurobiol*, *11*(4), 455-461. https://doi.org/10.1016/s0959-4388(00)00234-8

Kaas, J. H., Nelson, R. J., Sur, M., Dykes, R. W., & Merzenich, M. M. (1984). The somatotopic organization of the ventroposterior thalamus of the squirrel monkey, Saimiri sciureus. *J Comp Neurol*, *226*(1), 111-140. https://doi.org/10.1002/cne.902260109

Kumamoto, K., Senuma, H., Ebara, S., & Matsuura, T. (1993). Distribution of pacinian corpuscles in the hand of the monkey, Macaca fuscata. *J Anat*, *183 (Pt 1)*(Pt 1), 149-154. https://www.ncbi.nlm.nih.gov/pubmed/8270469

Kwon, S. E., Yang, H., Minamisawa, G., & O'Connor, D. H. (2016). Sensory and decision-related activity propagate in a cortical feedback loop during touch perception. *Nat Neurosci*, *19*(9), 1243-1249. https://doi.org/10.1038/nn.4356

Lalwani, A. K. (2002). Evaluation of childhood sensorineural hearing loss in the post-genome world. *Arch Otolaryngol Head Neck Surg*, *128*(1), 88-89. https://doi.org/10.1001/archotol.128.1.88

Lee, K.-S., Wagner, D. d. T., Sanders, M., & Huber, D. (2023). Emergence of a somatosensory tonotopic map for substrate vibration in the brainstem. *bioRxiv*. https://doi.org/10.1101/2023.09.26.559502

Lee, K. S., Loutit, A. J., de Thomas Wagner, D., Sanders, M., Prsa, M., & Huber, D. (2024). Transformation of neural coding for vibrotactile stimuli along the ascending somatosensory pathway. *Neuron*. https://doi.org/10.1016/j.neuron.2024.07.005

Lee, M. Y., Takada, T., Takada, Y., Kappy, M. D., Beyer, L. A., Swiderski, D. L., Godin, A. L., Brewer, S., King, W. M., & Raphael, Y. (2015). Mice with conditional deletion of Cx26 exhibit no vestibular phenotype despite secondary loss of Cx30 in the vestibular end organs. *Hear Res*, *328*, 102-112. https://doi.org/10.1016/j.heares.2015.07.018

Lehnert, B. P., Santiago, C., Huey, E. L., Emanuel, A. J., Renauld, S., Africawala, N., Alkislar, I., Zheng, Y., Bai, L., Koutsioumpa, C., Hong, J. T., Magee, A. R., Harvey, C. D., & Ginty, D. D. (2021). Mechanoreceptor synapses in the brainstem shape the central representation of touch. *Cell*, *184*(22), 5608-5621 e5618. https://doi.org/10.1016/j.cell.2021.09.023

Lesicko, A. M., Hristova, T. S., Maigler, K. C., & Llano, D. A. (2016). Connectional Modularity of Top-Down and Bottom-Up Multimodal Inputs to the Lateral Cortex of the Mouse Inferior Colliculus. *J Neurosci*, *36*(43), 11037-11050. https://doi.org/10.1523/JNEUROSCI.4134-15.2016

Liu, Y., Rutlin, M., Huang, S., Barrick, C. A., Wang, F., Jones, K. R., Tessarollo, L., & Ginty, D. D. (2012). Sexually dimorphic BDNF signaling directs sensory innervation of the mammary gland. *Science*, *338*(6112), 1357-1360. https://doi.org/10.1126/science.1228258

Loe, P. R., Whitsel, B. L., Dreyer, D. A., & Metz, C. B. (1977). Body representation in ventrobasal thalamus of macaque: a single-unit analysis. *J Neurophysiol*, *40*(6), 1339-1355. https://doi.org/10.1152/jn.1977.40.6.1339

Luna, R., Hernandez, A., Brody, C. D., & Romo, R. (2005). Neural codes for perceptual discrimination in primary somatosensory cortex. *Nat Neurosci*, *8*(9), 1210-1219. https://doi.org/10.1038/nn1513

Luo, W., Enomoto, H., Rice, F. L., Milbrandt, J., & Ginty, D. D. (2009). Molecular identification of rapidly adapting mechanoreceptors and their developmental dependence on ret signaling. *Neuron*, *64*(6), 841-856. https://doi.org/10.1016/j.neuron.2009.11.003

Luo, W., Wickramasinghe, S. R., Savitt, J. M., Griffin, J. W., Dawson, T. M., & Ginty, D. D. (2007). A hierarchical NGF signaling cascade controls Ret-dependent and Ret-independent events during development of nonpeptidergic DRG neurons. *Neuron*, *54*(5), 739-754. https://doi.org/10.1016/j.neuron.2007.04.027

Malmierca, M. S., Cristaudo, S., Perez-Gonzalez, D., & Covey, E. (2009). Stimulus-specific adaptation in the inferior colliculus of the anesthetized rat. *J Neurosci*, *29*(17), 5483-5493. https://doi.org/10.1523/JNEUROSCI.4153-08.2009

Martersteck, E. M., Hirokawa, K. E., Evarts, M., Bernard, A., Duan, X., Li, Y., Ng, L., Oh, S. W., Ouellette, B., Royall, J. J., Stoecklin, M., Wang, Q., Zeng, H., Sanes, J. R., & Harris, J. A. (2017). Diverse Central Projection Patterns of Retinal Ganglion Cells. *Cell Rep*, *18*(8), 2058-2072. https://doi.org/10.1016/j.celrep.2017.01.075

Matsuoka, T., Ahlberg, P. E., Kessaris, N., Iannarelli, P., Dennehy, U., Richardson, W. D., McMahon, A. P., & Koentges, G. (2005). Neural crest origins of the neck and shoulder. *Nature*, *436*(7049), 347-355. https://doi.org/10.1038/nature03837

Meredith, M. A., & Stein, B. E. (1983). Interactions among converging sensory inputs in the superior colliculus. *Science*, *221*(4608), 389-391. https://doi.org/10.1126/science.6867718

Mountcastle, V. B., & Henneman, E. (1952). The representation of tactile sensibility in the thalamus of the monkey. *J Comp Neurol*, *97*(3), 409-439. https://doi.org/10.1002/cne.900970302

Mountcastle, V. B., Talbot, W. H., Darian-Smith, I., & Kornhuber, H. H. (1967). Neural basis of the sense of flutter-vibration. *Science*, *155*(3762), 597-600. https://doi.org/10.1126/science.155.3762.597

Narins, P. M., Reichman, O. J., Jarvis, J. U., & Lewis, E. R. (1992). Seismic signal transmission between burrows of the Cape mole-rat, Georychus capensis. *J Comp Physiol A*, *170*(1), 13-21. https://doi.org/10.1007/BF00190397

Neubarth, N. L., Emanuel, A. J., Liu, Y., Springel, M. W., Handler, A., Zhang, Q., Lehnert, B. P., Guo, C., Orefice, L. L., Abdelaziz, A., DeLisle, M. M., Iskols, M., Rhyins, J., Kim, S. J., Cattel, S. J., Regehr, W., Harvey, C. D., Drugowitsch, J., & Ginty, D. D. (2020). Meissner corpuscles and their spatially intermingled afferents underlie gentle touch perception. *Science*, *368*(6497). https://doi.org/10.1126/science.abb2751

Nevo, E., Heth, G., & Pratt, H. (1991). Seismic communication in a blind subterranean mammal: a major somatosensory mechanism in adaptive evolution underground. *Proc Natl Acad Sci U S A*, *88*(4), 1256-1260. https://doi.org/10.1073/pnas.88.4.1256

Niu, J., Ding, L., Li, J. J., Kim, H., Liu, J., Li, H., Moberly, A., Badea, T. C., Duncan, I. D., Son, Y. J., Scherer, S. S., & Luo, W. (2013). Modality-based organization of ascending somatosensory axons in the direct dorsal column pathway. *J Neurosci*, *33*(45), 17691-17709. https://doi.org/10.1523/JNEUROSCI.3429-13.2013

O'Connell-Rodwell, C. E. (2007). Keeping an "ear" to the ground: seismic communication in elephants. *Physiology (Bethesda)*, *22*, 287-294. https://doi.org/10.1152/physiol.00008.2007

Oliver, D. L., & Morest, D. K. (1984). The central nucleus of the inferior colliculus in the cat. *J Comp Neurol*, *222*(2), 237-264. https://doi.org/10.1002/cne.902220207

Park, J. M., Hong, Y. K., Rodgers, C. C., Dahan, J. B., Harano, N., Schmidt, E. R. E., & Bruno, R. M. (2022). Deep and superficial layers of the primary somatosensory cortex are critical for whisker-based texture discrimination in mice *bioRxiv*. https://doi.org/10.1101/2020.08.12.245381

Perez-Gonzalez, D., Malmierca, M. S., & Covey, E. (2005). Novelty detector neurons in the mammalian auditory midbrain. *Eur J Neurosci*, *22*(11), 2879-2885. https://doi.org/10.1111/j.1460-9568.2005.04472.x

Pickles, J. O. (2015). Auditory pathways: anatomy and physiology. *Handb Clin Neurol*, *129*, 3-25. https://doi.org/10.1016/B978-0-444-62630-1.00001-9

Prsa, M., Morandell, K., Cuenu, G., & Huber, D. (2019). Feature-selective encoding of substrate vibrations in the forelimb somatosensory cortex. *Nature*, *567*(7748), 384-388. https://doi.org/10.1038/s41586-019-1015-8

Qi, L., Iskols, M., Greenberg, R. S., Xiao, J. Y., Handler, A., Liberles, S. D., & Ginty, D. D. (2024). Krause corpuscles are genital vibrotactile sensors for sexual behaviours. *Nature*, *630*(8018), 926-934. https://doi.org/10.1038/s41586-024-07528-4

Quy, P. N., Fujita, H., Sakamoto, Y., Na, J., & Sugihara, I. (2011). Projection patterns of single mossy fiber axons originating from the dorsal column nuclei mapped on the aldolase C compartments in the rat cerebellar cortex. *J Comp Neurol*, *519*(5), 874-899. https://doi.org/10.1002/cne.22555

Ribot-Ciscar, E., Vedel, J. P., & Roll, J. P. (1989). Vibration sensitivity of slowly and rapidly adapting cutaneous mechanoreceptors in the human foot and leg. *Neurosci Lett*, *104*(1-2), 130-135. https://doi.org/10.1016/0304-3940(89)90342-x

Rutlin, M., Ho, C. Y., Abraira, V. E., Cassidy, C., Bai, L., Woodbury, C. J., & Ginty, D. D. (2014). The cellular and molecular basis of direction selectivity of Adelta-LTMRs. *Cell*, *159*(7), 1640-1651. https://doi.org/10.1016/j.cell.2014.11.038

Saal, H. P., & Bensmaia, S. J. (2014). Touch is a team effort: interplay of submodalities in cutaneous sensibility. *Trends Neurosci*, *37*(12), 689-697. https://doi.org/10.1016/j.tins.2014.08.012

Salinas, E., Hernandez, A., Zainos, A., & Romo, R. (2000). Periodicity and firing rate as candidate neural codes for the frequency of vibrotactile stimuli. *J Neurosci*, *20*(14), 5503-5515. https://doi.org/10.1523/JNEUROSCI.20-14-05503.2000

Santiago, C., Sharma, N., Africawala, N., Siegrist, J., Handler, A., Tasnim, A., Anjum, R., Turecek, J., Lehnert, B. P., Renauld, S., Nolan-Tamariz, M., Iskols, M., Magee, A. R., Paradis, S., & Ginty, D. D. (2023). Activity-dependent development of the body's touch receptors. *bioRxiv*. https://doi.org/10.1101/2023.09.23.559109

Sathian, K. (1989). Tactile sensing of surface features. *Trends Neurosci*, *12*(12), 513-519. https://doi.org/10.1016/0166-2236(89)90112-4

Silfvenius, H. (1970). Characteristics of receptors and afferent fibers of the forelimb interosseous nerve of the cat. *Acta Physiol Scand*, *79*(1), 6-23. https://doi.org/10.1111/j.1748-1716.1970.tb04697.x

Stuttgen, M. C., & Schwarz, C. (2018). Barrel cortex: What is it good for? *Neuroscience*, *368*, 3-16. https://doi.org/10.1016/j.neuroscience.2017.05.009

Syka, J., Popelar, J., Kvasnak, E., & Astl, J. (2000). Response properties of neurons in the central nucleus and external and dorsal cortices of the inferior colliculus in guinea pig. *Exp Brain Res*, *133*(2), 254-266. https://doi.org/10.1007/s002210000426

Takada, Y., Beyer, L. A., Swiderski, D. L., O'Neal, A. L., Prieskorn, D. M., Shivatzki, S., Avraham, K. B., & Raphael, Y. (2014). Connexin 26 null mice exhibit spiral ganglion degeneration that can be blocked by BDNF gene therapy. *Hear Res*, *309*, 124-135. https://doi.org/10.1016/j.heares.2013.11.009

Talbot, W. H., Darian-Smith, I., Kornhuber, H. H., & Mountcastle, V. B. (1968). The sense of flutter-vibration: comparison of the human capacity with response patterns of mechanoreceptive afferents from the monkey hand. *J Neurophysiol*, *31*(2), 301-334. https://doi.org/10.1152/jn.1968.31.2.301

Tawil, R. N., Saade, N. E., Bitar, M., & Jabbur, S. J. (1983). Polysensory interactions on single neurons of cat inferior colliculus. *Brain Res*, *269*(1), 149-152. https://doi.org/10.1016/0006-8993(83)90972-1

Turecek, J., & Ginty, D. D. (2023). Coding of self and environment by Pacinian neurons in freely moving animals. *bioRxiv*. https://doi.org/10.1101/2023.09.11.557225

Turecek, J., & Ginty, D. D. (2024). Coding of self and environment by Pacinian neurons in freely moving animals. *Neuron*. https://doi.org/10.1016/j.neuron.2024.07.008

Turecek, J., Lehnert, B. P., & Ginty, D. D. (2022). The encoding of touch by somatotopically aligned dorsal column subdivisions. *Nature*, *612*(7939), 310-315. https://doi.org/10.1038/s41586-022-05470-x

Virant-Doberlet, M., Stritih-Peljhan, N., Zunic-Kosi, A., & Polajnar, J. (2023). Functional Diversity of Vibrational Signaling Systems in Insects. *Annu Rev Entomol*, *68*, 191-210. https://doi.org/10.1146/annurev-ento-120220-095459

Winter, D. L. (1965). N. Gracilis of Cat. Functional Organization and Corticofugal Effects. *J Neurophysiol*, *28*, 48-70. https://doi.org/10.1152/jn.1965.28.1.48

Wu, C., Stefanescu, R. A., Martel, D. T., & Shore, S. E. (2015). Listening to another sense: somatosensory integration in the auditory system. *Cell Tissue Res*, *361*(1), 233-250. https://doi.org/10.1007/s00441-014-2074-7

Xiong, X. R., Liang, F., Zingg, B., Ji, X. Y., Ibrahim, L. A., Tao, H. W., & Zhang, L. I. (2015). Auditory cortex controls sound-driven innate defense behaviour through corticofugal projections to inferior colliculus. *Nat Commun*, *6*, 7224. https://doi.org/10.1038/ncomms8224

Yau, J. M., Olenczak, J. B., Dammann, J. F., & Bensmaia, S. J. (2009). Temporal frequency channels are linked across audition and touch. *Curr Biol*, *19*(7), 561-566. https://doi.org/10.1016/j.cub.2009.02.013

Young, B. A., & Morain, M. (2002). The use of ground-borne vibrations for prey localization in the Saharan sand vipers (Cerastes). *J Exp Biol*, *205*(Pt 5), 661-665. https://doi.org/10.1242/jeb.205.5.661

Yu, Q., Wang, Y., Chang, Q., Wang, J., Gong, S., Li, H., & Lin, X. (2014). Virally expressed connexin26 restores gap junction function in the cochlea of conditional Gjb2 knockout mice. *Gene Ther*, *21*(1), 71-80. https://doi.org/10.1038/gt.2013.59

Zelena, J. (1978). The development of Pacinian corpuscles. *J Neurocytol*, *7*(1), 71-91. https://doi.org/10.1007/BF01213461

Zhang, H. Q., Murray, G. M., Coleman, G. T., Turman, A. B., Zhang, S. P., & Rowe, M. J. (2001). Functional characteristics of the parallel SI- and SII-projecting neurons of the thalamic ventral posterior nucleus in the marmoset. *J Neurophysiol*, *85*(5), 1805-1822. https://doi.org/10.1152/jn.2001.85.5.1805

Zhaoping, L. (2016). From the optic tectum to the primary visual cortex: migration through evolution of the saliency map for exogenous attentional guidance. *Curr Opin Neurobiol*, *40*, 94-102. https://doi.org/10.1016/j.conb.2016.06.017

Zhou, J., & Shore, S. (2006). Convergence of spinal trigeminal and cochlear nucleus projections in the inferior colliculus of the guinea pig. *J Comp Neurol*, *495*(1), 100-112. https://doi.org/10.1002/cne.20863

Zimmerman, A., Bai, L., & Ginty, D. D. (2014). The gentle touch receptors of mammalian skin. *Science*, *346*(6212), 950-954. https://doi.org/10.1126/science.1254229